MICROFLUIDIC DEVICES FOR GENENTIC ANAYLSIS AND GENE EXPRESSION STUDIES

Thesis by

Jian Liu

In Partial Fulfillment of the Requirements

For the Degree of

Doctor of Philosophy

CALIFORNIA INSTITUTE OF TECHNOLOGY

Pasadena, California

2007

(Defended September 29 th, 2006)

ACKNOWLEDGEMENTS

I would like to thank my advisor, Dr. Stephen Quake, for his great mentorship and consistent support over the years. He has led me into a very active and interesting research field of microfluidics. His advice has helped me out many times when I was struggling in my research projects. I appreciate his patient training, and the great opportunity of learning in his group.

I am deeply grateful to Quake group members. Dr. Markus Enzelberger kindly taught me the techniques of device fabrication and polymerase chain reaction (PCR). His help was invaluable when I just joined the group and knew little. Anne Fu and Todd Thorson gave me a lot of useful suggestions or tips on using the fluorescent microscope and working with PDMS devices. Dr. Ido Braslavski and Charles Spence were always patiently providing me with help whenever I needed them. I thank Dr. Yanyi Huang for his encouragement for my work and many communications on my career plan. I want to thank Carl Hansen, Frederick Balagadde, Sebastian Maerkl, Michael Vandam, and Mark Adams, with whom I have worked closely in the lab. I would like to extend my sincere gratitude to Dr. Marc Unger, Dr. Houpu Chu, Dr. Anne Leyrat, Dr. Rafael Gomez-Sjoberg, Dr. Yann Marcy, Dr. Michael Diehl, Dr. Jong Wook Hong, Luigi Warren, George Burkhard, Ziyang Ma, Emil Kartalov, and many other colleagues. I thank Dr. Jessica Melin and the microfluidic foundry at Stanford, as well as the other foundry at Caltech. Connie Rodriguez, Jody Joseph, Irene Leora, Dian Buchness, and Ali Ghaffari have kindly assisted me many times when I needed help.

Special thanks go out to a number of excellent academic collaborators. Dr. Brian Williams, Richele Gwirtz, and Dr. Barbara Wold kindly taught me the skills to perform conventional DNA microarray experiments and allowed me to use the facilities in their lab. I appreciate the collaboration with Maria Spletter and Dr. Liqun Luo, which was an excellent opportunity to learn some knowledge of neural science. I thank Tait Pottbaum for providing me with a computer program for temperature calibrations with TLC particles.

Many thanks also go out to my friends. I am indebted to Shuwei Li for his generous help and patient tutorship in my early graduate years at Caltech. I enjoy the warm-hearted friendship with Xin Weng, Jianming Xie, Donghua Xu, Robert Dirks, Jessica Mao, Xin Qi, Victor Wai Tak Kam, Claudiu Giurumescu, Bianxiao Cui, Haitao Zhu, Chunlei Wang, Tao Wei, Thomas Hall, Andy Pearce and many others. Especially, I want to thank Renee and James Masterson for their love and kind help after I relocated from Caltech to Stanford.

Finally, I thank my parents, Benming Kuang and Jide Liu, for their selfless love, understanding, and support all the time. The education that they gave to me started from my childhood. They helped me develop an enthusiaum for science. I am grateful to my parents-in-law, Jian Yu and Dezheng Cao, and my sister, Chang Liu, for being a continual source of encouragement and support for my life. I thank my wife, Chen Cao, very much for her love, patience, and support. I could not have done this without my dearest family.

Jian Liu

September, 2006

ABSTRACT

Microfluidic devices hold the promise of becoming the next-generation laboratory platforms by offering many possible benefits in chemistry, biology, and medicine. However, microfluidics is still in its infancy at present, requiring a great deal of work before it can become more than an active research field in academia. This thesis describes efforts by the author in developing microfluidic technologies for applications in genetics. Section I describes the development of miniaturized devices for genetic analysis. Successful nucleic acid amplifications by polymerase chain reaction (PCR) have been demonstrated within a reaction volume as small as 700 picoliters. In section II, the concept of a microfluidic matrix chip is described and has been experimentally realized to solve the "macroscopic/microfluidic" interface problem. The matrix chip also provides a flexible platform to perform combinatorial tests with high throughput performance. Section III presents an application example of the microfluidic matrix chip in gene expression studies, providing quantitative profiles of gene isoforms by alternative splicing in a high throughput manner. In the section IV, a microfluidic chaotic mixer has been developed to accelerate the process and enhance the hybridization signals of DNA microarray experiments. These devices represent significant advances in microfluidics, with the following goals achieved: improved sensitivity and reliability of assays, reduction of consumption of reagents or analytes into desired economies of scale, and dramatic reduction of the time and complexity of "hands-on" manipulations, therefore providing experimental results in a high throughput manner.

TABLE OF CONTENTS

FIGURES

Chapter 2

Chapter 3

Chapter 4

Chapter 5

TABLES

Chapter 1

OVERVIEW

Introduction

The completed human genome sequencing project is a landmark to understand our own DNA instruction book from a molecular level. In the past decade there have emerged many active research fields and opportunities. These include 1000-dollar genome sequencing project, functional genomics[1, 2], RNA regulations[3, 4], proteomics[5, 6], genetic diversity[7], and personalized medicine[8, 9]. However, most of the technologies currently available are still low throughput or price prohibitive to many labs. Taking human genome sequencing for example, current estimates of the cost range between 10 million to 25 million dollars[10, 11]. Scientists are expecting a next generation of technologies and platforms, which should feature high throughput processing, cost effectiveness, ease of automation, and reliable performance. A range of technologies are being directed toward this goal[10, 12-16]. Among them, the technology of microfluidics shows a promising future by offering many possible advantages[17-20].

Microfluidics is both a science and a technology, using channels with dimensions of tens to hundreds of micrometers to deal with fluids in small volume (10^{-9} to 10^{-18} liters)[21]. The ability to process small volumes, small quantities of reagents and analytes has placed it in a superior position than many conventional techniques. In bioanalysis for instance, the actual

concentration of analytes is increased dramatically when the reaction volume is reduced by several orders of magnitude using the microfluidic technology. Additionally, impure reagents can be partitioned into individual small volumes without affecting the reactions in other microchambers. Therefore, these advantages make microfluidics a very nice tool with extraordinary sensitivity for analytical chemists. Performing reactions in scaled-down volumes could also bring other benefits, such as reducing the cost of reagent consumption, or short time for analysis.

The combination of lithography and soft materials processing (like PDMS, a silicone rubber) has provided a convenient and robust approach for fabrication of microfluidic devices[22, 23]. The more recent advances using multilayer soft lithography (MSL) have realized large-scale integration of pneumatically activated valves, pumps, and mixers into a single microfluidic device[14, 17, 24, 25]. These methods have made tremendous impacts on a wide range of research fields, facilitating the cycle of constructing prototype devices, testing new ideas, and creating new knowledge. Highly integrated microfluidic devices inherently exhibit the functionality of high throughput performance and great potential of automation.

The physical properties of fluids in microchannels are significantly different from those more commonly seen in the macroscopic world[26]. The Reynolds numbers of microfluidic systems are typically smaller than 10^2. Laminar flow is always dominant is this regime. Even water as a fluid appears to be very viscous in microchannels. This feature of microfluidics has obtained many applications[19, 27-30]. One of the most straightforward cases

is hydrodynamic focusing[31-33]. Mixing subsequently becomes one of the central issues in microfluidics. Here in general, fluids do not mix convectively. The only mixing results from diffusion of molecules across the interface between any fluids[21]. The phenomenon of free interface diffusion has been exploited to grow a variety of protein crystals by the Quake group[18]. However, in many other cases, the efficiency of diffusive mixing is not enough. Various methods have been developed to introduce active mixing in microfluidic systems[34-37]. A significant part of this thesis is relevant to the topic of mixing in microfluidic channels or chambers.

The focus of this thesis is the development of microfluidic devices for genetic analysis and gene expression studies. This work is built on the cornerstone of the MSL technology (multilayer soft lithography), which is previously developed by Unger *et al.* in the Quake group[14]. The thesis describes the miniaturized devices using the MSL technology for polymerase chain reaction (PCR), which were the first few demonstrations of successful PCR amplifications on PDMS devices. These devices developed by the author became a part of important applications during the early growth of the MSL technology.

This thesis describes a huge effort by the author in the design and subsequent optimization of the microfluidic devices for various genetic research projects. It is indispensable in order to claim the possible benefits by microfluidics. For example, miniaturization of biochemical assays with microfluidic technologies promises a potential to save expensive reagents by several orders of magnitude as compared to conventional techniques. But this benefit is not necessarily the case in practice, because the microfluidic devices at some

point have to be interfaced to the tools in the macroscopic world, such as pipets or tubes, which handle the liquid at the scale of microliter or more. This question will be addressed in chapter 3. In general, good design and careful consideration of engineering issues are required for the development of microfluidics.

Organization and Collaborations

Chapter 2 begins with a rationale for miniaturizing polymerase chain reaction on the microchips. A microfluidic device was designed to perform PCR in various small volumes. PCR amplification in a volume as small as 700 picoliter was successfully demonstrated. PCR amplifications using microfluidic devices show improved performance over those with conventional tubes. Another microfluidic device with integrated micropump and microheaters is described for PCR in a compact spatial thermocycling mode. The concept of miniaturizing PCR on polydimethylsiloxane (PDMS) devices was brought up by Dr. Markus Enzelberger and Prof. Stephen Quake. The author implemented this idea.

Chapter 3 starts with an introduction to the volume mismatch between the macroscopic world and microfluidic devices. The challenge behind the problem is described, and then an effective answer is presented with the design of the microfluidic matrix chip. Two microchips (4 × 2 arrays and 20 × 20 arrays) exemplify the development of microfluidic matrix devices. These designs achieve two goals at the same time: significant decrease of reagent overhead from each pipetting step, and dramatic simplification of required pipetting operations. The matrix chip is a flexible platform for various formats of loading reagents,

essentially suitable for a variety of binding assays or screenings performed in a combinatorial manner. This “macroscopic/microfluidic” interface problem was brought up by Prof. Stephen Quake. The author made the major contribution to the development of the matrix chip and subsequent demonstration of matrix PCR. This work was collaborated with Carl Hansen.

Chapter 4 describes a high-throughput method to profile the gene isoforms by alternative splicing in fruit fly, which is also an application example of the microfluidic matrix chip. Quantitative profiles of the lola gene at different developmental stages of fruit fly are obtained by performing matrix PCR. This chapter explains that further information can be extracted to include absolute gene copy numbers. A theoretical development is introduced for decoding the mystery of extremely diverse Dscam isoforms by alternative splicing in fruit fly. Neural cell samples are provided by academic collaborators: Maria Spletter and Dr. Liqun Luo. George Burkhard wrote a prototype computer program for technical assistance.

Chapter 5 begins with an introduction of the technical problem of conventional DNA microarray experiments, that is, diffusion-limited hybridization. This chapter presents a method of microfluidic chaotic mixing to accelerate the process and enhance the signals of DNA hybridization. A microfluidic device is designed and constructed, with features of large hybridization chambers, integrated micropumps, and active mixing elements. Experiments show that these active mixing elements in our devices are very efficient, and critical in homogenizing the solution components at low Reynolds number. A second

generation of the device with larger hybridization chambers is demonstrated to be compatible with commercial high-density microarrays. In a series of side-by-side comparison experiments, the control experiments include the hybridization performed in a conventional static manner, or with a simple fluid circulation between the chambers. Our approach has achieved stronger signals, enhanced sensitivity, better signal specificity, reduced spot-to-spot variability, and faster hybridization process. RNA samples used in the experiments were provided by the following collaborators: Dr. Brian Williams, Richele Gwirtz, and Dr. Barbara Wold. Mouse-printed oligoarrays (17 K) for the trial experiments were generously provided by Yanxia Hao, and Christopher Baker. The work of evaluating mixing efficiency was assisted by Frederick Balagadde.

Chapter 2

GENETIC ANALYSIS USING MINIATURIZED DEVICES

Introduction

Nucleic acid amplification reactions such as polymerase chain reaction (PCR) have emerged as powerful tools in a variety of genetic analyses, medical diagnostics, and forensic applications[38-40]. These techniques are able to dramatically increase the concentration of target nucleic acids of interest, which are initially present at low levels in most cases. For example, a single target DNA molecule can be amplified to several million copies or more by PCR. PCR involves the repetition of heating (denaturation) and cooling (annealing and extension) cycles in the presence of a target DNA, two primers, deoxynucleotides, a polymerase and various cofactors. The prevalence of PCR-based methods in genetic analysis results from the advantages such as high sensitivity, reliable and robust performance, the vast amount of experience accumulated on DNA and DNA polymerase, and ease of automation. With the advent of the notion of "lab-on-a-chip" technology, the idea of making integrated microfluidic PCR chips has attracted the interest of many researchers[41-47]. Since the cost of PCR is dominated by the amount of reagents used, miniaturized devices are expected to dramatically reduce the cost for high throughput applications. Rapid results of assays may be provided by thermocycling a smaller volume of reagents in the microchips. They are also expected to be easily portable, making them useful for various field-testing situations ranging from crime scene forensics to biological

weapons detection. Finally, since PCR is exquisitely sensitive to cross-contamination, "lab-on-a-chip" devices provide a way to resolve this issue by performing all required analyses in a sealed, disposable device.

There are four key figures of merit that are important in the evaluation of a microfabricated PCR device. These include: (1) volume of sample consumption, (2) time to perform the reaction, (3) power consumption of the chip, and (4) ability to be integrated with other biological manipulations. Sample volume is a significant parameter in determining cost per reaction. With conventional techniques, a mixed solution of sample and reagents of around 20 microliters per assay is required to perform PCR. But miniaturized devices make it possible to reduce the reagent volume by several orders of magnitude. On the other hand, since the process time is often limited by the rate at which one can thermally cycle the reaction, much effort has been placed in reducing the sample volume in order to shorten the duration time of thermocycling. So far miniaturized devices have demonstrated reaction times ranging from 7 to 40 minutes[41, 48], while bench-top PCR machines still require 1 to 2 hours per reaction, typically. Power consumption is a critical issue for portable devices and can also be decreased by reducing the sample volumes. Finally, in many cases it will not be possible to reap the desired economies of scale without a scaleable technology that will allow integration of PCR with other manipulations such as reagent dispensing and subsequent analysis. Thus, it is clear that many of the important parameters for practical microfabricated PCR devices depend either directly or indirectly on one's ability to reduce the sample volumes involved.

A number of microfabricated and other miniaturized PCR devices have been demonstrated to date[41-47, 49, 50]. Most have large (>1 microliter) sample volumes, although samples as small as 240 nanoliters have been amplified[43]. There are two main classes of methods to conduct on-chip PCR. The most common approach is a time domain one, which is a direct miniaturization of bench-top methods. The reaction mixture is kept stationary while the temperature of the reaction chamber is cycled. This method requires fairly careful optimization of thermal mass in order to optimize reaction times and power consumption. The alternative is a space domain approach in which the device itself is not thermocycled, but the reaction mixture is moved in a flow channel through a series of zones with different fixed temperatures[42, 43]. This method can be conducted at relatively high speed because it is not necessary to heat and cool the device repeatedly, but it requires the use of relatively large sample volumes.

This chapter describes two representative devices that we have developed in an effort to miniaturize PCR on the chip. These include a microfluidic device containing a series of micro reactors with different volumes, and a "rotary PCR device" with integrated micro heaters[51]. Both devices are fabricated out of silicone elastomer, with integrated valves or pumps. These plumbing components are compatible with a high degree of integration, as shown by their use in microfabricated cell sorters and other integrated devices. In future devices, these plumbing components will be useful for metering small amounts of reagents. The former device uses the time domain method for temperature cycling, testing PCR within different volumes. PCR amplification in a volume as small as 700 picoliters has been successfully demonstrated with the device. The latter device integrates

microfabricated tungsten heaters on a glass slide, which provide different temperature zones on a planar surface. The fluidic channels are arranged in loop geometry with an inlet and outlet, and integrated pumps are designed to circulate the reagents along the loop channel through different temperature zones. This design allows compact spatial cycling with no sample loss or dilution during the amplification process. Previously such a rotary pump has been shown to accelerate chemical kinetics. Alternatively, the latter device can also be used with the temporal cycling scheme: the reaction loop channel can be sealed off with the valves and the temperature of the entire loop is cycled. We have demonstrated nucleic acid amplifications via both the Taqman PCR (2 steps) and standard PCR (3 steps) in these chips with fast process time. The elastomeric chips are disposable because they are significantly cheaper to mass produce than glass or silicon devices.

A Microfluidic Device to Perform PCR in Various Small Volumes

This miniaturized device was designed to scale down the conventional PCR techniques with a method of temporal thermocycling, and to test the reactions in various small volumes. The device is composed of two layers of silicone rubber (polydimethylsiloxane or PDMS), namely a control layer and a flow layer, sealed on a glass coverslip. As shown in figure 1, there are five winding flow channels (red) parallel to each other. Each of them has an independent inlet and outlet, and connects a series of chambers (reactors) with different volumes (from 14 nL to 700 pL). Actuation of the valves displayed in the ten parallel control channels (green) allows closing reaction chambers. All the control channels merge to a single hole for the manipulation with hydraulic pressure. In addition, multiple rows of

hydraulic guard channels (thin grey lines) in the control layer cover a large area of the microchip, reducing evaporation of the reagent solution during the process of thermocycling. Air can diffuse out of the control and guard channels under the hydraulic pressure because the material of PDMS is permeable to air. Therefore, water can fill in these dead-end channels.

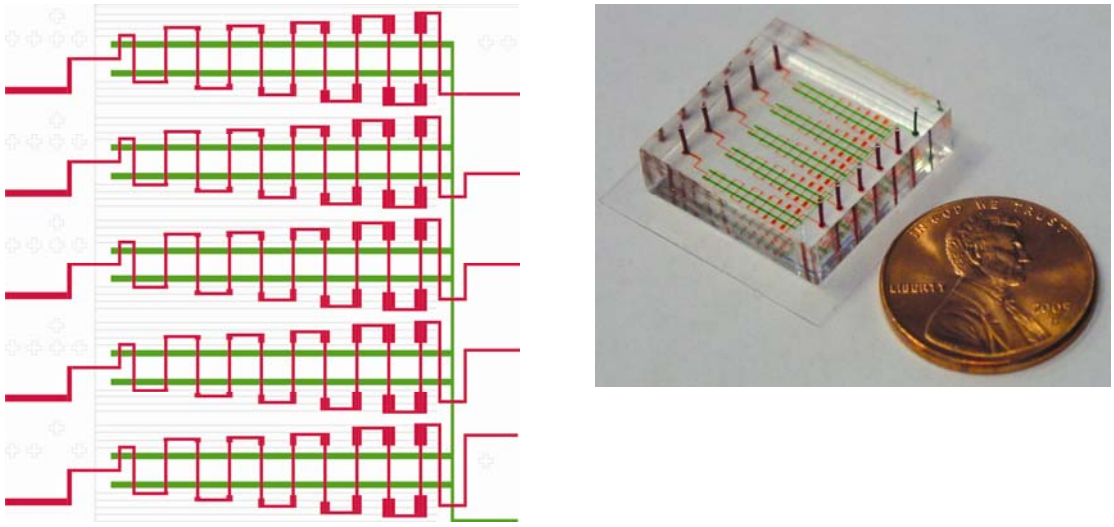

Figure 1: *A two-layer microfluidic device containing a series of reaction chambers of different volumes. Left: schematic drawing; right: optical micrograph. Control channels (green); Fluidic channels (red). Five parallel fluidic channels are displayed in the device. Each of them connects reaction chambers with the following volumes (from the right to the left):14 nL,12 nL, 9 nL, 6 nL, 4 nL, 3 nL, 2 nL, 1.5 nL, 1.35 nL, 0.7 nL. (The deam volumes of the connecting channels are taken into consideration in calculating the last two values.)*

The microfluidic devices were fabricated by multilayer soft lithography techniques[14]. The techniques were applied to fabricate a variety of microfluidic devices described in the

subsequent chapters, in some cases with otherwise specified changes. Here the main procedure is described as follows: After the chip patterns were designed using AutoCAD or other graphic software tools, the files can be sent out for a printing service. The masks were printed on transparency films by a high-resolution printer (3556 dpi). Molds were prepared by spincoating photoresist (Shipley SJR5740) onto silicon wafers (3000 RPM for 60 seconds) which had been pretreated with Hexamethyldisilazane (HDMS). The wafers were heated at 110 ^{o}C for 90 seconds, after which the channel patterns were exposed onto them by ultraviolet light with a mask aligner (Karl Suss). The patterns were developed by 5:1 (v/v) developing solution (Shipley 2401). Then molds were put onto a hot plate (125 ^{o}C) for 30 min to round the remaining photoresist. The features on the molds were approximately 10 microns high. After that, the flow mold was processed again in a way similar to the above description, using a negative mask and photoresist (SU8-50, MicroChem Co.) to obtain chambers as high as 50 microns.

The devices were made from GE RTV 615, a two-component poly(dimethylsiloxane) elastomer. A 20:1 mixture of RTV was spincoated on the fluid channel mold at 1500 RPM for 30 seconds, resulting in a thin layer of about 70 μm (by estimation). 5:1 RTV was poured (or spincoated) on the control channel mold, with an option to improve the mechanical properties by an additional layer of 10:1 RTV onto the top. After baking both molds in an oven of 80 ^{o}C for 45 minutes, the RTV block on the control mold was peeled off to punch air supply through-holes. Then it was aligned and pressed against the thin RTV layer on the flow mold. After a bake at 80 ^{o}C for 2 hours, the multilayer RTV was peeled off the mold to punch fluid through-holes. Finally, the device was made by sealing

the multilayer RTV onto a glass coverslip at 80 ^{o}C for 2 hours. As a reminder, before these layers were assembled together, the channels on the surface of each layer were open. After the layers were bond together, the ceiling of the lower layer (flow) became the floor of the upper layer (control), therefore forming the complete channels in the upper layer. Similarly, sealing a glass coverslip formed complete channels in the lower layer (flow). It was optional to pre-spincoat another thin layer of RTV on the glass coverslip, therefore the flow channels would entirely be comprised of RTV, instead of hybrid of RTV and glass substrate.

This device was tested to PCR amplify a 294 bp segment of human beta-actin gene. The signals of amplification from micro reactors were read out by the fluorescence change with the technique of Taqman probes. Briefly, the Taqman probe is an oligonucleotide containing a reporter dye (FAM) in the 5' end and a quencher dye (TAMRA or BHQ1) in the 3' end. It is cleaved during PCR by the 5'-3' nuclease activity of DNA polymerase, releasing the fluorescent reporter. Therefore, this technique allows quantitative detection of PCR product with high specificity, showing a dramatic fluorescent increase at the wavelength for FAM (figure 2).

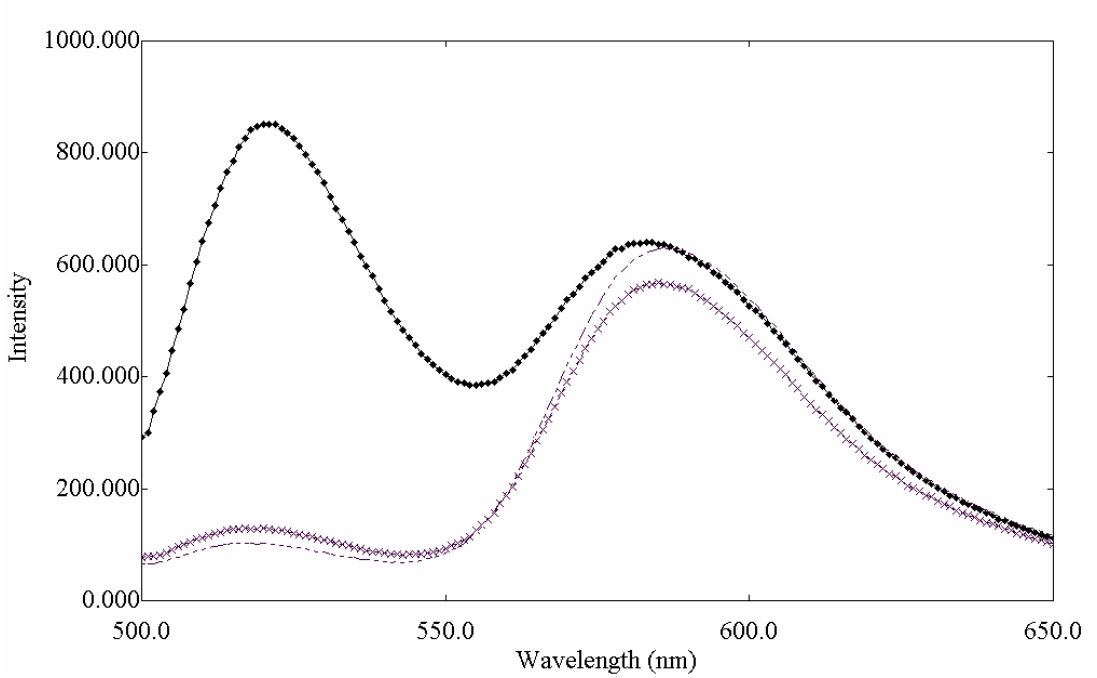

Figure 2: *The emission spectra of the sample (before and after) and the negative control (no DNA template). -♦-: sample; -×-: no template contro;. ---: Sample before PCR.*

The Taqman PCR amplifications were performed in conventional tubes with a bench-top PCR machine (MJ Research). Note how the fluorescent peak at 518 nm appears in the sample after PCR, while there is virtually no peak from the negative control or the sample before PCR. The cycling program was described in the section2.3: 2 minutes at 50 ^{o}C; 10 minutes at 95 ^{o}C; 40 cycles: 15 seconds at 95 ^{o}C; 1minute at 60 ^{o}C.

An amplification protocol suggested by the supplier (Applied Biosystems) was optimized to perform PCR on the microfluidic devices. The DNA template was available from the kit by Clontech (cDNA) or Applied Biosystems (gDNA). Forward primer and reverse primer were the following: 5'-TCA CCC ACA CTG TGC CCA TCT ACG A-3' and 5-'CAG CGG AAC CGC TCA TTG CCA ATG G-3', respectively. Taqman Probe: 5'-(FAM)ATG

CCC-X(TAMRA)-CCC CCA TGC CA CCT GCG T-3', A solution of the following reagents was prepared in the microtube: template, 0.2ng/μL (cDNA); primers, 500nM; Mg^{2+}, 4 mM; dATP, 200μM; dCTP, 200μM; dGTP, 200μM; dUTP, 400μM; Dynazyme, 0.05 U/μL; AmpErase UNG, 0.01 U/μL; Probe, 200nM; lambda DNA carrier, 2ng/μL; PEG 8000, 0.75%; BSA, 0.25μg/μL; Gelatin, 0.001%; TritonX-100, 0.025%. In this optimized recipe, lambda DNA was used to reduce the issue of absorption of DNA template on the inner walls of microchannels. And a cocktail of additives as described as above may help to stabilize the components of PCR in the solution[52]. A bench-top PCR machine (PTC200, MJ Research) with a flatbed heating block was used to cycle the temperature of the whole microfluidic device: 2 minutes at 50 ^{o}C; 10 minutes at 95 ^{o}C; and then 40 cycles: 15 seconds at 95 ^{o}C; 40 seconds at 60 ^{o}C.

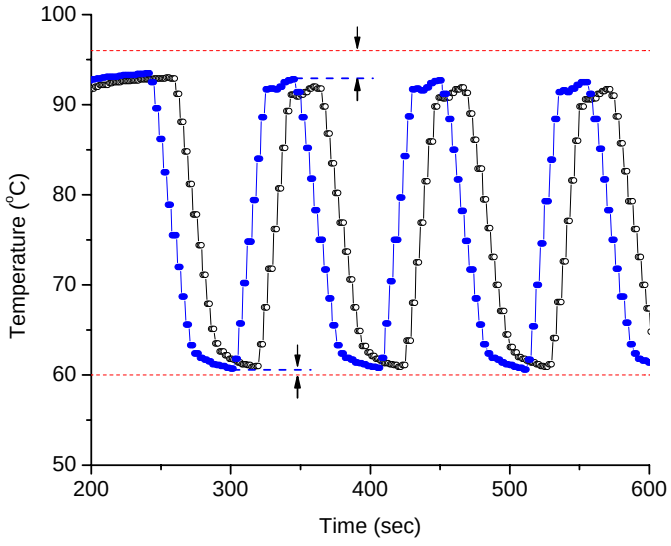

Figure 3: *Temperature difference across the glass coverslip (0.17mm) of the microchip. Red dashed lines: setup temperature of the flatbed heating block of the thermocycler (PTC200, MJ Research), cycled between the high end and low end (96 ^{o}C, 20 sec; 60 ^{o}C, 30 sec). Blue (with mineral oil interfacing the block surface and the glass) and black (without mineral oil) lines: temperature profiles measured by the thermal couple (K type) embedded in the PDMS device (touch the glass substrate). The temperature differences (indicated by arrows) with mineral oil are approximately 3.5 ^{o}C (high end) and 1.0 ^{o}C (low end), respectively. They become slightly larger without mineral oil interfacing. Note: this graph does not show whether mineral oil interfacing reduces the delay of temperature response or not.*

A PDMS device embedded with a K-type thermal couple (Omega, standard limits of error 2.2 ^{o}C) was used to measure the temperature difference across the glass coverslip (0.17 mm). As shown in figure 3, the temperature difference was approximately 3.5 ^{o}C for the high end (denaturation), while it reduced to less than 1 ^{o}C for the low end (annealing and extension). The temperature differences were taken into account in setting up the thermocycling profiles with the flatbed heating block. After thermocycling was complete, the fluorescence emission (reporter at 519nm and passive reference at 570nm) from the PCR products in the chip was imaged using a DNA array scanner (Applied Precision).

In the experiment, the reagent solutions containing DNA template or no template control were alternately loaded into the flow channels. The control channels were pressurized to form closed reaction chambers in the flow layer. As shown in figure 4a, the reaction

chambers containing all the components produced positive signals as expected. There was a significant fluorescent increase at the wavelength of 519 nm from these micro reactors (green). On the contrary, the reaction chambers without DNA template did not show an increase in fluorescence (except for one false positive reaction), thus they appeared to be indistinguishable from the background. One of them in the second row gave a false positive signal, which might derive from contamination of DNA template during pipetting operations. The reaction chambers, including the positive and negative controls, were imaged at the wavelength of 570nm for the fluorescent emission of passive reference dye molecules, as shown in figure 4b.

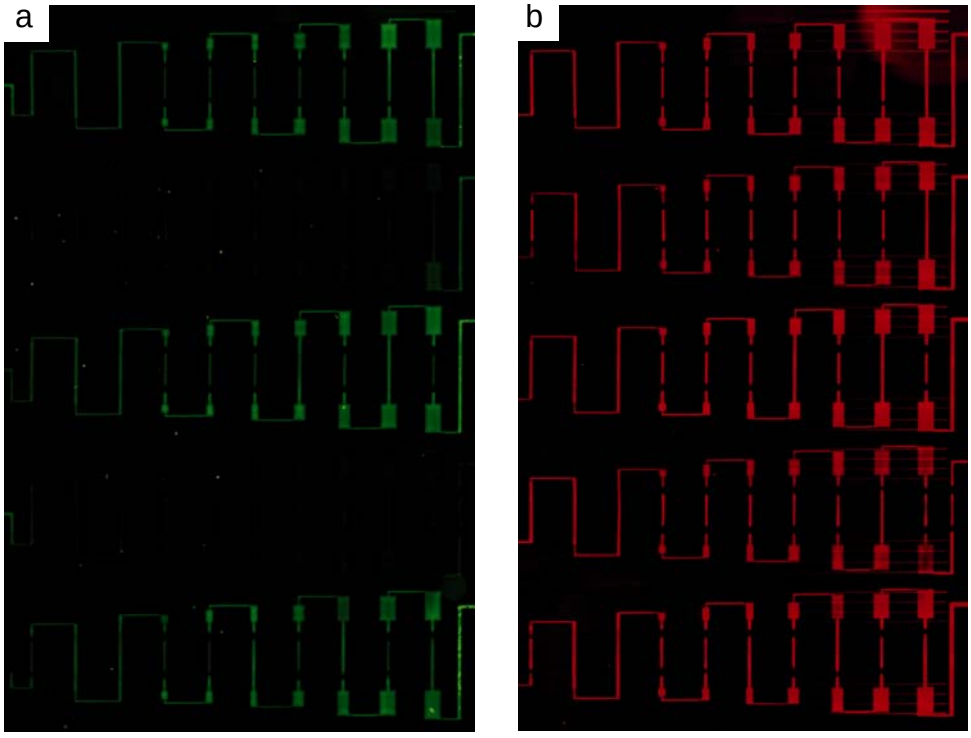

Figure 4: *Fluorsecent images of PCR within a series of reaction volumes in the microchip. Left(a): at the wavelength for fluorephore FAM (519 nm). The bright green color shows an*

array of reaction chambers containing the DNA samples (52 copies/nL), connected by three independent rows of winding fluidic channels. The rest reaction chambers in row 2 and row 4 are almost invisible because they are negative control (without DNA template) except for one false positive reaction in row 2. Right(b): at the wavelength for fluorephore ROX (570 nm), as a passive reference (as shown red).

We attempt to investigate the limit of miniaturization of PCR by estimating the availability of the "building blocks" of the amplicons for the amplification. These include the molecules of primers and deoxynucleotides (dNTP).

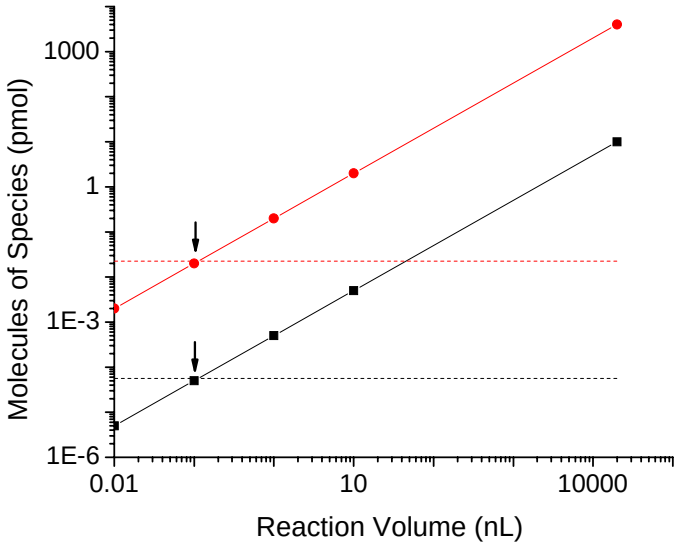

Figure 5: *Limit of miniaturization determined by the availability of the "building blocks" of PCR amplicons. The molecules of primers in the specified volume are represented by the black line; those of dNTP by the red line. The dashed lines, in the black (primers) or in the red (dNTP), represent the minimun necessary molecules for detectable signals. The arrows*

points to the minimum necessary volume to accommodate the required molecules. The typical concentrations of primers and dNTP are used in the calculation.

As shown as figure 5, the molecules of primers (black line) and dNTP (red line) in each chamber decrease linearly with miniaturization of the reaction volume. Based on our experience, the fluorescent signal becomes detectable after around 25 cycles (CT) of PCR amplification from a single copy of DNA template. Then the number of amplicons are $2^{25} \approx$ 34 million, which subsequently requires at least the same number of primers (black dashed line) available for PCR amplification. The threshold molecules for dNTP (red dashed line) can also be calculated, with a practically reasonable assumption that each amplicon is composed of several hundred dNTP. Therefore, it is approximately estimated that a volume of at least 100 pL is necessary to provide sufficient molecules of the "building blocks" for PCR. A reaction volume less than 700 pL may be able to work, but generally speaking, a volume of several hundred picoliter seems safe to perform PCR on miniaturized devices. However, the above discussion represents a conservative estimation of the miniaturization limit for PCR. Even smaller volume of PCR amplifications might be realized if there occur new breakthroughs in the detection or imaging technologies.

Here it has successfully been demonstrated that the reaction volume of PCR amplification can be miniaturized as small as 700 pL with 52 copies/nL *DNA template,* using this microfluidic device. Miniaturization of PCR can not only save expensive reagents dramatically, but also bring up many other benefits including improved sensitivity for each individual reaction (assay).

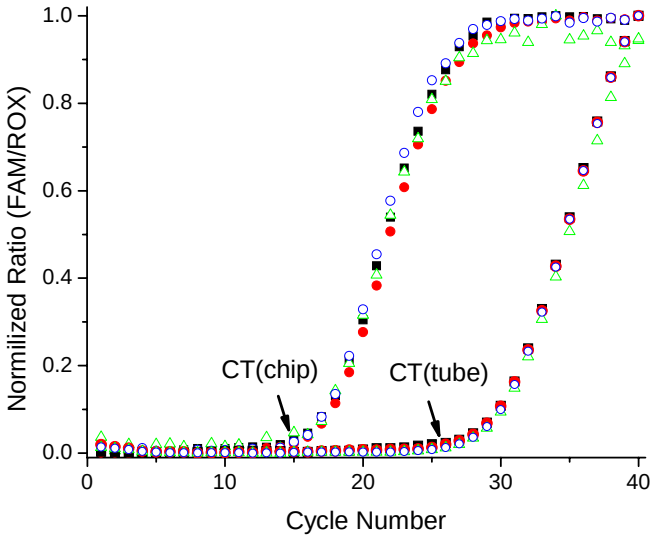

Figure 6: *Real time curves of PCR (with the identical copy number of DNA template) performed in the microchip and conventional microtubes. The volume of individual reactor in the microchip is 10 nanoliter, while the reaction volume using conventional microtube is 20 microliter. The solutions were prepared to include identical concentration of PCR components except for DNA template. For the reactions in the microtube, the concentration of DNA template was diluted by a factor of 2000, which matched the volume difference between the chip reactor and tube. Therefore, it allowed comparison of PCR with the same copy number of DNA template per assay. CT (chip): 15.3±0.4 (standard deviation); CT (tube):26.6±0.5. ΔCT≈11 cycles.* 2^{11}*=2048, which matches the volume difference (fold = 2000) between the tube and the chamber of the chip. Each reaction was performed in the microchip or tube with a repetition of 4 (shown with different colors and shapes). The curves were obtained from different readout system, and normalized for comparison. In these experiments, an isoform of lola gene from fruit fly was amplified. More details of the reaction are describe in the chapter 4.*

As shown in figure 6, performing PCR in the microchip (10 nL/chamber) shows a critical threshold (CT) of 11 cycles earlier than its macroscopic counterpart (20 microliters/tube) with the same copy numbers of DNA template. A single copy of DNA template per reaction (in a view of stochastic effect) can reliably be amplified using microfluidic devices. These phenomena can be explained by the tremendous increase of valid concentration of DNA template after the volume of the reaction is scaled down by several orders of magnitude. On the other hand, there is a noticeable difference in amplification kinetics between the conventional techniques and microchips. As shown as figure 7, chip-based PCR amplifications tend to display steeper increases of fluorescence and reach the plateau area earlier, compared with PCR in conventional tubes. The phenomenon might result from reduced side reactions in microchips. Generally speaking, there are always a low percentage of impure reagents in the actual PCR solutions. The side reactions by the impure reagents could be one of the factors of decreasing efficiency of PCR amplification. Using conventional techniques such as tubes cannot avoid undesired reactions. However, the situation can be quite different when it comes to microchips. Since the volume of individual reactors on the microchip is reduced by several orders of magnitude, there is a very high probability that the individual chamber contains much less or no impure reagents at all. The impure reagents could be out of the reaction chambers or isolated into several individuals without affecting the other separate reactors. Our experiments (figure 7) support that chip-based PCR exhibits more efficient amplifications.

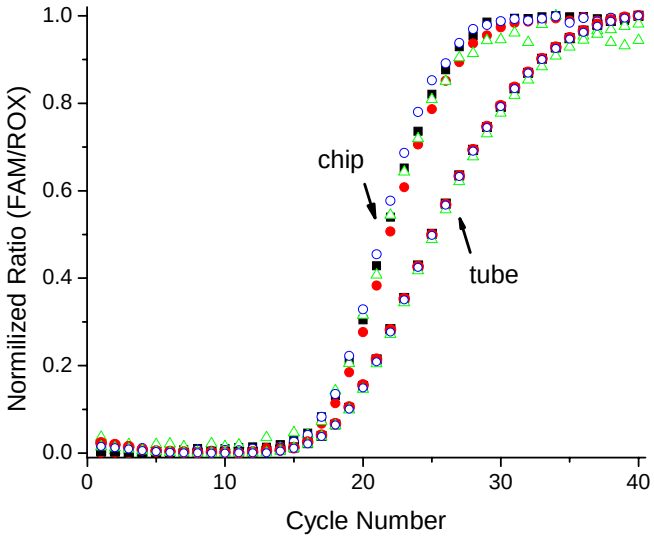

Figure 7: *Comparison of real time PCR curves (with identical concentration of DNA template) in the microchip and conventional microtubes. The same PCR curves as figure 4 from chip-based experiments are displayed for the purpose of comparison. And the experiment conditions were similar to the description of figure 4, except that identical concentration of DNA template (without dilution) was used for tube-based experiments. CT (tube):15.9±0.1. Notice that these two methods of PCR show different features of the plateau effect.*

A "Rotary PCR Device" with Integrated Heaters

Temporal thermocycling usually takes longer in the PCR experiments because of the time spent on temperature ramping. Therefore, we developed a "rotary PCR device" with integrated heaters, using spatial cycling to provide rapid results of PCR experiments[51].

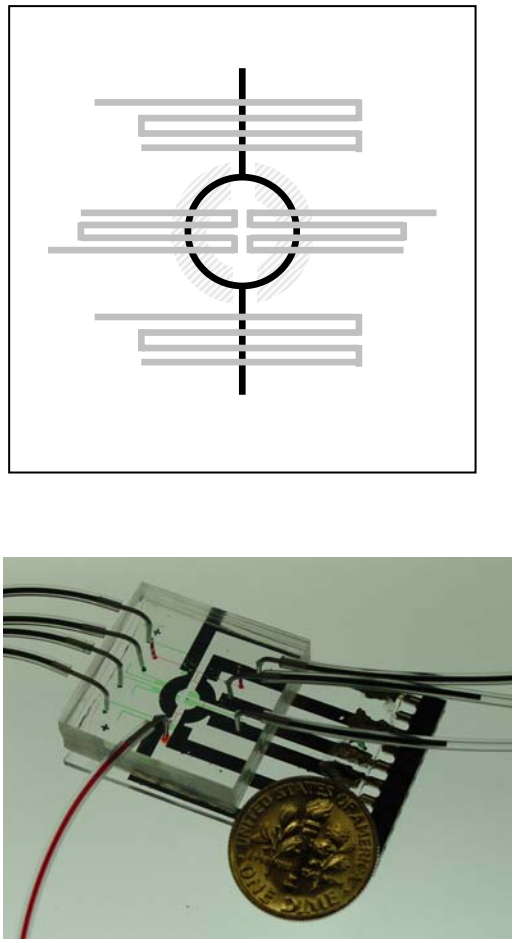

Figure 8: *A PDMS rotary PCR microchip with integrated heaters. Top: schematic. The control channels appear in grey; the fluid channel in black; heaters in grey with fill pattern of upward diagonal. Three heaters arranged in the following order (clockwise from upper right): denaturation, annealing, and extension. In the Taqman PCR experiments, only the heaters for denaturation and extension were used. Bottom: an optical micrograph. The layout of the fluid and control channels are slightly different from the schematic on the top.*

As shown schematically in figure 8, the flow channel is a central loop with an inlet and an outlet; fluid can be circulated in the loop channel using the integrated pump in the control

layer. We have previously shown applications of this rotary pump in mixing and surface binding assays. The volume of the loop channel is approximately 12 nL. The dimensions of the central loop are a radius of 2.5 mm and height of 8.5 μm. The width of the loop channel is asymmetric: 120 μm on the left semicircle; 70 μm on the right semicircle. In such a pattern the fluid velocities in the two parts are different from each other. Therefore, the time that the fluid resides in different temperature zones can be adjusted either by the width of flow channel or the length of the heater.

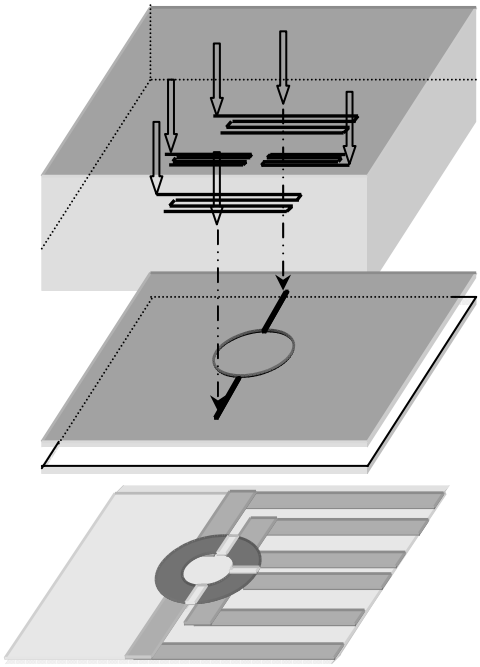

Figure 9: *Assembly of the rotary microchip and the heaters. From the top to the bottom: RTV block with control channels at the bottom surface; thin RTV layer with fluid channel at the bottom surface; glass coverslip; heaters with leads (sputtered onto a glass slide). Arrows indicate the air and fluid through-holes.*

The heaters were made of thin layers of tungsten (heating component) and aluminum (electrical leads) sputtered onto a glass microscope slide (figure 9). Similar to the fabrication of molds as described previously, a negative pattern of photoresist was developed onto a piece of a glass microscope slide (40mm × 26mm × 1.1mm). Then a thin layer (around 500 Angstroms) of tungsten was deposited on the sample by a direct current (DC) sputter system. Acetone was used to remove the remaining photoresist in order to get the designed tungsten pattern. The procedure was repeated in order to sputter another thin layer of aluminum as the electrical leads for the heaters.

Calibration of the microfabricated heaters was performed via a two step process. The heater for denaturation was calibrated with thermochromic liquid crystals (BM/C17-10, Hallcrest Inc.) They belong to a class of organic cholesteric molecules exhibiting an intermediary phase between the solid and liquid states. Within a particular temperature range, these molecules can change colors from red to blue as a function of the surrounding temperatures. Therefore, encapsulated liquid crystal particles with a non-reactive polymer coating can be applied to probe the temperature on the surface or in the fluid. In the experiment of calibration, the "rotary PCR" device was mounted on the slide with microfabricated heaters. Then the particles of liquid crystals were loaded into the fluidic channel of the device. They were imaged at various heater currents with a color camera (KR222, Panasonic) and a stereomicroscope (ASA012-3449, Japan). The temperature response of the TLC was separately calibrated by imaging the device containing TLC particles on the heating block with determined temperatures[53, 54]. Briefly, images of the TLC particles were digitized and average hues of them were calculated, with outliers

discarded. As shown in figure 10, hue and temperature have a fairly linear relationship from 75 to100 ^{o}C, sufficient to determine the denaturing temperature.

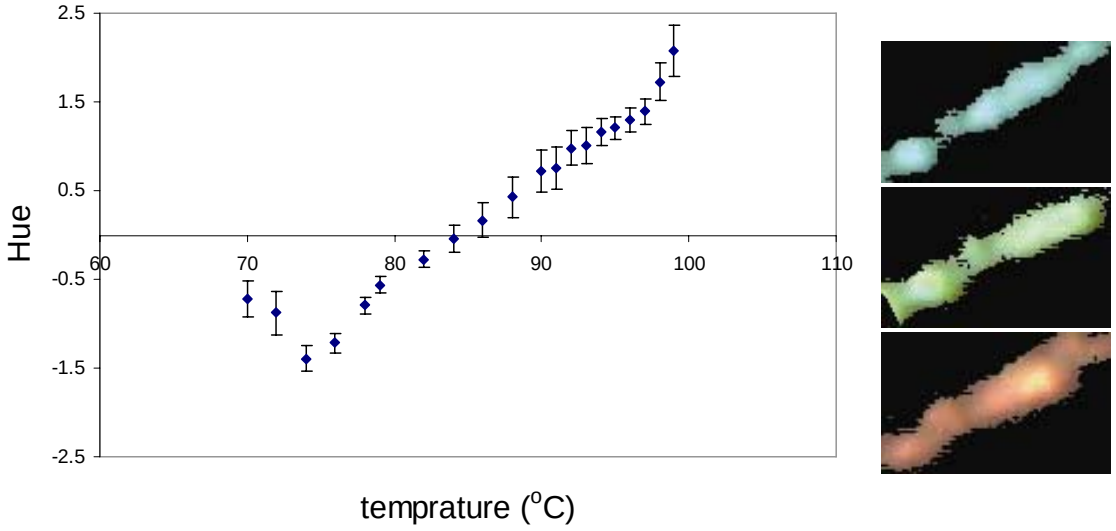

Figure 10: *Calibration of the thermochromic liquid crystal particles (BM/C17-10, Hallcrest Co.) The insets on the right show three representative images of a segment of fluidic channel containing TLC at the following temperatures: Red (76 ^{o}C), Green (86^{o}C), Blue (96 ^{o}C).*

The lower annealing/extension temperatures were calibrated using the thermistors (B05KA103N, Thermometrics, Inc.). They belong to a category of thermistors with negative temperature coefficients (NTC type). Each thermistor must be individually calibrated over the operating temperature range before it can be put into the use. Many approaches of calibration have been developed to meet various requirements in terms of measurement accuracy or operating temperature range. For example, three-point calibration (Steinhart and Hart model) provides a high degree of accuracy (around 0.001 ^{o}C) over a

broad temperature range, while one- or two-point calibration may be limited by a narrow operating temperature range and reduced accuracy[55]. On the other hand, PCR is a robust reaction with a capacity to tolerant inaccuracy of annealing temperature or extension temperature up to several degrees. Therefore, we took the two-point method to calibrate these thermistors. An electrical circuit was connected to measure the output voltage of the thermistor (figure 11), thus allowing calculation of its resistance at the setup temperatures.

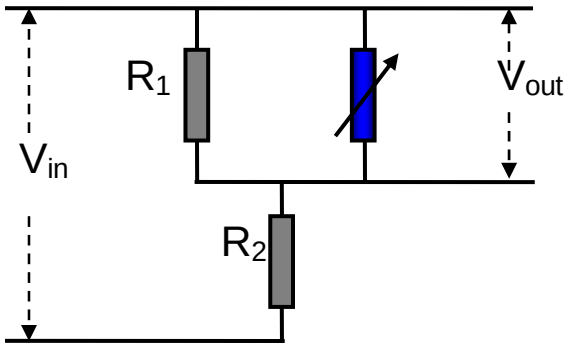

Figure 11: *Schematic drawing of the electrical circuit for calibration or measurement using themistors. The thermistor is represented by the blue. R1 = 0.62 KΩ, R2 = 1.0 KΩ. V_{in} = 5.06 V. In the calibration of the independent thermistors, they were immersed into an oil bath. Then one thermistor was chosen and embedded in a PDMS device for actual temperature measurements.*

The thermistor was immersed into a small vial containing mineral oil, which was subsequently put into a bath of ice and water (H_2O triple point: 273.16 K) for half an hour or more before any measurement. The second of point of calibration was obtained by using

a bath of boiling water (373.15 K). Over a relatively narrow temperature range, the logarithm of the thermistor's resistance is linearly related to its inversed temperature,

$$\ln R/R_0 = \beta_M \left(1/T - 1/T_0\right)$$

The material characteristic is represented by β_M (in Kelvin), which is generally considered temperature independent. However, it varies from thermistor to thermistor because of manufacturing tolerances. Based on two points of data, we calculated the values of individual thermistors (Table 1), therefore obtaining the relationships between their resistances and temperatures.

Table 1. *Material characteristic constant βm and resistance (0 ^oC) of five thermistors*

	β_M (Kelvin)	R_0 ($K\Omega$)
#1	3694	27.54
#2	3544	26.53
#3	3507	25.58
#4	3555	23.11
#5	3177	21.71

The coefficient of variance of β_M among these thermistors was about 5%. The temperature inaccuracy by the two-point method was estimated to be around 2 degrees, although smaller errors can be obtained using a modified method of two-point calibration[55]. For the two-step PCR experiment with the Taqman probe, the denaturing temperature was set at 95

^{o}C, and the annealing temperature at 60 ^{o}C. Two independent resistive heaters were used to heat the microchip to set temperatures. The power consumed by the heaters was around 380mW and 75mW, respectively.

The valves or pumps integrated with the device were actuated using a pneumatic controller supplied by Fluidigm, Inc. The Fluid Controller system allows selective actuation of valves to seal off the loop as well as peristaltic pumping at variable rates within the loop. Typical actuation pressures were around 12 psi; the pumping frequency was 20 Hz. During operation of the rotary pump, the sample liquid is transported around the loop at an average rate of 2 or 3 revolutions per minute. In the chip's control layer, we initially used three separate valves to peristaltically pump the fluid[14, 56]. Then we found that one S-shaped channel could accomplish the same peristaltic pumping as three separate channels. In addition, the S-shaped channels provide more secure closing of the inlet and outlet than a single channel.

The fluid motion in the channel was characterized by using a solution of 2.5 μm beads. In order to mimic the actual conditions of the experiments, we used the same concentration of PCR buffer in the bead solution. At room temperature, the speed of beads was about 3.4 mm/second in the narrow channel and 1.5mm/second in the wide channel. However, the velocity was slowed down when the device was run at its operating temperatures, resulting in about 20 or 30 second per full cycle (by estimation). The reason of the decrease in velocity might result from the thermal expansion of RTV or small bubbles in the liquid after heating.

PCR Amplification with Spatial Cycling or Temporal Cycling

There are two different modes available for the use of the "rotary PCR device" in terms of temperature cycling, including a spatial approach and a temporal one. In the spatial cycling mode, the reagent mixture for PCR was loaded into the loop channel through the inlet hole. Then the valves controlling the inlet and outlet were actuated with hydraulic pressure to form a closed loop for the reaction. The rotary pump was actuated in order to circulate the solution around the loop. Therefore, the reagent solution repeated flowing through the desired temperature zones provided by the tungsten heaters. A segment of the loop channel, which was not shaded by the heaters, was monitored with the fluorescence microscope (IX50, Olympus, objective 20×, NA 0.5). The filters (Chroma) in the fluorescence microscope were chosen as follows: Exciter, HQ 470/40x; Dichroic, Q 495LP; Emitter, HQ 525/50m. A cooled CCD camera (ST-7, Santa Barbara Instruments Group) was used to acquire fluorescent images (figure 12) of the specified channel segment every few minutes during the PCR. The images were analyzed with the CCDOPS (SBIG) software in the following way: in each picture, three squares (25 pixels on a side) inside the fluid channel were chosen to get an average value of the fluorescence intensity. Similarly, three squares outside the channel were selected to make another average value as the background of this picture. The latter value was subtracted from the former to obtain the fluorescence of the solution inside the fluid channel.

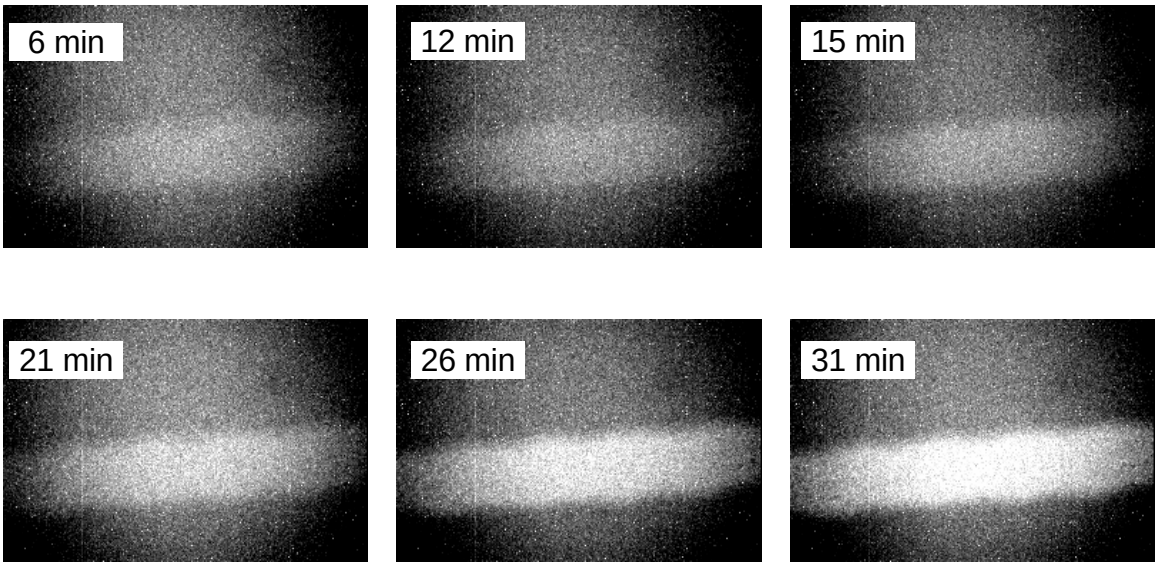

Figure 12: *Snapshot images of the rotary PCR device (one segment of the fluidic channel) during spatial thermocycling. Camera: SBIG Model ST-7; Microscope: Olympus IX50. Objective: 20X. Width of the flow channel: 70 μ.*

The rotary PCR device was tested with the spatial cycling mode to amplify a segment of the human β-actin gene. The preparation of the sample and reagent mixture was similar to previous descriptions. After the sample solution was circulated in the loop channel and the temperature was cycled for about 15 minutes, the fluorescent intensity of the solution started a rapid increase (figure 12 and figure 13). When the sample solution was spatially thermocycled for about 30 minutes, there was an increase of more than fourfold in fluorescence intensity in the present of DNA template, while the no-template control remained flat (except for small fluctuations) all the time. This was consistent with the features of macroscopic real-time PCR. As experiments of calibration, we loaded the PCR products from amplification with conventional bench-top techniques into the flow channel

of the devices, and then imaged the fluorescence of the channels. These experiments showed that the recorded increase in fluorescence from amplification on the chip was comparable to that of 30 to 35 cycles of PCR product by a bench-top PCR machine (PTC200 Peltier Thermal Cycler, MJ Research).

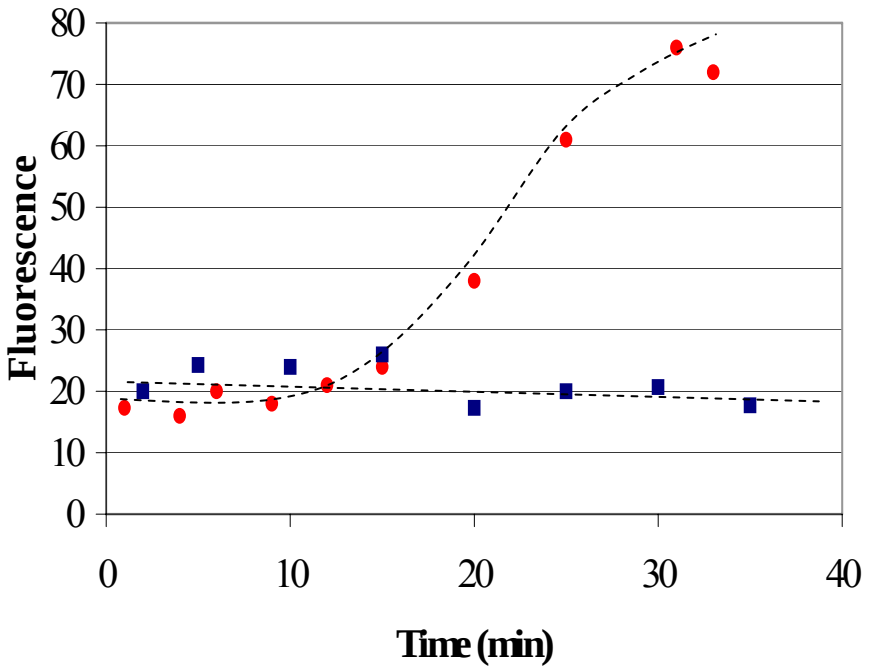

Figure 13: *Fluorescence increase in spatially cycled Taqman assay performed on the rotary-chip. Fluorescence was monitored in the channel with the camera during the process of amplification (human beta-actin gene). Red dot: sample; blue square: no template control. The dashed curves are a guide for the eye.*

We also used our microchips to perform a three-step PCR reaction in which we directly monitored the creation of amplification product using intercalating dye molecules of SYBR Green I (Molecular Probes). A segment (199 bp) of λ phage DNA was selected for

amplification; forward primer and reverse primer were the following: 5'-GGT TAT CGA AAT CAG CCA CAG CGC C-3' and 5'-GGA TAC GTC TGA ACT GGT CAC-3', respectively. The temperatures were set as follows: 94 ^{o}C for denaturation, 55 ^{o}C for annealing; and 72 ^{o}C for extension. figure 14A shows the fluorescence difference before and after PCR, indicating that amplification occurs relative to the no-template control. Our design of spatial cycling provides a compact format to thermocycle the sample solution. This method reduces the time of temperature ramping to a minimum level, therefore providing a rapid result of the PCR experiment. The device allows dynamically loading fresh solutions of the reagents into the central loop via the inlet. For example, additional polymerase can be introduced into the reaction to maintain the enzyme activity level during thermocycling; water can be loaded to compensate for dehydration due to evaporation. In addition, it is optional to withdraw a portion of the circulating solution via the outlet for time course studies if necessary.

Then the device was tested to amplify the segment of λ phage DNA using the more conventional temporally cycled mode. In this experiment, after the sample solution was loaded into the microchip, we sealed off the inlet and outlet of the flow channel by actuating the valves. Afterwards, we did not pump the solution to flow in the loop channel; instead, the whole device was manually thermocycled using the tungsten heaters. The heaters were adjusted to identical temperatures so that the contents of the device were uniformly heated; the temperature steps were as follows: 15 seconds at 94 ^{o}C; 30 seconds at 55 ^{o}C; 30 seconds at 72 ^{o}C. 23 cycles were conducted in the experiment. The change of fluorescence during PCR was monitored by the same optical setup every few cycles. The

increased fluorescence over the time suggested a successful amplification of DNA template within the microchip using the method of temporal cycling (figure 14B).

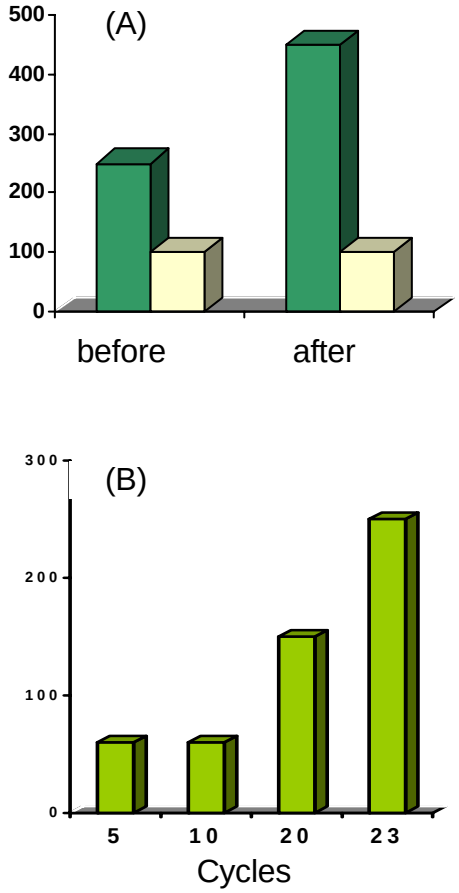

Figure 14: *Three-step PCR. A segment of λ DNA was amplified; the creation of product was monitored directly with the use of the intercalation dye Sybr Green 1. Top (A): Spatial cycling. The reagents were pumped through three different temperature zones: denaturing (94 ^{o}C), annealing (55 ^{o}C), and extension (72 ^{o}C). The graph shows fluorescence intensity (AU) measured in the channel before and after 40 minutes of pumping. Dark: PCR process with DNA template. White: negative control without template. Bottom (B): Temporal cycling. The entire loop chamber was heated to the designed temperature simultaneously.*

This temperature was manually ramped between the designed temperatures of denaturing, annealing and extension.

Each temperature cycle with this temporal approach took about 6 minutes, which was slower than the spatial thermocycling mode. Compared with conventional techniques of temporal thermocycling, smaller volume of reagents per assay is the benefit of using the rotary microchip. The loop channel of the rotary device consumes only about 12 nL of the sample solution. Previously we have demonstrated that miniaturized PCR can be performed in a volume as small as 700 pL with the device containing a series of reaction chambers. Combining these facts, it is apparent that the microfluidics devices would become a promising platform in order to reduce the consumption of reagents. However, at present the minimum sample volume required to be loaded is mainly limited by the amount that can be loaded on the chip using conventional macroscopic tools, for example, by pipetting. These tools can handle the liquid in the order of 1 or 2 μl. The mismatch of the volumes is huge between macroscopic tools and microfluidic devices. A solution to this conundrum will be presented in Chapter 3.

Concluding Remarks

We have demonstrated successful nucleic acid amplifications by miniaturizing PCR on microfluidic devices. A device containing a series of reaction chambers of different volumes has been tested, showing that the volume of PCR may be reduced as low as 700 pL or even less. Performing the reactions in small volume provides many advantages, compared with conventional bench-top techniques. These benefits include saving the

reagents, improving the sensitivity per assay, and being compatible with the requirement of highly parallel processing. In addition, a rotary microfluidic device has been developed to perform PCR in a compact format with optional modes of spatial cycling or temporal cycling. This microchip consumes only 12 nL of reagent mixture, realizing nucleic acid amplification with integrated heaters. For both devices as above, the microfabricated structures, including channels, chambers, and integrated valves or pumps, should allow a high degree of future integration. The PDMS microchips are disposable, reducing the chances of cross-contamination during the reaction procedure.

The microfluidic devices that we have developed are compatible with many other assays for genetic analysis, including restriction digests of nucleic acids and SNP analyses[57, 58]. For example, the invader DNA assays take use of a cascade of cleaving events of oligo probes to recognize a specific nucleic acid target. They allow identification of a single nucleotide mutation of the DNA molecule with amplified fluorescent signals[59]. Our microfluidic devices provide a flexible platform to perform these assays. Miniaturization of the assays on the chip would dramatically reduce the consumption of the expensive reagents such as enzymes or fluorescent probes, providing a cost-effective method to apply them for genetic diagnostics. Overall, the microfluidic devices should be able to find a wide range of applications in rapid medical diagnostics, food control testing, and biological weapons detection.

Finally, we wish to point out a possible future application enabled by the unique geometry of the rotary device. Since it is possible to modify the surface chemistry of the channels,

and indeed to specifically attach proteins, one could conceivably immobilize DNA polymerase in the extension region of the chip. Then in the spatially cycling mode, the enzyme is kept at a constant temperature and in particular is not exposed to the denaturing temperature. This is significant because a tremendous amount of effort has been spent on developing DNA polymerases that are both thermostable and of high fidelity, at the expense of other desired qualities, such as turnover rate. By relaxing the thermostability requirement, one could perform efficient PCR with enzymes from non-thermophilic organisms that have been optimized for other parameters, such as fidelity and speed. Thus this particular format of the PCR may allow a number of enzymological advances to play a role in future nucleic acid amplification technology.

C h a p t e r 3

MICROFLUIDIC MATRIX: INTERFACING "WORLD-TO-CHIP"

Introduction and Motivations

Microfluidic technology offers many possible benefits in chemistry, biology and medicine[60-63], not least of which is to automate rote work while reducing the consumption of expensive reagents to the nanoliter or subnanoliter scale. For example, Hadd et al. developed a microchip for performing automated enzyme assays, in which precise concentrations of substrate, enzyme, and inhibitor were mixed in nanoliter volumes using electrokinetic flow[64]. Fu et al. reported an integrated cell sorter with a 1 picoliter minimum active volume by the actuated valve.[65] However, since microfluidic devices must at some point be interfaced to the macroscopic world [66] there is a minimum practical volume (at the scale of 1 μl) that can be introduced into a device. The so-called world-to-chip interface problem[67] has plagued the microfluidic field since its inception: it is questionable how the desired economies of scale in microfluidics can be practically achieved unless an effective approach is developed to solve the mismatch between those two scales of volume.[68] Although integrated glass capillaries have been used to reduce sample consumption for simple titrations between two reagents, these devices are fundamentally serial and have the possibility of sample cross-contamination during the loading process.[66, 69, 70] On the other hand, there has been an effort to develop techniques to concentrate analytes from a large input volume with techniques such as microfluidic isoelectric focusing (IEF) [71] and

temperature gradient focusing (TGF),[68] but only a limited species of samples have successfully been demonstrated so far.

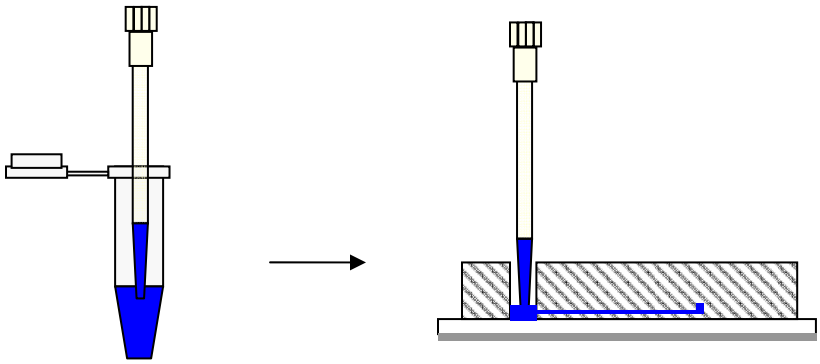

Figure 1: *Schematic of the process of loading the sample solution from the microtube to the inlet of the microchip. Notice that the volume mismatch is up to three orders of magnitude or more between the macroscopic vials and the micro reactors on the chip. Typical bench-top facilities such as microtubes or microplates deal with liquid reagents in the volume of dozens of microliters. Pipets can reliably dispense the solution on the scale of microliters. The volume of the inlets of microchips is approximately one microliter or more. However, the volume of individual reactors in the microchip is three or four orders of magnitude less, on the scale of nano or subnano liters. In the diagram these volumes are not drawn to scale. In the actual experiment, reagents are generally loaded into the reactors of the microchip by applying pneumatic pressure at the end of the pipet tip or the steel syringe tip. An alternative option is available by applying pressure on all the loaded input holes simultaneously with a customized cover. This option provides ease of compatibility with conventional liquid handling systems of high-throughput performance.*

The challenge associated with realizing the desired economies of scale in microfluidic devices is to simultaneously reduce the number of pipetting steps needed to load the devices, while amortizing the sample volume from each pipetting step over a large number of independent assays. Microfluidic matrix geometries offer the advantage of performing N^2 independent reactions with only $2N$ pipetting steps;[72] N=2 matrices have been used for chemical synthesis[73] and N=5 passive matrices have been used to demonstrate two-component biochemical assays such as optical detection of enzymatic activity[74]. However, in those devices the reagent consumption scaled only with N, which was so small that there was little practical savings. Passive devices also have technical limitations in sample metering [73] and device operation. For example, precise pressure balancing was required during operation, and the kinetics of mixing were limited due to the static nature in the devices.[74]

This chapter presents the development of microfluidic devices with the geometry of matrix in order to solve the "world-to-chip" interface problem[75]. These devices are designed to have different sizes of matrix, including 4 × 2 arrays, 10 × 10 arrays, and 20 × 20 arrays. They integrate a number of valves (up to thousands in the 20 × 20 matrix chip), allowing more complex three-component reactions to be studied. Variations in the chip design provide two options to mix the reaction components inside individual micro-reactors. These include passive diffusion, or active circulation of the solutions. Two representative devices are described in this chapter, including a 4 × 2 matrix chip with diffusion-controlled mixing, and a 20 × 20 matrix chip with active mixing. The devices scale the savings of the most precious reagent by N^2 (or $N \times M$). Take the 20 × 20 matrix chip for

instance. N^2 = 400 distinct PCR reactions can be performed with only $2N$+1 = 41 pipetting steps, consuming only a single 2 μl aliquot of DNA polymerase that was distributed over all 400 independent reactions. Performing the same set of reactions by hand or with a robot would require orders of magnitude more reagents and $3N^2$ = 1,200 pipetting steps, each of which introduces the possibility of mistake or cross-contamination.[76] Our approach has simultaneously achieved two important goals in solving the macro/micro interface problem that has thus far limited the impact of microfluidic technology. The matrix device that we developed has an immediate application in medical diagnosis and gene testing by performing biological and chemical assays in a combinatorial manner.

4 × 2 Matrix Chip with Diffusion-Controlled Mixing

The matrix chip was made by sealing a PDMS device composed of a control layer (top) and a flow layer (middle) onto the glass coverslip (bottom). A routine procedure of fabrication was followed to prepare the molds and 2-layer PDMS devices. The protocols using multilayer soft lithography (MSL) have been previously described.[65, 77, 78] Eight identical reactors (4 × 2 arrays) are displayed in the schematic drawing of the device (figure.2). These reactors are the flow channels partitioned by the control channels. Four independent input holes (blue) are available to address the reactors in rows, with another four independent holes as outputs. The reactors are also accessible in columns through another set of independent input or output holes (red). A single input or output hole (yellow) is connected to all the reactors. This feature of design allows loading the most

expensive reagent through one input hole and simultaneously amortizing it over all the reactors to perform distinct assays, therefore saving the reagent and reducing pipetting operations. The matrix chip with small arrays (4 × 2) was designed and tested for the purpose of proof of principle. The matrix chip with larger arrays, for example, 20 × 20 arrays as demonstrated subsequently, can facilitate saving the reagents in a more economic scale and reducing the number of pipetting steps dramatically.

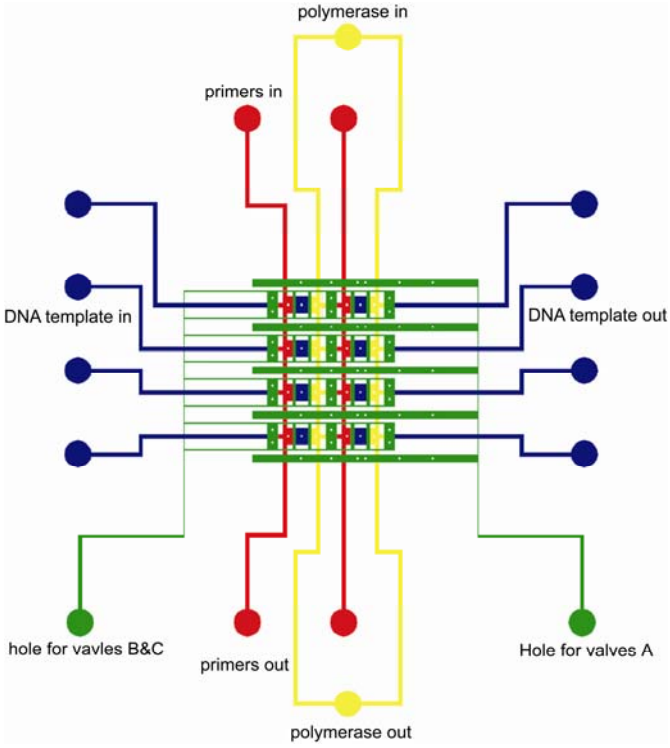

Figure 2: *Schematic diagram of the matrix chip (4 × 2 arrays). In this design, mixing of reagents is performed in a diffusion-controlled manner. Colors are coded to indicate control lines (green), primers (red), template sample (blue), DNA polymerase (yellow).* $V_{primers}$ *:* $V_{template}$*:* $V_{polymerase}$*: ≈ 5:4:5. The volume of individual reactors is approximately 4.1 nanoliter.*

The valve system in the control layer essentially consists of two sets of independent valves, marked with the color of green in the schematic drawings of figure 2 and figure 3. One set of valves (A, 220 μ wide) are designed to isolate individual reactors in the same column from each other. The other set of valves include parallel large valves (B, 270 μ wide) and small valves (C, 96 μ wide), arranged in multiple rows.

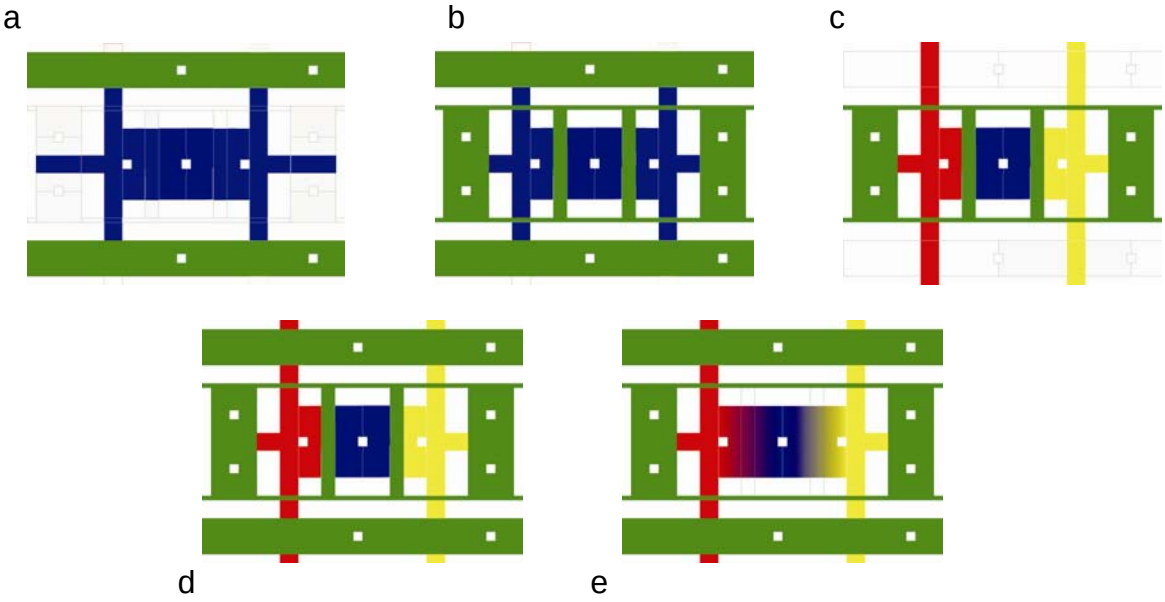

Figure 3: *Schematic diagrams of valve operations for loading the reagents into the matrix chip (4 × 2 arrays) in a sequential order. The code of colors is consistent with figure 2. figure 3(a): Actuation of valves A allows DNA template to be loaded into the micro reactor. 3(b): Actuation of large valves B and small valves C isolates the solution into the three compartments. 3(c): Primers and DNA polymerase are loaded into the chip after valves A are open, flushing the extra solution of DNA template to the waste. 3(d): Actuation of valves A again isolates primers and DNA polymerase into the desired compartments. 3(e): Small valves C are selectively open, allowing the three components to mix by diffusion. Note: In the control layer, the narrow channels (42 μ wide) connecting valves cannot*

switch off the flow channels. Micro posts (white squares) are designed to prevent collapse of channels or chambers.

The program of loading reagents starts with actuation of the first valve set (A). Then the solutions containing the component (blue, either DNA template or no-template control) of PCR assays can be loaded into each row of reactors (figure 3a). Actuation of the second valve set (B and C) partitions the loaded solutions in each compartment (figure 3b). Valves A are then opened to allow for the loading of primers (red) down each column while DNA polymerase (yellow) is simultaneously introduced to all reactors from a single inlet. Loading primers and DNA polymerase flushes the extra solutions of DNA template to the waste (figure 3c). But the solutions of DNA template isolated in the central compartments by small valves (C) are left intact in a well-defined volume. Afterwards, valves A are once again actuated, defining the desired volumes of primers and polymerase and isolating each reactor (figure 3d). Large valves (B) differ from small valves (C) in terms of the membrane area, requiring relatively lower threshold pressure to actuate. Thus, adjusting the pressure allows selectively switching on the small valves, while keeping large valves closed. Then inside individual reactors, the components may be mixed by passive diffusion (figure 3e). It is noteworthy that these valve operations are performed in a parallel fashion over the reactor arrays in the matrix chip. In total only two holes in the control layer are required to connect the pressure source.

The matrix chip allows distinct combinations of DNA templates and primers tested in individual reactors with DAN polymerase loaded from a single input hole. A matrix chip of 4 × 2 arrays was tested to amplify a 294 bp segment of the human β-Actin cDNA fragment

(1.8 K bp, Clontech). Forward primer, reverse primer, and Taqman probe were the same as before (see Appendix A). An amplification protocol supplied by Applied Biosystems (http://www.appliedbiosystems.com) was modified to include the use of DyNAzyme II (Finnzymes OY) and a cocktail of additives [52]. The solutions loaded onto the chip were prepared with one component of the template, primers or polymerase, and all other necessary PCR reagents and additives. The pattern of PCR assays was arranged to perform 4 reactions with the cDNA template, and the other 4 reactions of no-template control.

The chip was mounted onto the surface of a flatbed heating block of a thermocycler (PTC-200, MJ research). Mineral oil was used to increase the thermal contact between the glass substrate of the chip and the surface of the heating block. All the reactors in the chip were isolated by the hydraulic control channels, which reduced the evaporation of the reagents in the fluidic channels to a negligible level. The PCR conditions were verified with conventional methods to show that there are no detectable side products from the non-hot start condition. The whole chip was thermocycled: 2 minutes at 50 ^{o}C, and 1 minute at 96 ^{o}C; then 30 cycles: 20 seconds at 96 ^{o}C; 40 seconds at 60 ^{o}C. Including the thermocycler's ramp times, the total thermocycling time was approximately one hour. Then the chip was removed from the heating block, followed by a cleanup of the glass substrate with acetone, ethanol, and napkin. The chip was mounted onto the stage of a microscope (TC200, Nikon). Individual reactors were imaged using an objective (20X, NA 0.5) and a cooled CCD camera (ST-7, Santa Barbara Instruments Group) for fluorescent measurement. The field view of the CCD camera allowed imaging only a part (about 1/4) of each reactor of

the chip (figure 4). But the fluorescent intensities of different parts of the same reactor were generally comparable to each other.

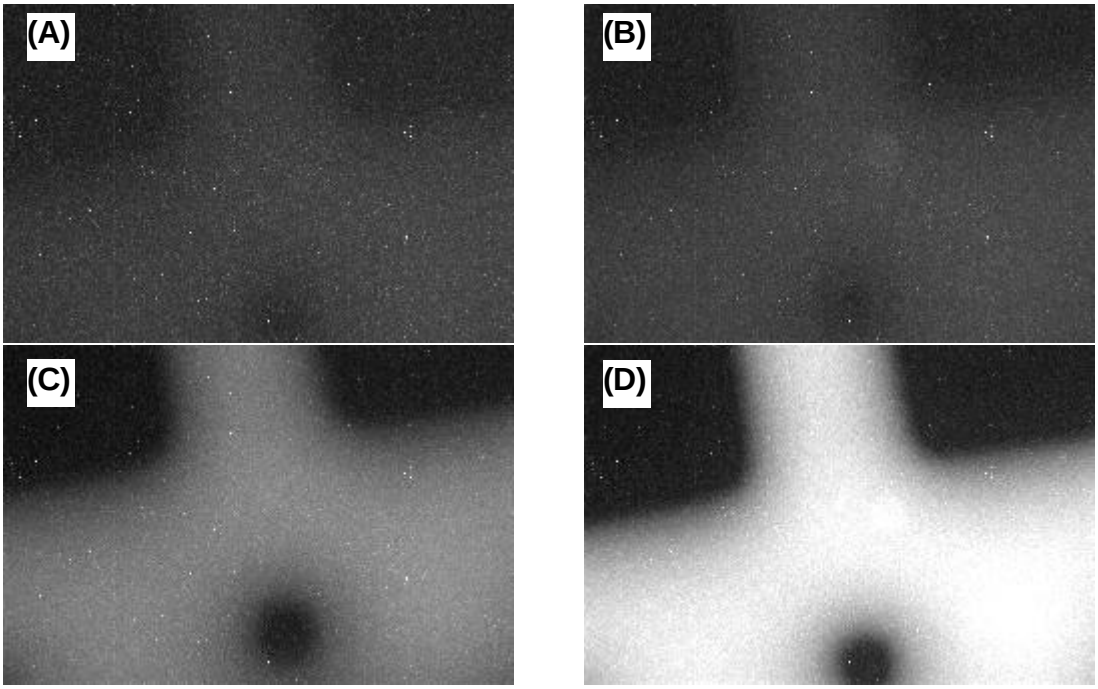

Figure 4: *Performing PCR on the matrix chip (4 × 2 arrays). There was apparent difference of fluorescent intensity between the reactors with DNA template (D) and the negative control (C). The images of (A) and (B) were taken before thermocycling; (C) and (D) were end-point measurements after thermocycling. The images of (B) and (D) show the same part of a reactor loaded with DNA template; while (A) and (C) are respectively their counterparts without DNA template (negative control). The reactor of negative control shows a slight increase in fluorescence, indicating contamination of the DNA template.*

The reactors containing cDNA template show a significant increase in fluorescent intensity at 519 nm after thermocycling, compared with the reactors of no-template control (figure 4 and figure 5). The experiment result supports the idea of the matrix chip, which tests the

DNA samples and primers combinatorially, while only requiring the most expensive reagent (DNA polymerase) loaded through a single input hole. However, the mixing of components is controlled by diffusion in this design, which requires more time to set up the reactions than active mixing. In addition, we observed a slight increase of fluorescence (519 nm) in the reactors of negative control, indicating a problem of contamination with DNA template.

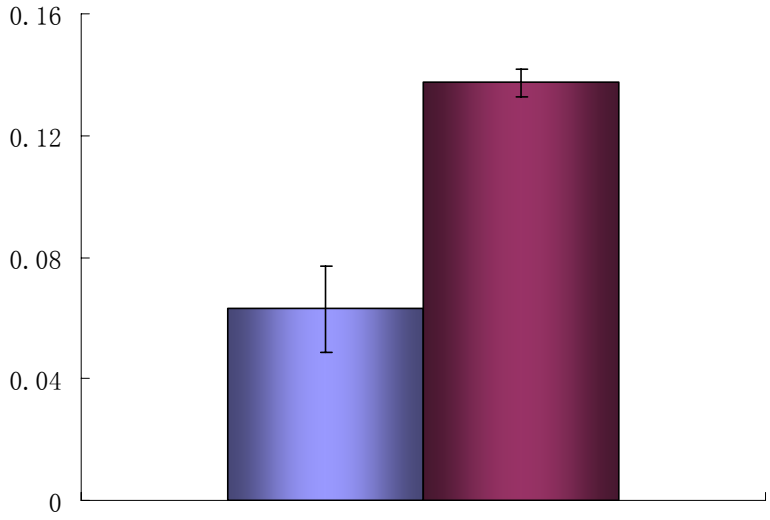

Figure 5: *Averaged ratio of fluorescent intensity at 519 nm/570 nm, after performing PCR reactions in the matrix chip (4 × 2 arrays). Red: 4 reactors loaded with DNA template; blue: the other 4 reactors without DNA template (negative control). Error bars are shown as standard deviation. The passive reference is measured at 570 nm.*

This problem may be explained by the particular sequence of loading reagents, as discussed as follows. In the experiment, the solutions containing cDNA or no-template control were loaded and then isolated into the central compartments (blue, figure 3C) of individual

reactors. Then the extra solution of cDNA template in each reactor was flushed down to waste by loading the other two components: primers and DNA polymerase. This sequence is optimal for mixing reagents by diffusion because of its spatial arrangement of the components in each reactor: cDNA template located in the center, while primers and polymerase in the surroundings (figure 6).

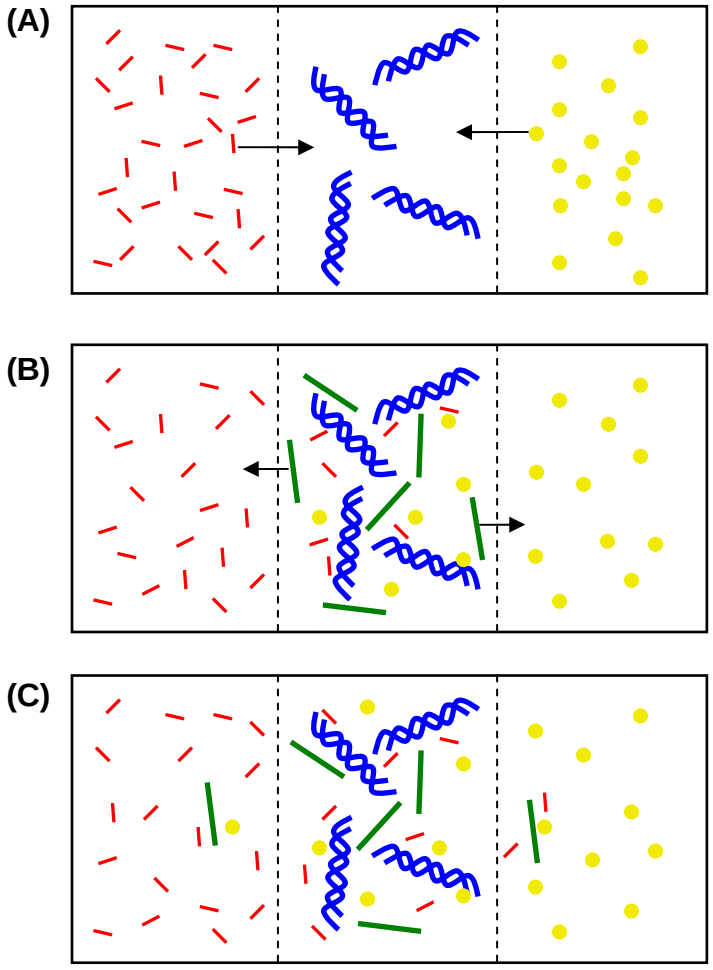

Figure 6: *Schematic diagrams of the mixing of the three components for PCR by diffusion. DNA template (blue helix), primer (red short line), DNA polymerase (yellow dot), amplicon (green long line). The whole rectangle represents a micro reactor on the*

matrix chip (4 × 2), which is partitioned into three compartments by the dashed lines. figure 6(A): primers and DNA polymerase diffuse into the central compartment, where the slowest component (DNA template) is located. figure 6(B): amplicons of PCR in the central compartment diffuse more quickly than DNA template. figure 6(C): PCR amplification is available in the surrounding compartments.

The lengths of cDNA template are typically around several thousand base pairs (the diffusion coefficient is at the scale of 10^{-8} cm^2/s), while those of gDNA can be several orders of magnitude more. DNA template has the smallest mobility by diffusion, compared with the other two components of primers (10^{-6} cm^2/s) and DNA polymerase (10^{-7} cm^2/s). Therefore, the designed locations as described as above allow an optimal combination of mobilities of these three components under the circumstance of passive diffusion. Additionally, once the amplification begins, the amplicons (only several hundred base pairs) of PCR have a better chance to diffuse all over the reactor than the original cDNA template, which is helpful for PCR in the surrounding compartments (figure 6C). On the contrary, it will become more difficult to mix the components of PCR and start amplification if DNA template is initially loaded to the compartment on either side. However, this loading scheme allows DNA template eventually flowing through one reactor to another in the same column. It may cause contamination in the downstream reactors since PCR is very sensitive to any trace amount of DNA template. This problem can be solved by the matrix chip with active mixing in the subsequent development.

20 × 20 Matrix Chip with Active Mixing

The new matrix chip keeps the essential features of the previous version of 4 × 2 arrays. But there are also considerable changes in the design. As shown in figure 7 and the schematic layout of figure 8, the chip is composed of glass substrate and three PDMS layers with distinct functions: a matrix flow channel structure sandwiched between two layers with integrated hydraulic valves (green) and pneumatic pumps (white). In the fluidic layer (middle), channels are approximately 106 μm wide and 12 μm high. Each vertex of the matrix contains a ring shaped channel (reactor) of approximate 3 nanoliter. Each row of reactors is connected to a separate input hole (about 625 μm in diameter) through which unique primers may be loaded. Each column can similarly load the reactors with different DNA templates. A single input for the addition of polymerase is connected to all the reactors in the matrix. In the control layer (top, green), the valve system is designed to load each reactor with the three separate reagents while preventing cross contamination. In total, 2860 valves displayed horizontally or vertically are controlled by only 2 independent pressure supply through-holes. The large valves (B in the inset of figure 1, 270 μm wide) or the small valves (C, 96 μm wide) can selectively be actuated because they have a different threshold of the hydraulic pressure.[77,17] Reagent loading is not blocked by the narrow control channels (42 μm wide) connecting the valve system because their tiny membrane does not deflect at the actuation pressure used.[77] The third layer uses a 20 × 20 array of rotary pumps (bottom) in order to facilitate mixing the reagents.[79,80] Its layout has been simplified from a previous version (shown in figure 9) to the current design.[81]

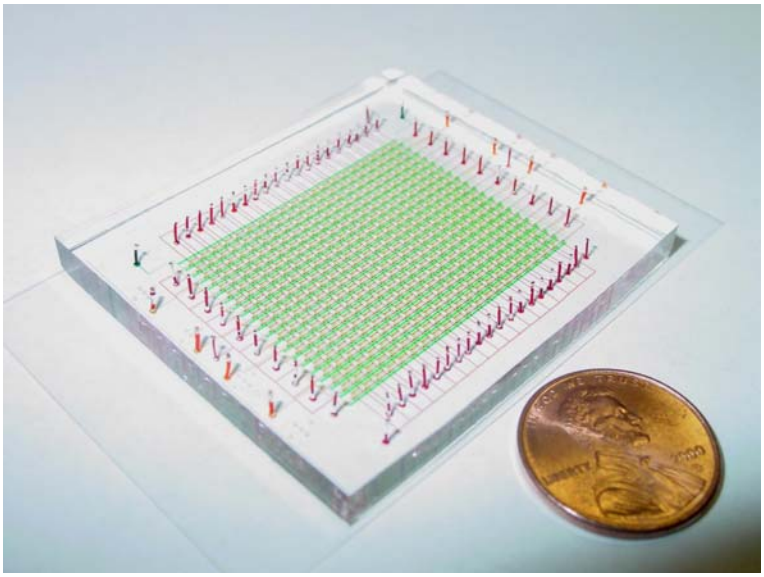

Figure 7: *Optical micrographs of the matrix device (20 × 20 arrays) with the design of active mixing.*

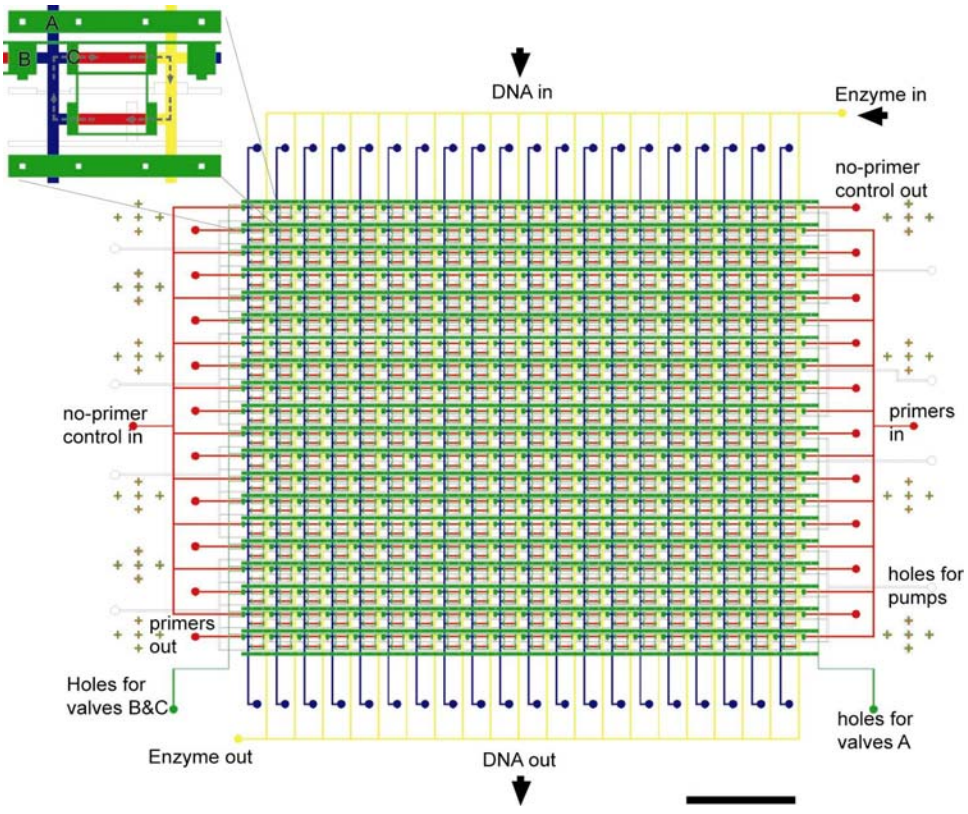

Figure 8: *Schematic diagram of the matrix chip (20 × 20 array) shows the various input, output and control ports. Inset: a single reactor which is color coded to indicate control lines (green), template sample (blue), DNA polymerase (yellow), primers (red), and rotary pump (white).* $V_{template}$:$V_{polymerase}$:$V_{primers}$ *= 3:3:4. Scale bar, 6.4 mm.*

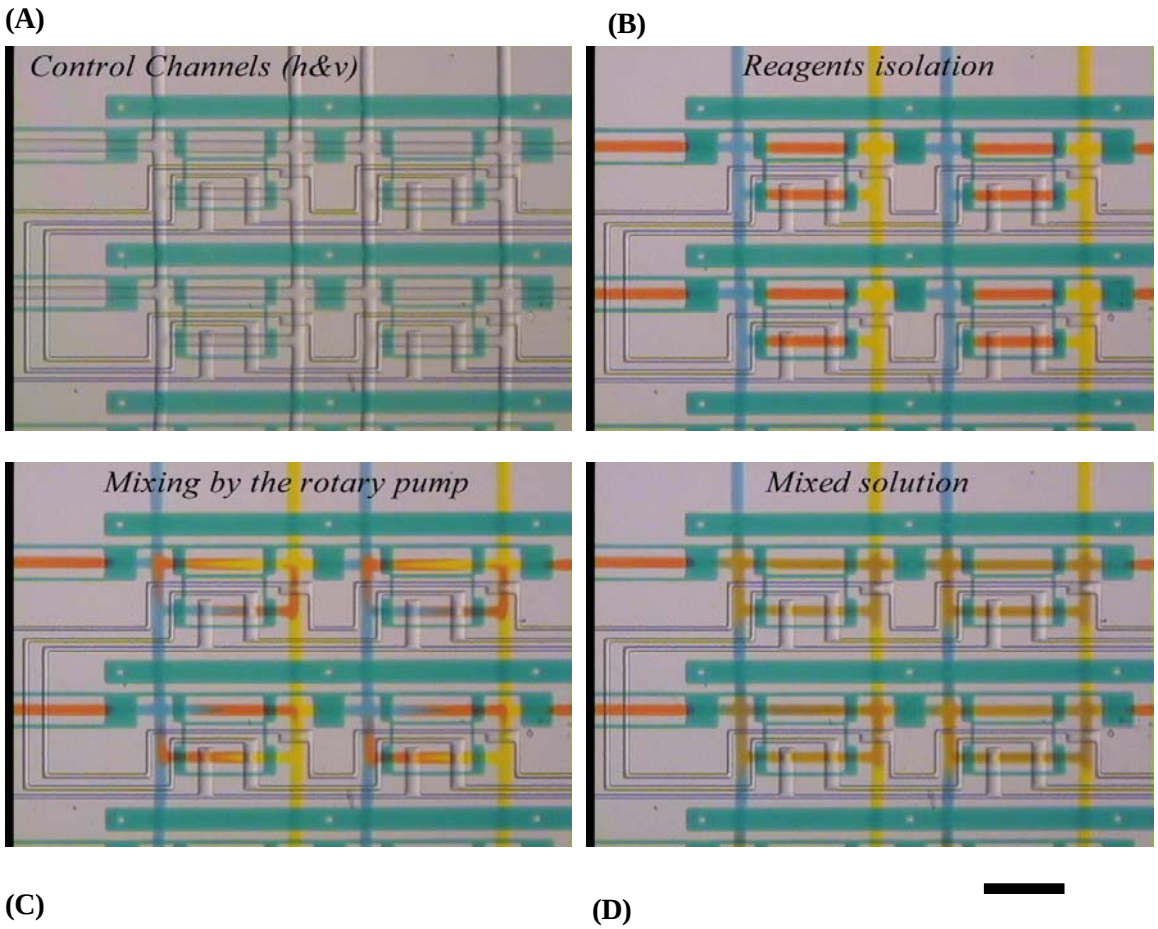

Figure 9: *Set of optical micrographs illustrating the isolation and active mixing of different dye solutions. Four reactors are imaged. (A) The "dead-end" control channels are filled in with the green dye solution. It is feasible because PDMS is gas-permeable. (B) Different dye solutions are isolated into volume-defined compartments of the individual reactor. (C) The parabolic profile of the Poisueille flow stretches the*

interfaces of the reagents along the loop channel, producing long and thin interlaced steams which quickly mix by diffusion (shown here with food dye). Because of the valve ordering, the solutions are moving counter-clockwise in the first row of reactors, while clockwise in the second row. (D) The color-mixed solution results from the rotary pumping for half a minute. A video of the loading and mixing sequence with food dye is available at http://thebigone.stanford.edu/quake/matrix. Scale bar, 600 μm.

Regarding fabrication of the 20 × 20 matrix chip, here we only specify the necessary modification to produce the three-layer elastomeric devices. Three separate molds for the different layers were prepared with UV-lithography. The photoresist (Shipley SJR5740) line height was 12 μm on the fluidic layer mold or the pump layer mold; while the control layer mold had higher lines of 25 μm, which prevents collapse of the thin elastomeric membrane of the fluidic layer. To fabricate the control layer, General Electric RTV 615 A and B components were mixed in a 4:1 ratio using a Keyence Hybrid mixer. Then the mixture was poured onto the control layer mold in a foil-coated petri dish and baked in the oven at 80 ^{o}C for 30 minutes to obtain a thick PDMS block (3 or 4 mm). At the same time, a 25 μm thick elastomeric layer with a 20:1 ratio was spin-coated on the fluidic layer mold at 1600 RPM for 65 seconds, then cured at 80 ^{o}C for 35 minutes. After incubation, the control layer was peeled from the mold and punched with through-holes for pressure connection. It was aligned on the thin fluidic layer and then baked at 80 ^{o}C for 45 minutes. Meanwhile, a third pump layer was spin-coated with the RTV615 mixture (20:1) at 2200 RPM for 65 seconds, and then incubated at 80 ^{o}C for 45 minutes. Next, the bonded device containing the former two layers was peeled and through-holes were punched for loading

fluidic samples. It was aligned onto the third pump layer and baked at 80 ^{o}C overnight. Then the rest through-holes were punched on the device for air injection in pumping. After that, the three-layer device was sealed with a piece of glass coverslip (#1, Lakeside microscope accessories) and incubated at 80 ^{o}C for no less than 3 hours.

Reagents can be loaded into the 20 × 20 matrix chip by manipulating the valve system in a similar manner as described previously. The spatial arrangement of reagents in each reactor is changed purposely to reduce the problem of contamination. Since mixing efficiency of reagents is not limited by passive diffusion in the new matrix chip, it becomes a more flexible platform to load any component into the desired compartment. Here primers are loaded into the central compartments of the ring-shaped reactor, while DNA template and polymerase are loaded into the remaining compartments of each reactor. This new loading scheme requires flushing the extra solution of primers through downstream reactors to the waste. Since PCR is not sensitive to small amounts of undesirable primers, the problem of contamination by the loading scheme can be reduced to a negligible level. In addition, to simplify the pipetting steps for the checkerboard experiments, two sets of $N/2$ inputs/outputs are connected together for primer loading. As shown in figure 8, after all the components for PCR are loaded into the desired compartments, small valves C can be selectively switched on, thus bringing the components into fluidic contact within each reactor. Peristaltic pumps in the bottom layer allow for the rapid rotary mixing[79] of all reagents within the reactors (figure 9C). An efficient mixing of the reagents can be achieved by actuating the rotary pumps with two pneumatic controllers (Fluidigm Inc.) at 10Hz for 5 minutes. After thermocycling the whole matrix chip, a modified DNA array

scanner (Applied Precision) is available for imaging the fluorescence emission from the PCR products in the chip (519nm and 570nm).

Combinatorial Tests between Samples and Primers

To test the performance of the chips, we alternately loaded each row of reactors with primers and no-primer controls; and then loaded each column of reactors with the cDNA template and no-template controls. The DNA template concentration was titrated along the positive control columns in order to test sensitivity. The polymerase was loaded from the single inlet and amortized over all the independent reactors.

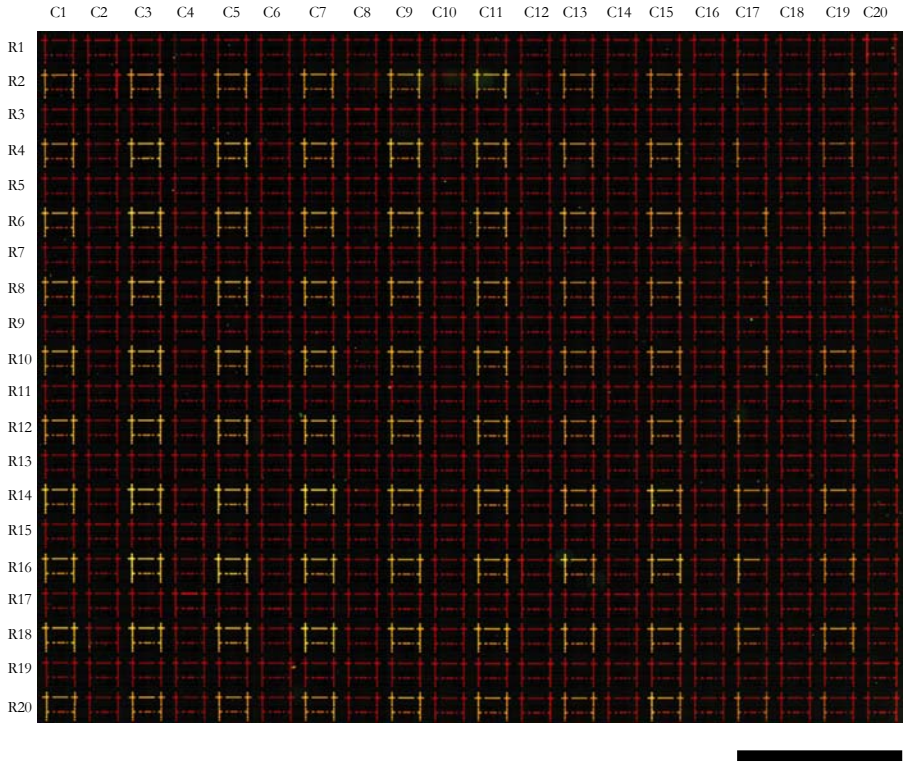

Figure 10: *Two-color image of fluorescent emission from a 20 × 20 matrix chip. Yellow indicates a positive signal from the sample. The no-template or no-primer controls show*

a dim red produced by the passive reference dye in the buffer. The concentration of the DNA templates is as follows (copies per reactor): C1 and C3 (6,100), C5 and C7 (3,050), C9 and C11 (610), C13 and C15 (305), C17and C19 (61). A threshold fluorescent ratio is established to define the false positive/negative signal. Some reactors in columns 17 and19 do not show the desired positive signals, establishing the sensitivity of the chip. Scale bar, 6.4 mm.

As shown in figure 10, the reactors containing all the necessary reagent components for PCR produced the positive signals (yellow, a mixed color of green and dim red); while those reactors that missed one or two reagent components showed a color of dim red, which derived from the passive reference dye in the buffer solution. The expected image is a checkerboard pattern, and any cross-contamination or leakage between compartments will be evident (figure 11, reactor C6R9). The chip's plumbing layout and the sample loading sequence are specifically designed so that DNA template contamination among independent reactors is only possible if the valve system fails. This is important because the high sensitivity of the PCR assay can easily turn any carry-over contamination between DNA samples into a false positive signal. In this device, the only opportunity for potential carry-over contamination is between the primer sets during the sample loading sequence; PCR is not sensitive to small amounts of primer contamination and channel flushing while loading the other reagents should reduce any primer contamination to negligible levels. Possible primer contamination can be further reduced by extended channel flushing with additional buffer solution before loading the DNA templates or polymerase.

In the experiment the reagent volumes necessary for loading can be as few as 1 μl cDNA or no-template control for each column of reactors; 3 μl primers or no-primer control, and 2 μl polymerase for the whole matrix chip. Using the 20 × 20 matrix chip, the sample solution (1 μl) containing cDNA template from each pipetting step has a chance to be tested with 20 distinct primer pairs. On the other hand, the solution (3 μl) containing primers from each pipetting step can be used to test 20 different samples with 1 to 10 repetitions, depending on the availability of wiring the input holes. Most strikingly, an aliquot of 2 μl polymerase from a single input hole can be introduced into the chip and amortized over all the 20 × 20 reactors (3 nl each) to perform distinct reactions. Therefore, we have demonstrated that this approach can dramatically improve the efficiency of reagent consumption, thereby providing an effective answer to the "macroscopic/microfluidic" interface problem.

The demonstrated volumes mentioned as above may not be the minimum ones. However, there exist some dead volumes in the channels connecting the reactors or the input holes to the reactors, which are unavoidable. The risks, including incomplete flushing of reagents or trapped air bubbles in the flow channels, may be raised if the volumes of transferred reagents are reduced inappropriately during loading.

This device greatly reduces the time spent on sample setup step for PCR by requiring merely 41 pipetting steps for 400 reactions, as opposed to the 1,200 that would be required for microtiter-plate-based assays. Without use of the chip, sample setup would probably be the single largest time consuming step of the process. With the chip, the

most time consuming step is the thermocycling, which in turn is limited by the thermal mass of the cycler. The microfluidic volumes being cycled have a very low thermal mass, and it is possible in to decrease the time for the assay by using integrated heaters to effect local thermocycling[82] or to take advantage of the ring reactor to move the sample into different regions of constant temperature[80].

Combinatorial Tests between Forward Primers and Reverse Primers

The matrix chip with active mixing is a flexible platform, with the capability of testing any two components of assays combinatorially and loading a third universal component from a single input hole. Figure 11 shows a 10 × 10 matrix chip in which an alternative format was used for loading reagents.

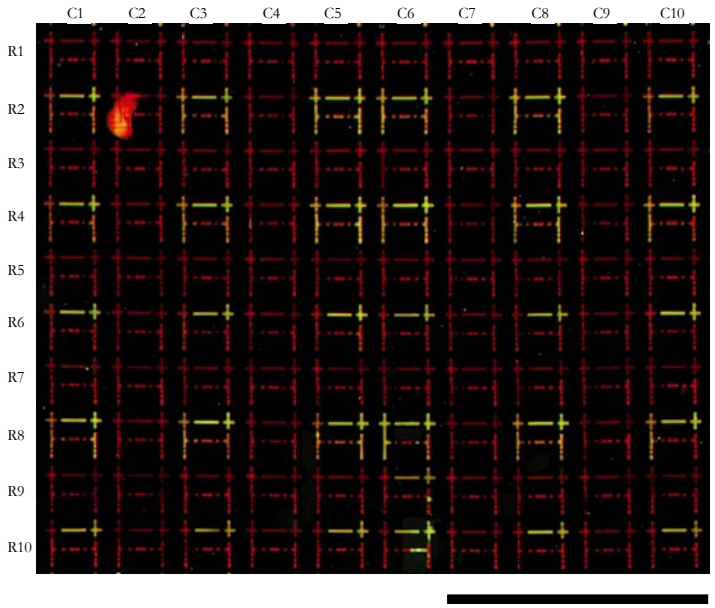

Figure 11: *A scanned fluorescent image illustrating use of the matrix chip to explore combinations of forward and reverse primers. Even-numbered rows are loaded with the*

correct forward primers, while odd rows are negative controls. Columns 1, 3, 5, 6, 8, and 10 are loaded with the correct reverse primers, while the remainder columns are negative controls. Thus, one should only observe successful PCR reactions in those reactors at the vertices of correct forward and reverse primers, as shown. Reactor C6R9 shows a false positive signal, which possibly resulted from the contamination of the forward primer of the neighboring reactors in the same column (C6). Scale bar, 6.4 mm.

The three main components with all the other necessary PCR reagents and additives were as follows: component I included both the cDNA template and the polymerase; components II contained forward primers while component III contained reverse primers. Components II and III were loaded in the rows and columns of the matrix, respectively. Then component I, which contained both the cDNA template and the polymerase, was loaded into all the reactors from the single input. In this manner, all possible combinations of forward and reverse primers can be tested with each other on a common DNA template. This format is particularly useful in optimizing forward and reverse primer pairs for PCR, and mapping exons or profiling gene isoforms from a complicated mixture of transcripts.

Overall Performance of the Matrix Devices

In order to evaluate the performance of the matrix devices, we repeated the experiment of PCR with a number of chips that we fabricated. In all, 6 separate 20×20 matrix chips and 8 separate 10×10 matrix chips were tested for a total of 3,200 reactions. 24 out of 1550 positive control reactors produced false negative signals; in 18 of these cases the DNA

concentrations were close to the detection limit. The other 6 reactors failed, possibly because of dust blocking the channels or other fabrication defects. 35 out of 1,650 negative controls showed false positive signals, perhaps due to the reagent leakage. In total, 98% of the 3,200 reactors tested produced the expected results (figure 12).

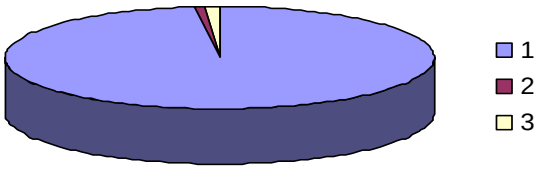

Figure 12: *Statistical survey of performance of matrix chips. More than 98% of reactors produced expected signals, based on repeated experiments on 6 separate 20 × 20 matrix chips and 8 separate 10 × 10 matrix chips. The color of blue represents expected signals, including true positive and true negative ones. The red represents false negative signals, while the yellow represents false positive signals.*

By titrating the concentrations of DNA template, we established the detection limit of the chip to be around 60 template copies per reactor (figure 13). These testing experiments were performed with only 30 thermocycles. Now we have demonstrated that a single copy of DNA template can reliably be detected in the matrix device with PCR amplification (40 thermocycles).

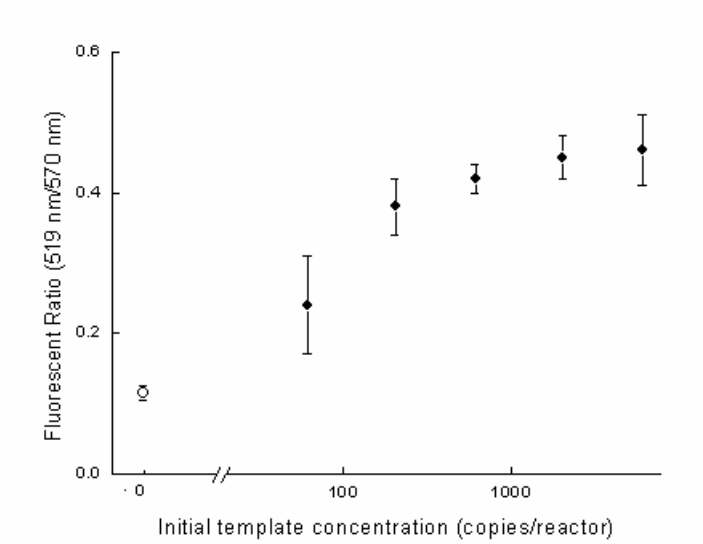

Figure 13: *Fluorescent ratio vs. the initial concentration of the cDNA templates. Each symbol represents the averaged ratio of 20 reactors containing the same template concentration, with an error bar showing the standard deviation. There is no significant difference between the no-template control and the no-primer control. As the concentration decreases to the limit of detection, the standard deviation increases due to a mixture of positive and false negative results.*

In one experiment we managed to recover the PCR product from the 20 × 20 matrix chip and analyzed it with conventional gel electrophoresis. Positive samples containing cDNA template were loaded into every reactor in order to collect as much PCR product as possible. The scanned fluorescent image (not shown) demonstrates that all the 400 reactors worked as expected. The chip pattern was slightly modified to connect together all the inputs/outputs for primer loading/unloading. Thus, the PCR product could be flushed with TE buffer solution (about 40 μl) and collected with a pipette tip plugged into

the wired outputs. The solution of the extracted PCR amplicon was concentrated into a volume of about 5 μl by evaporation. The quality of this pooled amplicons was then verified by gel electrophoresis (figure 14). As a positive control experiment, a solution containing identical PCR components was thermocycled in the microtube, and then aliquots of the PCR product solution were loaded into the gel.

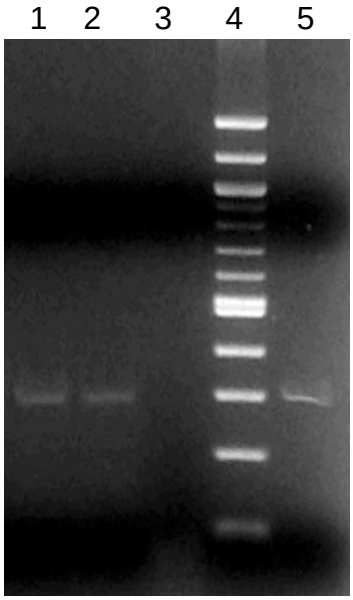

Figure 14: *Agarose gel electrophoresis of the PCR amplicon by the chip or by a microtube. Lane 1: 1 μl PCR amplicon by the microtube; Lane 2: 0.5 μl PCR amplicon by the microtube; Lane 3: negative control by the microtube; lane 4: 100 bp DNA ladder; lane 5:extracted PCR amplicon (400 reactors x 3 nl/reactor) by the matrix chip. Displayed in 2% Agarose gel with easy-cast™ electrophoresis system (Model B1A,VWR); stained with Sybr Green I; documented by the Kodak electrophoresis system.*

As shown in figure 14, the length of the amplicons recovered from chip-based PCR (lane 5) is around three hundred base pairs as expected. It shows comparable or slightly stronger signal than its counterparts from the bench-top controls (lane 1 and lane 2). In future devices it should be possible to integrate on-chip capillary electrophoresis for *in situ* product analysis beyond the information provided by the Taqman assay.

Concluding Remarks

The microfluidic matrix device offers an effective solution to the "world-to-chip" interface problem by accomplishing two important goals: an economy of scale in reagent consumption is achieved, while simultaneously minimizing pipetting steps. We have demonstrated that N^2 independent assays can be performed with only 2N+1 pipetting steps, using a single aliquot of the enzyme that can be amortized over all the reactors. Thus, the chip reduces labor relative to conventional fluid handling techniques by using an order of magnitude less pipetting steps and reduces cost by consuming two to three orders of magnitude less reagents per reaction.

Our microfluidic matrix device has immediate applications in medical diagnosis and gene testing. The demonstrated PCR format allows N samples from patients to be simultaneously screened for N mutations or pathogens. The features of high throughput performance and economic saving of the reagents make the matrix chip an attractive option for clinical research, where a large number of samples are required to be assayed routinely. In addition, our approach simplifies the pipetting operations dramatically. With conventional fluid handling systems much more complicated pipetting operations would

be required to perform the same number of assays. Setting up the reactions can become the most time-consuming step because of the extra operations, which unfortunately also raises the risk of introducing pipetting errors or contamination of the reagents. Other applications of interest include investigations of antibody/antigen interactions, or gene expression analysis, where reverse transcriptase PCR can be used to query *N* mRNA samples for the expression levels of *N* different genes. Besides PCR techniques, other techniques, such as invader assays or fluorescently labeled mismatch-binding proteins, can potentially be used in the device for diagnostic purpose. These methods share a common feature of using the technology of fluorescent probes, which is sensitive and compatible with format of multiple assays in a parallel fashion. It should be quite straightforward to adapt the matrix chip to these analysis methods. On the other hand, the use of the matrix chip may not be limited by fluorescent techniques. Other optical properties, such as absorption or opacity, can potentially be applied to monitor the assays in the matrix chip.

The matrix chip may also find application in the studies of cell biology[25, 61] or screening of drugs. For example, antibiotic synergy tests screen a large number of antibiotic combinations to find out the optimal synergy effect to kill disease microbes[83]. Biologists are interested by the advances in this field because of possible benefits such as extension of antimicrobial spectrum and minimization of side effects on the human body. But the conventional techniques using petri dishes or microplates to perform the tests are low throughput and labor intensive. It is not surprising that the results from conventional techniques usually provide only limited information. The microfluidic matrix chip is a

potential platform for antibiotic synergy tests. The advantages include improved throughput and ability for real-time monitoring the dynamics of cell behaviors. Particularly, the microfluidic matrix chip that we developed provides a unique benefit of reducing bias of pre-treatment of bacterial cells. They can be loaded through the single input hole and amortized over all the reactors on the matrix chip, with a solution containing the neutral/optimal buffer for the bacteria. Since the valve system of the matrix chip secures the isolation of individual compartments, the bacterial cells will not be affected by any antibiotic before they are allowed to contact each other. Once the small valves are open, a rapid mixing will present the target bacteria in a desired solution of antibiotics. On the contrary, other methods may allow the bacterial cells to contact either antibiotic before they are put into the final formulated solutions. Thus there is a chance to bring up undesired response from the cells to the first antibiotic, causing a different result in antibiotic synergy tests.

Beyond the demonstrated format of performing a large number of parallel assays, the matrix chip has a capacity to perform assays requiring multiple steps within a single chip. After the reactions of the first step are completed in the formats that we have demonstrated, the products may be isolated into the central compartments with the well-defined volume of individual reactors. The other compartments may then be filled with the reagents for the downstream assays by operating the valve systems exactly in the same way as before. Therefore, the intermediate products need not be extracted off the chip, facilitating the automation of the multistep assays and simplifying chip design and

operation. Furthermore, this approach can save the unavoidable loss or dilution of product in the dead volume of the chip and the outlet port.

In general, the microfluidic matrix chip provides a universal and flexible platform for biological and chemical assays that require parsimonious use of precious reagents and highly automated processing.

Chapter 4

PROFILING DIVERSE ISOFORMS OF ALTERNATIVE SPLICING WITH MICROFLUIDIC PCR DEVICES

Introduction

Alternative splicing gives rise to mRNA isoforms by including/excluding particular exons or introns, thus providing an important mechanism of genetic regulation in higher eukaryotes[84]. It is one of the key figures in explaining the mystery that diverse proteins can be encoded by several orders of magnitude fewer genes in many organisms[85]. Alternative splicing can affect many aspects of protein function, including determination of cellular and subcellular localization, modulation of enzyme activity, and so on[84, 86]. The biological role of alternative splicing can frequently be extended if the protein isoforms thereby produced are important elements (transcription factors, hormone receptors, or ion channels) in the regulatory cascade[86]. Therefore, early events of alternative splicing can be involved with regulating entire developmental pathways of biological targets of interest. The isoforms by alternative splicing share extensive regions of identity, while varying in specific domains[86]. Figure 1 shows the difference between normal splicing and alternative splicing. There exist various patterns of alternative splicing. Noteworthy, a single pre-mRNA can exhibit multiple sites of alternative splicing, which dramatically increases the complexity of variants. In recent years, emerging cases of alternative splicing have been discovered in a

variety of organism including fruit fly, mouse, and human. It is estimated that up to 60% of human genes are involved with alternative splicing[84, 87].

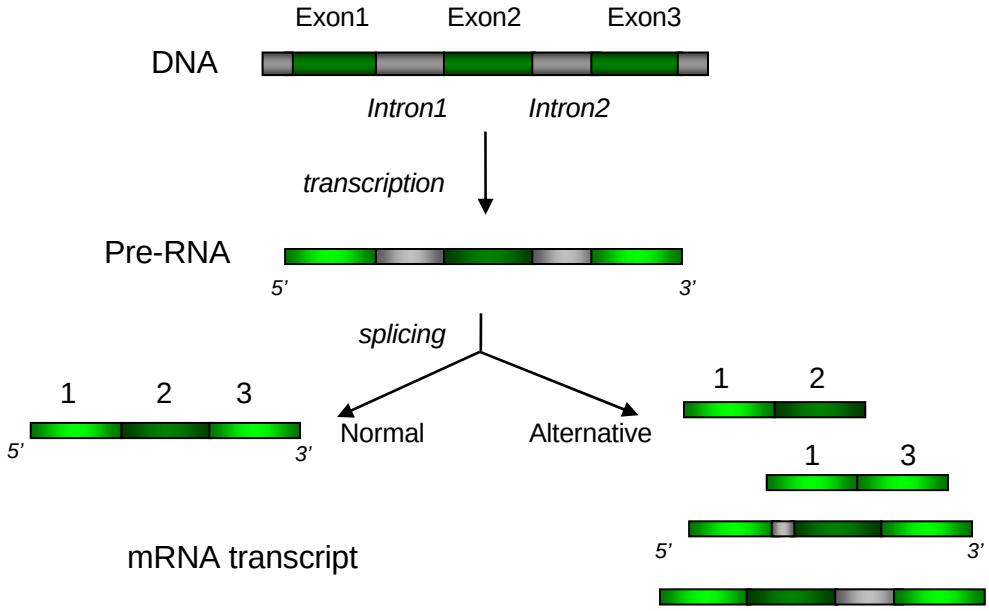

Figure 1: *Schematic of alternative splicing (right), compared with normal splicing (left). Exons are shown in the color of green, while introns are shown in grey. Alternative splicing may enrich the library of mRNA transcripts.*

Drosophila melanogaster is a fruit fly. For a very long time it has been used as a classical model organism for research, particularly in genetics and developmental biology. The life cycle of Drosophila consists of a sequence of stages including embryo, larva (first, second, third and final instar), pupae, and adult. Typically only 11 or 12 days are required to complete one cycle at room temperature (21 to 23 ^{o}C), though variations in the generation time exist, resulting from different temperatures. Drosophila has only 4 pairs of

chromosomes. Its genome is approximately composed of 165 million base pairs, containing around 14,000 genes by estimation[88]. Drosophila lola (longitudinal lacking) gene encodes a transcription factor and produces a family of about 20 isoforms by alternative splicing (figure 2)[89, 90].

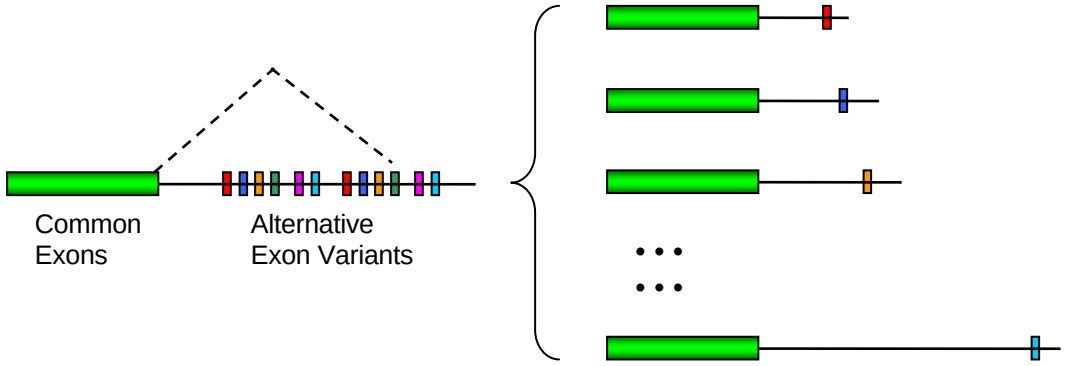

Figure 2: *The lola gene of fruit fly gives rise to a family of around 20 isoforms by alternative splicing. These isoforms share a region of several constant exons (shown in green), varying in their tails with a alternatively spliced exon (shown in different colors). The lines (solid and dashed are a guide for the eye.*

This gene is required for a number of axon guidance decisions in the developing nervous system of *D. melanogaster.* Previous studies suggest that various isoforms of lola gene by alternative splicing are involved with the process of axon guidance decisions[89, 91]. However, quantitative profiles of these isoforms expressed at various developmental stages are missing. This information should be critical for the investigation of how the specific neural activities are determined by the isoforms. We are interested in applying the microfluidic devices onto quantitative analysis of the lola gene expression, in order to

obtain insightful links from genes to gene functions regarding the nervous development of fruit fly. Another interesting gene is *Drosophila* Dscam (the Down syndrome cell adhesion molecule), which encodes an axon guidance receptor. This gene displays an amazing diversity: theoretically its pre-mRNA can be alternatively spliced into over 38,000 different isoforms, 2 or 3 times the number of predicted genes in the entire organism of fruit flies[92]. Only a small percentage (less than 1%) of the potential isoforms have been confirmed by experimental results so far[92-94]. It is unknown how many isoforms are actually expressed in fruit flies, or whether each neural cell makes a random or pseudorandom set of these isoforms. Little is known whether the set made is continuously variable over the time of the nervous development. Answers to the above questions will deepen our understanding of biological significance of the Dscam gene, for example, in terms of specificity of neuronal connectivity[93] or complexity of immune system of insects[95].

This chapter describes our work on quantitatively profiling the lola isoforms from selected samples using microfluidic PCR devices. Neural cells at different developmental stages of fruit fly were selected using laser capture microdissection (LCM). Standard procedures were followed to extract, purify and preamplify RNA samples, and then to obtain cDNA samples. Subsequently matrix PCR assays were performed by loading the cDNA samples and the designed primer pairs into the microfluidic device combinatorially. Quantitative profiles show distinct patterns of combination of lola isoforms at different developmental stages. The expression levels of individual isoforms can be different from one another by nearly two orders of magnitude at the same developmental stage. Furthermore, information

including absolute copy numbers of interested genes can be extracted with careful calibration. This chapter introduces a theoretical development for decoding the mystery of extremely diverse Dscam isoforms by alternative splicing in fruit fly, which is useful for future experiments.

Sample Preparation

Fly stocks were raised on standard media at the room temperature in Dr. Luo's lab. White pre-pupae were collected and considered to be 0 hour after puparium formation (APF). Pupae (0 hour or 20 hour) or larva at the third instar were lined up in a small tissue block, covered with OCT (Microm, Germany) and frozen on dry ice. Animal samples can be stored for up to 2 weeks at −80 ^{o}C. Samples were sectioned on a cryostat. Tissue sections were collected on PEN-membrane covered slides and immediately place in a storage box on dry ice. Tissue samples should be prepared for laser capture microdissection (LCM) as soon as possible (no longer than 8 hours at −80 ^{o}C or dry ice). The slides were removed from dry ice and rinsed through a standard ethanol dehydration series: 70%, 95%, 100% EtOH for 5 minutes each. Then slides were washed in xylene for 2 minutes with gentle agitation. After xylene was drained, slides were allowed to dry and transferred to a clean container to start LCM capture immediately (no longer than 1 hour at room temperature).

The target cells were projection neurons of antenna lobes, which had been fluorescently labeled using the standard transgenic techniques (UAS-CD8-GFP fusion protein driven by the Gal4-GH146 insertion)[96, 97]. As shown in figure 3, selected cell samples were cut and

captured into a cap of a PCR tube, using a Leica LCM microscope with epifluorescence for identification of antenna lobes. Routinely, each tube of sample contained 5 (up to 30) captures, corresponding to 5 (up to 60) cells by estimation. A control sample was created by scraping the PEN membrane containing sections into a separate PCR tube.

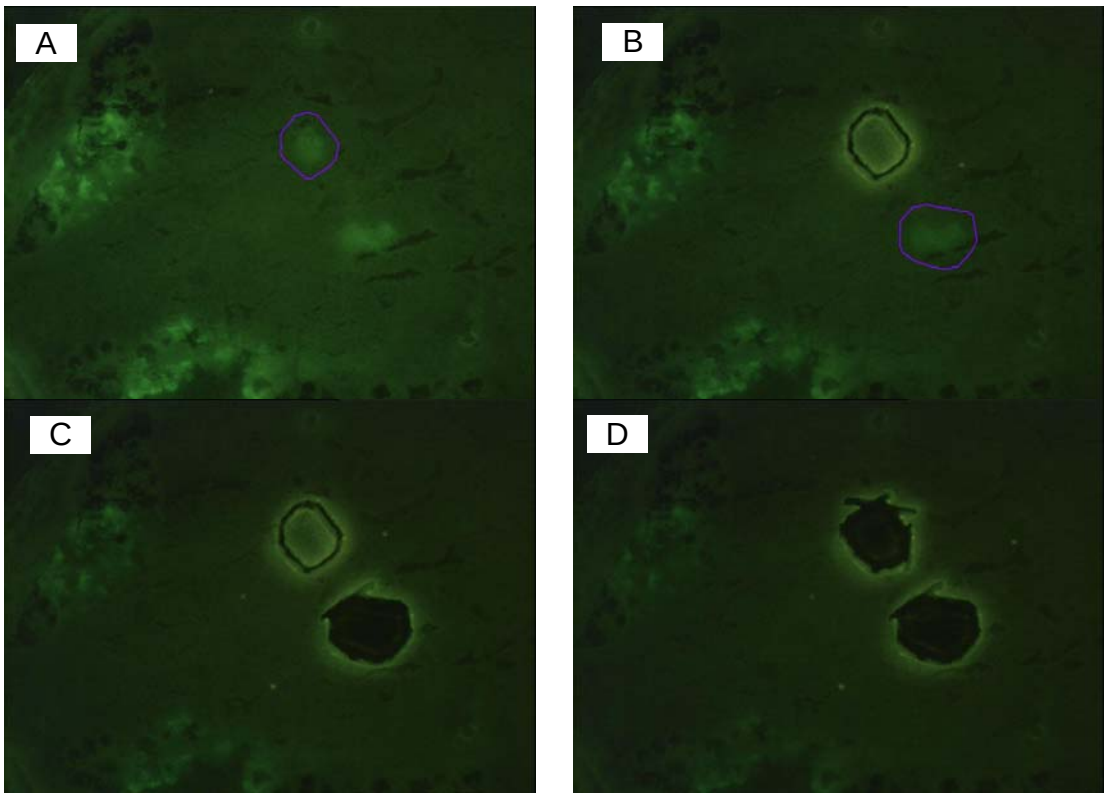

Figure 3: *Selection of cells using laser capture microdissection (LCM). Target cells (projection neurons in antenna lobes) were labeled with GFP. Usually the cells appeared in a pair from each tissue sample. A: One target cell was circled by the virtual purple line with the software of a Leica LCM microscope. B: A laser cut along the virtual purple line, but the cut sample hung around on the slide. The cutting route was chosen for another target cell. C: The second cell was cut and captured into the container. D: Caputring the first target cell was successful after a make-up cut.*

The tubes containing captured cells were transferred to dry ice and stored no longer than 1 day at −80 ^{o}C before RNA isolation. Total cellular RNA was recovered using the Arcturus Pico-Pure RNA isolation kit. This kit includes a buffer solution to break down the cells and extract RNA, and then purify RNA samples with the column membrane. Small amounts of RNA from a few cells can reliably be recovered in our experiments with the standard protocol.

RNA samples were preamplified using a MessageAmp II aRNA amplification kit (Ambion Inc.). Briefly, a reverse transcription primed with oligo(dT) bearing a T7 promoter was applied to produce high yields of first-strand cDNA, templated by the mRNA in our samples. Then the cDNA underwent second-strand synthesis and cleanup to become a template for *in vitro* transcription catalyzed by T7 RNA polymerase. The pre-amplifications of RNA samples were very efficient.

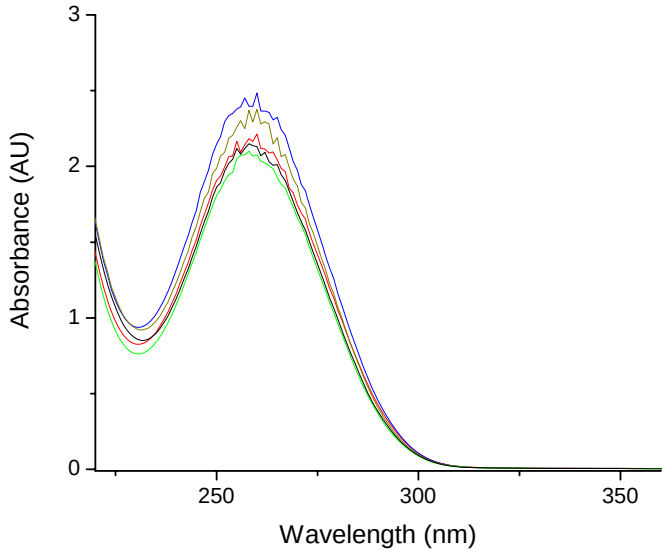

Figure 4: *UV spectra of RNA samples after linear preamplification. The concentrations of RNA samples can be determined by their absorptance at 260 nm. Commercial poly(A)RNA samples with defined amounts were included in the tests. It was estimated that one round of preamplification can enrich the RNA by around 2,300-fold. A second round of ampfilication can subsequently be performed if necessary.*

We routinely achieved a yield of around 2,300-fold increase in our experiments (figure 4), which matched the expected yields according to the kit manual by the supplier. The high quality of the cRNA samples after preamplification was verified using Bio-RAD bioanalyzer. Amplified RNA samples appeared as a smear from 300 to 3000 nt as expected.

The cRNA samples were used as template for another round reverse transcription (#18080-051, Invitrogen), producing high yield of cNDA. The reactive capacity of each kit was taken into account when assembling the cocktail solutions. The cDNA samples were aliquoted and stored at –20 ^{o}C before the use.

Unique primer pairs and Taqman probes were designed for individual lola isoforms and other interested genes, using an online software Primer3 (http://frodo.wi.mit.edu/cgi-bin/primer3/primer3_www.cgi). The oligos were synthesized by Integrated DNA Technologies, Inc. The primer pairs and Taqman probes were prepared in stock concentrations, and then diluted into work concentrations. Each work solution contained 9 **m**M forward and reverse primers, as well as 2.5 **m**M Taqman probe. Both the probe solutions and cDNA sample solutions can be stored in minitubes (minitube system, Axygen

Scientific Inc). With this system, the tubes can be arranged in a format similar to a 96-well microplate, therefore compatible with 8-channel or 12-channel pipets for high throughput liquid handling. On the other hand, individual minitubes are conveniently changeable with one another without affecting the others. Optimized rubber cap stripes can seal the tubes very well.

Profiles of Lola Isoforms at Different Developmental Stages

Microfluidic matrix chips (48×48 arrays, figure 5) were applied to perform PCR assays in a high throughput manner, providing quantitative profiles of the lola gene isoforms and other genes of interests.

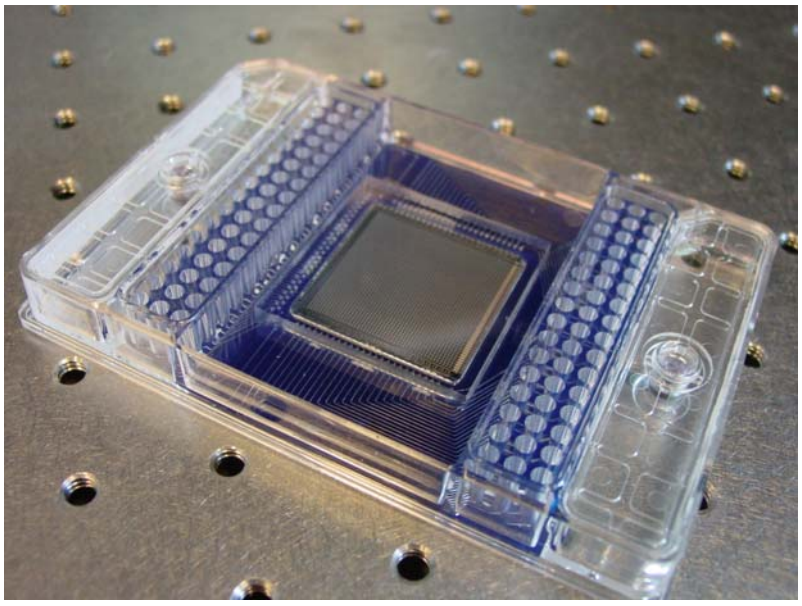

Figure 5: *An optical micrograph of the matrix 48 × 48 chip. The concept of microfluidic matrix chip has been patented and commercialized by Fluidigm Inc.*

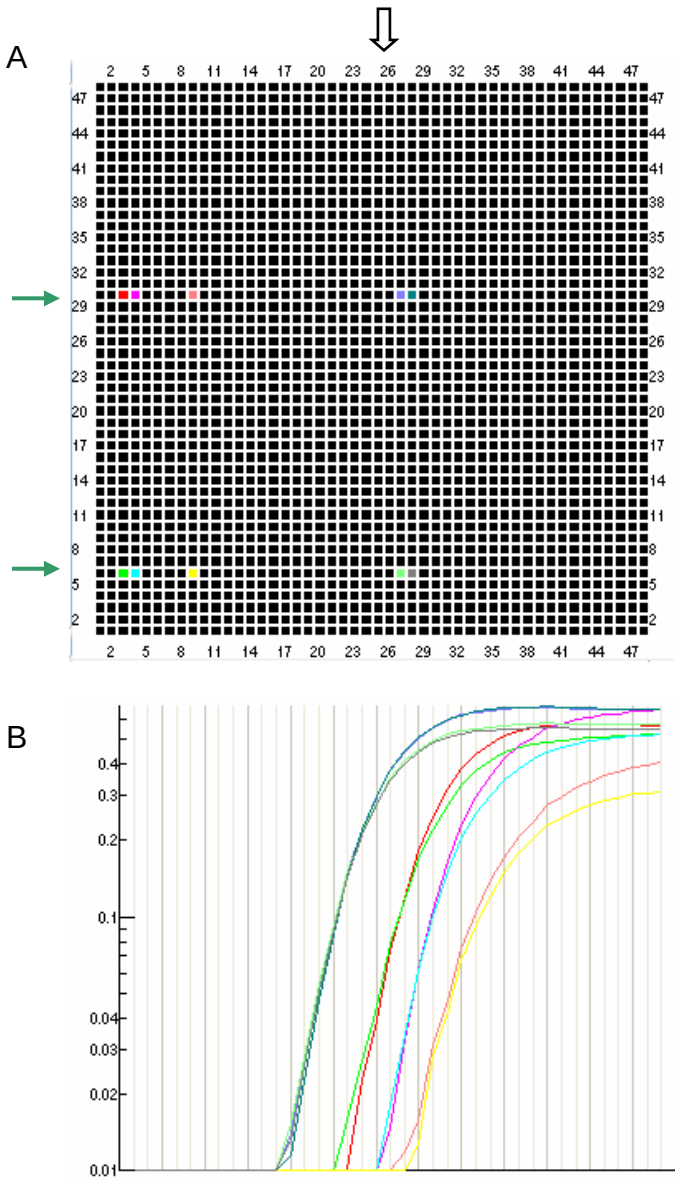

Figure 6: *Matrix PCR assays provide a high throughput method of gene expression profiling. In this experiment (figure 6A), multiple cDNA samples were loaded in rows, while primer pairs were loaded in columns (block arrow). For each cNDA sample, two identical concentrations were tested in independent rows of reactors (green arrows). The PCR experiments were highly repeatable on the chip. Figure 6B shows the real-time PCR*

curves for two identical cDNA samples in independent rows of reactors (three lola isoforms A in column 3, B in column 4, I in column 9, and Actin 42 in column 27 and 28).

As shown in Figure 6, the primer pairs including Taqman probes were pipetted into the input holes and then loaded into the chip in columns, while multiple cDNA samples with other PCR components in the mother solutions were loaded into the matrix chip in rows. They mixed with each other in the designed reaction chambers of the chip without cross-contamination. Therefore the primers and cDNA samples can be tested combinatorially. An instrument (Topaz FID crystallizer, Fluidigm Inc.) was used for loading and mixing the reagents/analytes in a programmed procedure. The matrix chip was removed and mounted on a flatbed heating block of a thermocycler. A large area CCD camera with high resolution was applied to monitor the fluorescence from PCR reactions in real time. The performance of matrix PCR was reliable. We obtained consistent CT values (less than 1 cycle variation) from any identical PCR assays on the chip (with only a few exceptions). As shown in figure 6B, the real-time PCR curves from identical samples were almost superimposed upon each other.

The housekeeping gene of Actin 42 was chosen as an internal control of the experiments. We performed PCR tests many times using the devices for independent cDNA samples prepared from separate batches. As shown in figure 7, the expression levels of Actin 42 were very consistent for all these independent samples (unselected or LCM selected). In addition, our experiment suggested that the gene of Actin 42 can be used to normalize the expression level of other interesting genes over the time course (figure 8).

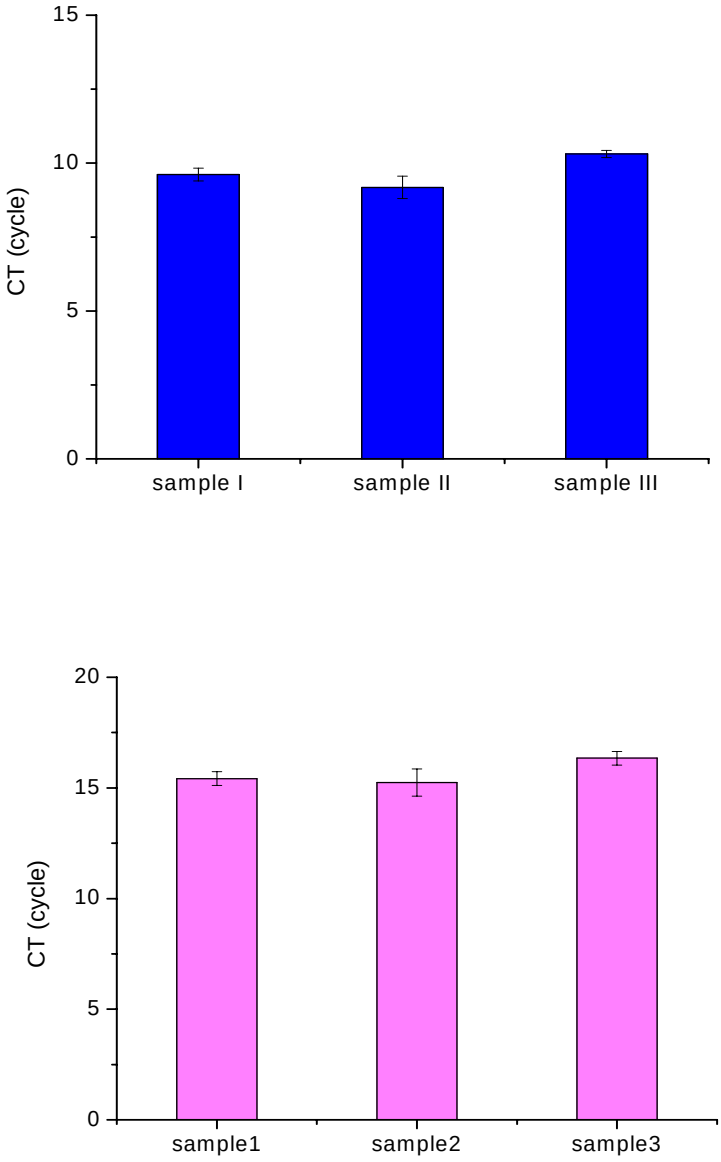

Figure 7: *Independent tests of housing keeping genes (Actin42) from separate batches of samples. Top: unselected samples (0 hour APF), scratched directly from the wax member containing the tissue sections. Bottom: LCM selected AL samples (0 hour APF), normlized*

to a single capture. Each sample was indepedently tested 5 times on the chip. Error bar: standard deviation.

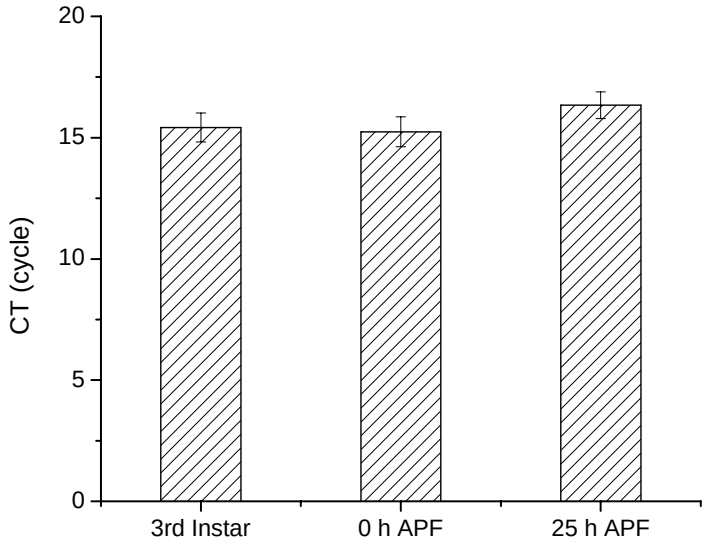

Figure 8: *Expressions of housing keeping genes (Actin42) at different developmental stages. Samples: antennal lobe (AL) selected by LCM. Error bar: standard deviation.*

Figure 9 demonstrates the robustness of our preparation procedure of the samples and reliability of the PCR assays using our matrix devices. In this figure, the columns represent the levels of RNA expression of lola isforms averaged from 3 independently samples (error bar, standard deviation). Each sample was independently tested 5 times for all the primer pairs of lola isoforms using the matrix devices. We were able to obtain consistent results from our measurements. The CT values of any repetitive reactions of the identical sample were very close to each other, with a difference of smaller than 1 cycle (data not shown).

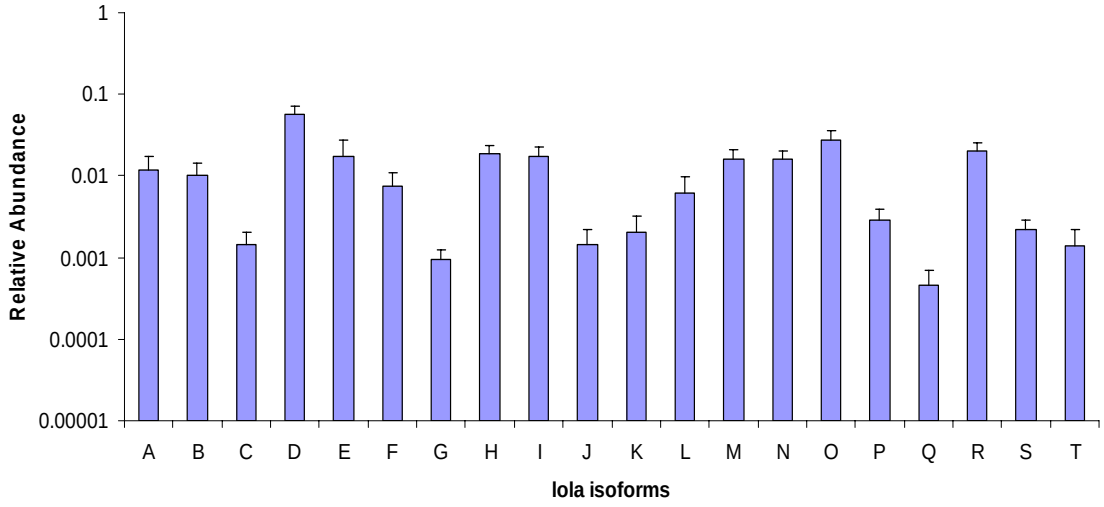

Figure 9: *Expressions of the lola isoforms from unslectled samples. The levels of expression are normalized and shown relative to the housekeeping gene Actin42. Error bars represent standart deviation from 3 independent samples, and samples were independently tested 5 times.*

Figure 10 shows the expression profiles of the lola isoforms at different developmental stages. The samples were selected by laser dissection microscopy (LCM). Within the setting-up, we did not achieve single cell resolution, but the selection allowed us to profile mRNA expression in a small subset of enriched neurons. Based on our experiments, different combinations of lola isoforms were expressed over the time course, in terms of presence/absence and abundance. At each developmental stage, we detected a significant difference in the levels of RNA expression between individual isoforms. For example, several isoforms (D, H, and R) in the AL sample at 0 hour APF (figure 10A, black) were meausured more abundant than isoform L or S by nearly two orders of magnitude. The distinct patterns of abundance of lola isoforms over the time course suggest that some of

them, for instance, E, H, I, M, and Q in antennal lobe, might be regulated along with the growth of the insects (figure 10A). Separate tissues may exhibit different features of which isoforms of lola are developmental regulated (figure 10A and 10B).

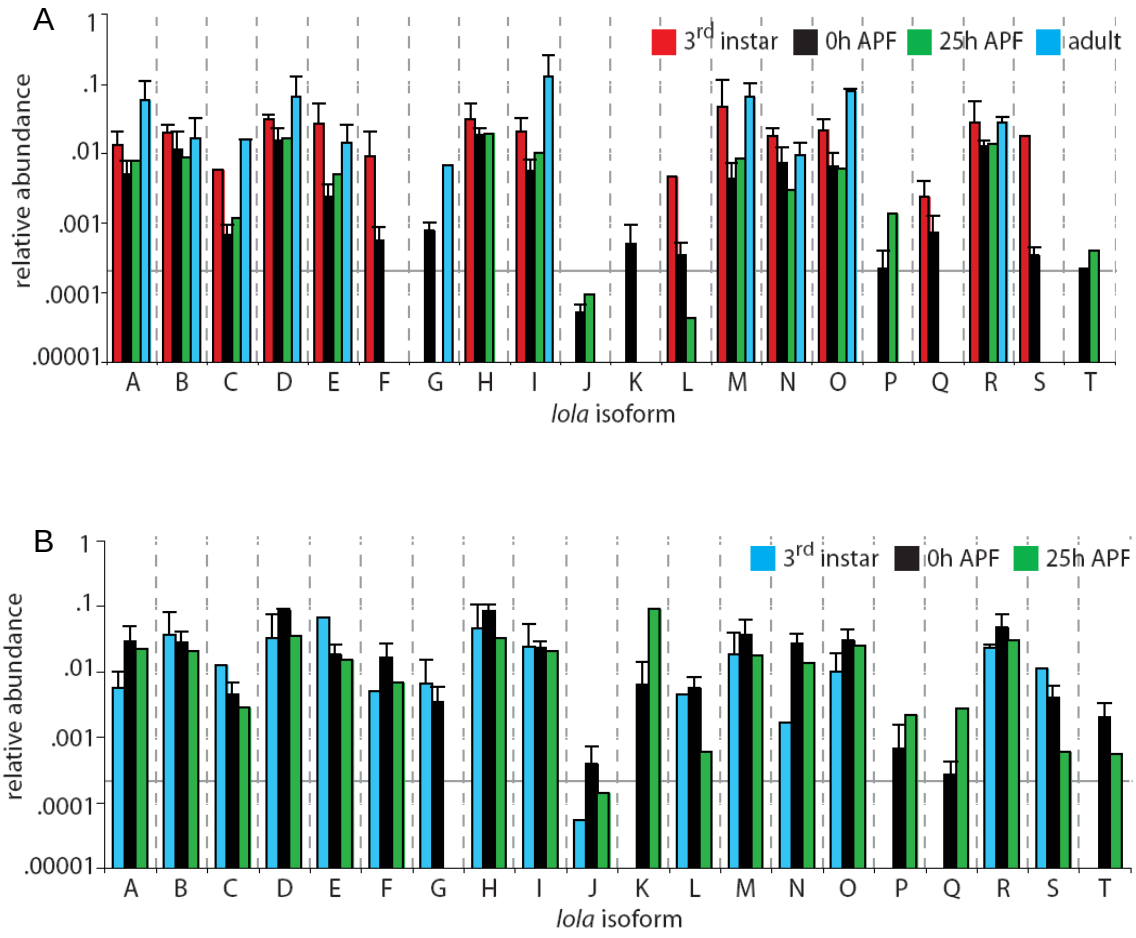

Figure 10: *Expressions of the lola isoforms from selected samples by LCM at different developmental stages (coded with distinct colors). Their abundances are normalized and shown relative to the housekeeping gene Actin42. (A) antennal lobe at 3rd Instar (red), 0 hour APF (black), 25 hour APF,(green), and adult (blue). (B) optic lobe at 3rd Instar (blue), 0 hour APF (black), 25 hour APF (green). Error bars represent standart deviation*

from at least 2 independent samples, and samples were independently tested 5 times. Samples lacking error bars failed to produce in 1 or more samples, resulting in a single data point. Horizontal solid line represents a confidence limit of the average relative expression near the detection limit based on CT vaules and reproducibility.

Quantification with Information of Absolute Gene Copy Numbers

Here we attempt to develop an effective method for gene expression profiles with information of absolute abundances. Matrix PCR has provided a high throughput approach to profile the relative abundances of multiple genes for multiple samples. The information of absolute copy numbers of interested genes can be further obtained by using a microfluidic digital PCR chip (manufactured by Fluidigm Inc.). The digital PCR chip functions by large-scale partitioning the PCR mix into hundreds of micro chambers simultaneously, so that eventually one micro chamber contains either a single copy of DNA template or no DNA template. After thermocycling the PCR chip, each chamber containing DNA template will produce a positive signal, which accounts for "1" and can be added up. The other chambers containing no template can serve as negative controls (figure 11). Therefore, digitally counting the numbers of chambers with positive signals and adding them up allow us to calculate the absolute gene copy number over the total volume of all micro chambers. The DNA sample must be diluted properly before loading, so that the chance of multiple copies of DNA template present in one microchamber can be reduced to minimum level. The current version of digital PCR chip includes 12 blocks. Each block consists of an array of 765 microchambers (around 7nL/chamber).

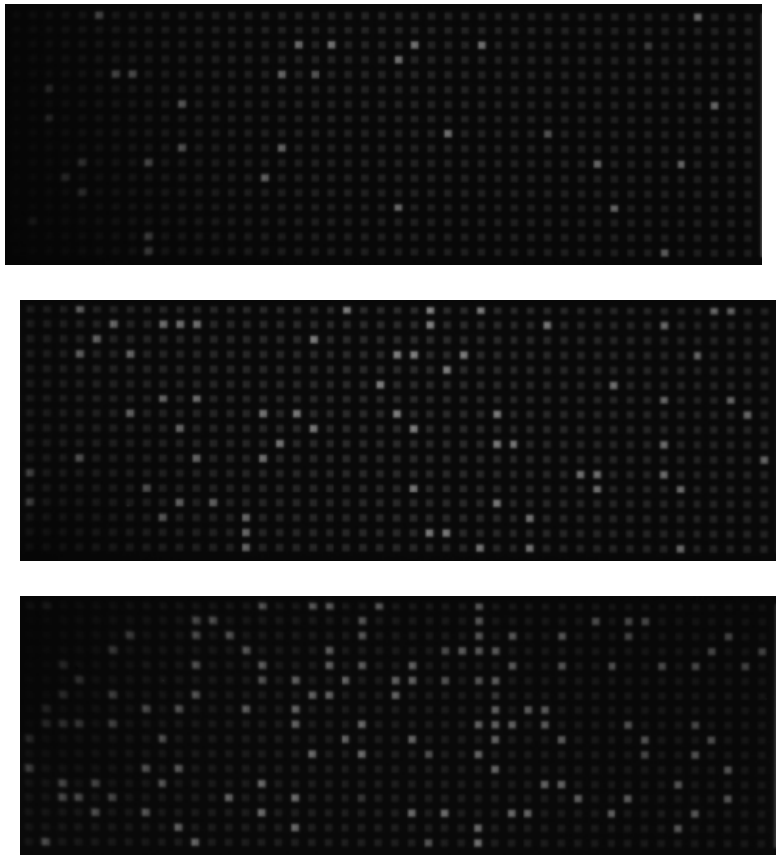

Figure 11: *Digital counts of the absolute gene copy numbers. Brighter spots: positive signals; dim spots: negative reaction chambers (their visibility may be attributed to the background fluorescent in the PCR solution). Sample: selected antennal lobe at 3 rd instar of larva. It was diluted, pre-mixed with primer pairs, and then loaded into the digital PCR chip (manufactured by Fluidigm Inc.). Top graph: lola isoform A, middle: lola isoform R, bottom: Actin42.* A*t least two blocks were tested with the identical solutions with endurable variation of counts. These panels show representative images.*

The selected AL sample at the 3rd instar of larva was tested here. The cDNA sample was aliquoted and diluted with a reference of the individual CT values from the matrix PCR experiments. The diluted cDNA samples were mixed with a selection of primers/probes,

including lola isoforms M, N, lim1 gene, and Actin 42. The mixed solutions were loaded into the digital PCR chip for the test.

As shown in figure 11, each block displays a number of random bright spots (positive signals) and dim spots (negative reaction chamber). The absolute copy numbers for these selected genes were obtained by counting the positive spots in each block. The variations between redundant blocks with identical samples were very small. After we took into account of the dilution factor by pipetting operations and the efficiency of pre-amplification, we can estimate the absolute copy numbers of interested genes per capture (1 or 2 cells/capture). Taking the gene of Actin 42 for example, it was estimated to be expressed around 56,000 copies per capture. Immediately, the absolute abundances of other gene isoforms can be calculated using their "ratios" (relative abundances) and the calibrated copy number of Actin 42 gene. Based on our calculation, the majority of lola isoforms are in medium-low abundances (around or fewer than 1000 copies per capture). This result seems reasonable, given the fact that they function as transcription factors. As an experiment of quality control, the calculated abundances using the "ratios" were double checked by digitally counting a few random chosen lola isoforms or other interesting genes. The results of these two methods match each other, suggesting that both the "ratios" method and digital counting are reliable (figure 12). However, there exists a remarkable difference in throughput performance between them. The method of digital counting is limited by its small capacity of performing independent assays. Even applying multicolor and multiplex PCR on digital chips can only improve its throughput by a factor of two or three. On the contrary, the method of using the "ratios" can provide a capacity of profiling

several orders of magnitude more targets simultaneously, requiring only one-point calibration with the help of digital PCR chip to obtain absolute abundances.

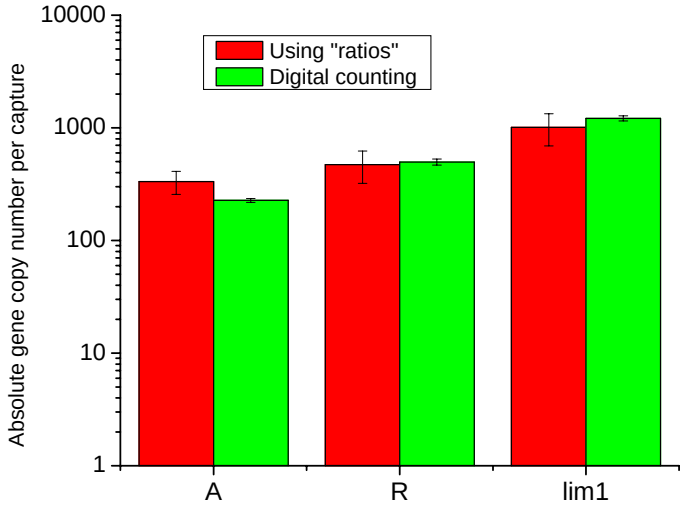

Figure 12: *Comparison of calculated gene copy numbers using the "ratio" method (matrix PCR chip) and more direct digital counting (digital PCR chip). The gene of lim1 is a candidate downstream gene target regulated by lola. The results of these two methods match each other very well.*

Devolving Extremely Diverse Isoforms of Dscam Gene

Dscam, the Down syndrome cell adhesion molecule, is an immunoglobulin superfamily member. *Drosophila* Dscam gene encodes an axon guidance receptor. It consists of clusters of variable exons sandwiched by constant exons. In the year 2000, Schmucker et al. discovered an amazing feature of this gene from the fruit fly: there are 12 variants of exon 4, 48 variants of exon 6, 33 variants of exon 9, and 2 variants of exon 17. Therefore, there

exist 38,016 potential different mRNA isoforms by combinations of the above variants (figure 13)[92].

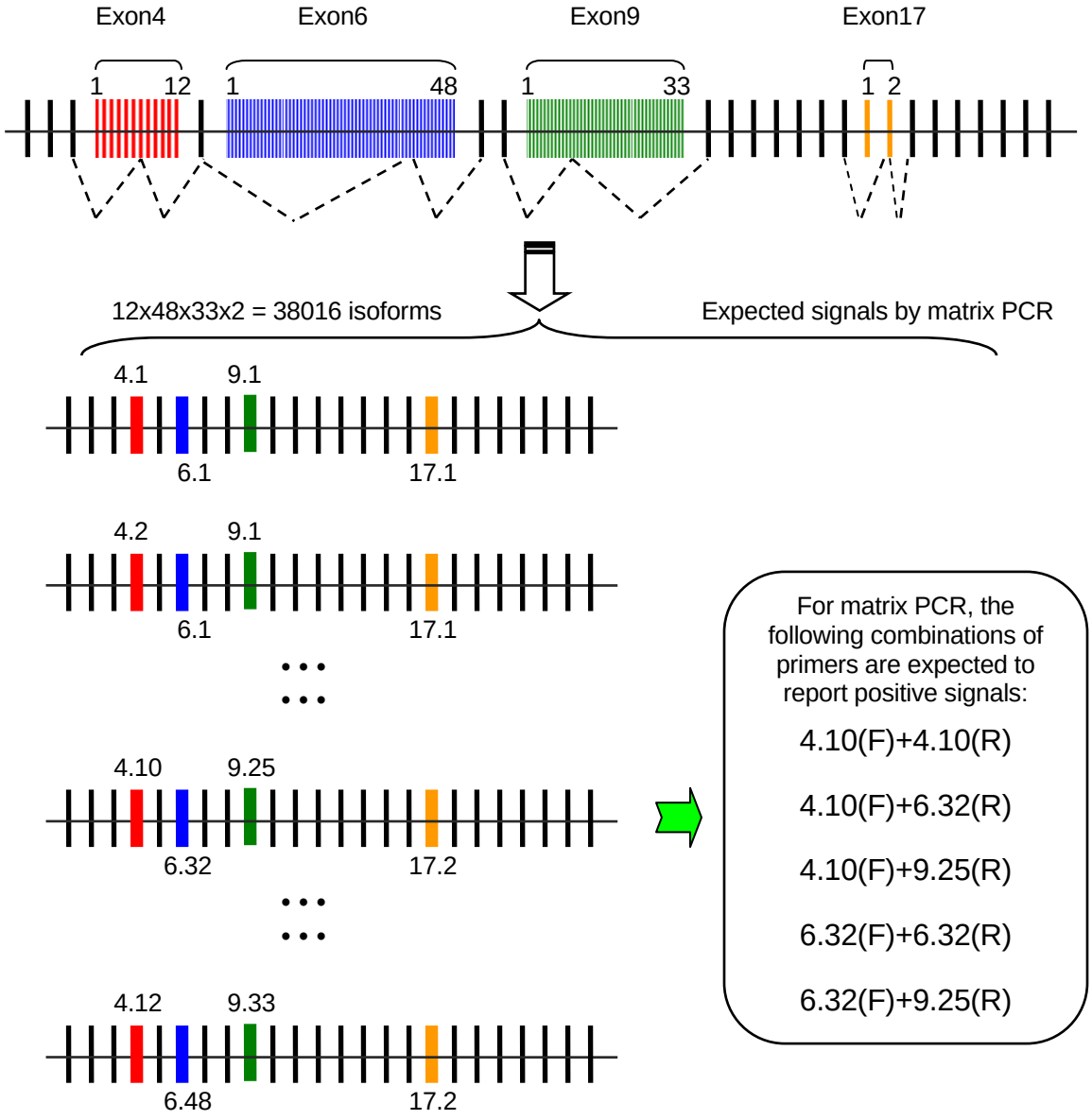

Figure 13: *Alternative splicing of Drosophila Dscam gene. Constant exons are represented by the vertical black rods in genomic DNA or RNA transcripts. Mutually exclusive*

alternative splicing occurs for exon 4 (red), exon 6 (blue), exon 9 (green), and exon 17 (orange). There are 12 variants for exon 4, 48 variants for exon 6, 33 variants for exon 9, and 2 variants for exon 17. As exemplified in the box at the bottom right corner, particular combinations of primer pairs are expected to report positive signals in the presence of specified Dscam isoforms (ID: 4.10-6.32-9.25). Exon 17 is passed presently because it is too far from the other regions of interests.

Interestingly, *Drosophila* Dscam transcripts always contain one variant exon at each position, yet never more than one variant. The original article confirmed 49 unique isoforms out of randomly sequenced 50 clones of the gene. Regarding the composition of these confirmed isoforms, 11 of 12 exon 4, 30 of 48 exon 6, and 25 of 33 exon 9 were detected[92]. The data suggested a high possibility of utilizing all the alternative exons *in vivo*. However, whether or not the extraordinary diverse mRNA isoforms are expressed might be a different story from utilization of those exons. Since only a small portion of the clone samples were sequenced in their study, it is still a mystery how many of the potential isoforms are actually expressed *in vivo*. Little is known whether each neural cell makes a random or pseudorandom set of these isoforms, or whether the set made is continuously variable over the time of the nervous development.

Here we introduce a unique approach to devolve the extremely diverse Dscam isoforms of fruit fly, by taking advantage of large-scale combinatorial tests with the microfluidic matrix chip. A pair of forward and reverse primers is designed for each individual exon variants of *Drosophila* Dscam gene. (12 pairs for exon 4, 48 pairs for exon 6, 33 pairs for exon 9; exon

17 is passed because it is far away from more interested sites.) In total, this set is composed of 93 forward primers and 93 reverse primers. The quested cDNA sample can be included in the mother solution and amortized to all the reactions along with DNA polymerase. Then performing quantitative matrix PCR reactions on four chips (M48 × 48, supplied by Fluidigm) allows us to plumb all the combinations of forward and reverse primers (93x93). Essentially, the tests with complete combinations of forward and reverse primers can tell us not only the presence of individual exon variants, but also the information of which exon variants link together with one another (that is, signature of individual isoforms, as schemed in figure 13). In addition, our approach may provide quantitative information of the abundance of individual Dscam transcript. In brief, our approach of matrix PCR offers the crucial benefits as follows: isoforms orientated, high throughput, minimum hands-on processing, quantitative results, and super detection limit down to a single transcript. Our approach is a perfect tool for decoding the mystery of *Drosophila* Dscam isoforms. In the future, the application of this approach might be extended to various gene expression studies, including quests for unknown genes.

***Table 1*:** Throughputs using matrix chip (48×48) and conventional 96-well microplates.

	48 × 48 Matrix	96- well microplate
Required number of devices	4	92
Required pipetting operations	384	17664
Required reagent volume (μL)	92[a]/1,920[b]	176,640[c]
Required time (hour)	10	230

[a]: 92 µl is the total volume of all the micro reactors (10 nl each) of the chips;

[b]: 1920 µl is calculated including the reagent overhead. (5 µl for each input hole);

[c]: 176640 = 8832 x 20 µl/each well.

Table 1 shows that the efficiency of our approach is matchless. Briefly, nearly 9000 independent PCR assays are required for a complete test of one sample. 4 matrix chips (48×48 arrays) can make a complete test, but it would require around 92 microplates with much more complicated pipetting operations to perform these assays. The method of microplates would require such a large volume of reagents/samples, which is technically and financially impossible. The experiment using matrix chips can be finished in one day; but it would require weeks if using microplates. Other available techniques include clone sequencing[92], DNA microarrays[95], and polymerase colony (Polony)[99] suffer from serious drawbacks. Clone sequencing is inherently a blind test and a procedure of very low throughput. The method of using DNA microarrays is out of focus, only providing the information of separate exon variants instead of the isoforms. The method of Polony is technically unavailable because it would require more than 90 rounds of repeated processing of hybridization and dehybridization. To our knowledge, the approach of matrix PCR is the best tool for decoding the mystery of Dscam isoforms.

A Qualitative View and Mathematical Perspective

We find out a one-to-one correlation between the mixture of transcripts by alternative splicing and the signal pattern from matrix PCR experiments, which is an essential element

of our approach. figure 14 schemes this one-to-one correlation using a subset of representative sequences of the *Drosophila* Dscam isoforms.

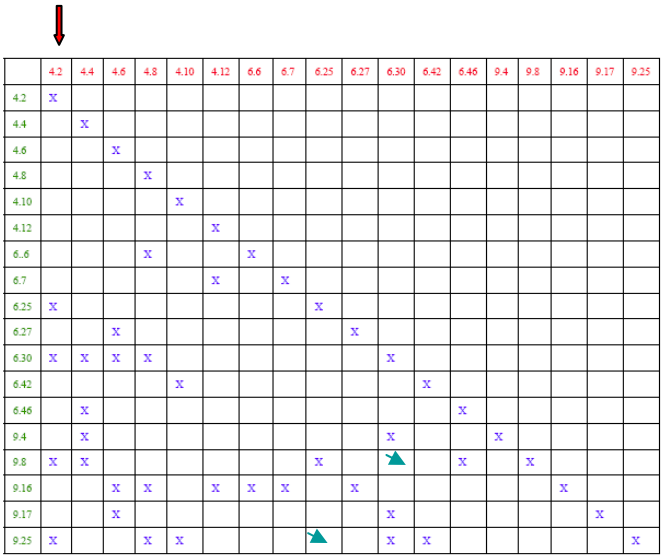

cDNA	Exon 4	Exon 6	Exon 9
20	4	46	8
46	10	42	25
18	4	30	4
27	6	30	17
41	8	30	25
26	6	27	16
8	2	25	8
48	12	7	16
39	8	6	16
Touchstone	2	30	25

Figure 14: *One-to-one correlation between the mixture of transcripts and the signal pattern from matrix PCR experiments. The table (on the right) lists the exon identification of the isoforms which are numbered consistently with the original research article. In the signal pattern (on the left), the forward primers for individual exons are in red (X-axis), while the reverse primers are in green (Y-axis). Positive signals are marked by x, while negative signals are left blank. A putative cDNA which has not been reported is added to the subset of selected isoforms on purpose as a touchstone of our proposed method. The red and green arrows are indicators (see text).*

The table on the right lists the exon identification of the isoforms which are numbered consistently with the original research article (the first column). Assuming that we prepare a cDNA sample containing exactly this subset of isoforms (10) and perform matrix PCR on

the chip, we should obtain the signal pattern from the reactions, as shown by the table on the left of figure 14. In this signal pattern, the forward primers for individual exons are in red (X-axis), while the reverse primers are in green (Y-axis). All the appropriate combinations of primer pairs templated by the corresponding cDNA produce positive signals. These reactors are marked by x in the table of signal pattern. On the contrary, those reactors containing inappropriate primer pairs will serve as negative controls, represented by blanks in the table. This signal pattern has been simplified by erasing certain rows (reverse primers) and columns (forward primers) because the corresponding exons are not expressed in any transcript of selected subset. The reactors on the upper-right of the diagonal are always blank because all of them contain inappropriate primer pairs.

On the other hand, assuming that we have obtained such a table of signal pattern from a blind test, we can devolve all the cDNA isoforms completely based on the information from the table. For example, we observe five positive signals in the column of forward primer 4.2 (red), indicated by the red arrow. This information can be deduced to include four potential isoforms, (a) 4.2-6.25-9.8, (b) 4.2-6.25-9.25, (c) 4.2-6.30-9.8, (d) 4.2-6.30-9.25. But it is not necessary that all the four potential isoforms exist in the sample. As we notice only two positive signals in the column of forward primer 6.25 (red), we can immediately rule out one putative isoform (b) 4.2-6.25-9.25, because an addition positive signal (indicated by the green arrow at the red 6.25 and green 9.25) would be expected if there were the putative isoform (b). Therefore, it is sure that the isoform (a) 4.2-6.25-9.8 should exist in the sample. In fact, the cDNA (8) in the table of isoforms confirms our deduction. Similarly, after we combine all the information in row 9.4 (green), column 4.4

(red), row 9.17 (green) and column 4.6 (red), we should be able to tell the existence of isoforms (d), which is the cDNA (touchstone) in the right table. With similar processing all the other initial isoforms in the selected subset can be devolved from the signal pattern exactly. To draw an analogy, the deduction in our approach is somewhat similar to solving a "sudoku puzzle" game.

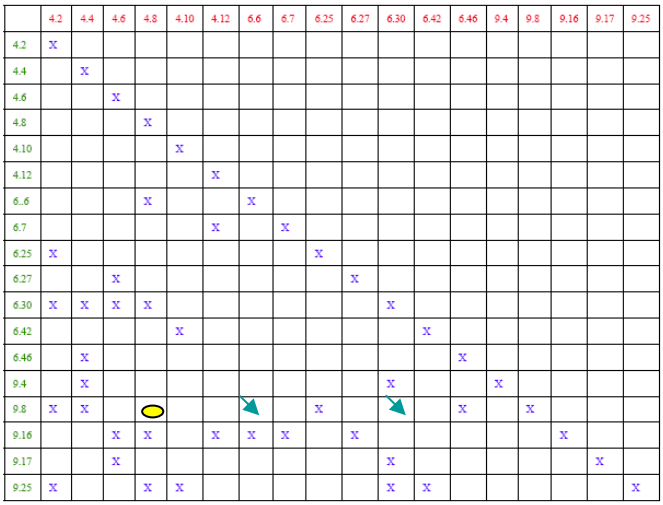

Two putative isoforms:
4.8-6.6-9.8
4.8-6.30-9.8

cDNA	Exon 4	Exon 6	Exon 9
20	4	46	8
46	10	42	25
18	4	30	4
27	6	30	17
41	8	30	25
26	6	27	16
8	2	25	8
48	12	7	16
39	8	6	16
Touchstone	2	30	25

Figure 15: *Schematic showing our approach can screen out false signals. The yellow oval and green arrows are indicators (see text).*

Interestingly, our approach is able to screen out some false signals from the experiment using the redundant information of the signal pattern. Assuming a random false positive signal occurs in the reactor (indicated by the yellow oval at red 4.8 and green 9.8), it may add two more putative isoforms (e) 4.8-6.6-9.8 and (f) 4.8-6.30-9.8 when we read out the column 4.8 (red). However, after we consider the negative signal in the reactor (the green arrow at red 6.6 and green 9.8), we can determine that isoforms (e) is not expressed in the

selected subset. Similarly, putative isoform (f) can be ruled out by reading out the reactor (the green arrow at red 6.30 and green 9.8). Of course, the tolerance of false signals of our approach is not unlimited. For example, if there happen to be another false positive signal in the check reactors, or distinct isoforms composed of 4.X-6.6-9.8 or 4.X-6.30-9.8 are expressed in the sample, then either of the above two putative isoforms can not be ruled out. In practice, repeated experiments should be performed to reduce the uncertainty of false signals to a minimum level.

Ultimately, our goal is to read out the information of the signal pattern of matrix PCR and determine which transcript isoforms by alternative splicing are expressed, and the abundance of individual transcript isoforms in a pool of mRNA. A gene is treated as a set of exons G = $\{E_1, E_2, E_3, E_4, E_5, \cdots, E_n\}$, with each alternative splicing transcript isoform containing a subset of the exons. And we define a vector $\hat{t}$ for each transcript as follows:

Transcript 1 = $\{E_1, E_2, E_5, \cdots, E_{n-1}, E_n\}$, $\hat{t}_1$ = (1, 1, 0, 0, 1, 0, 0, …, 1, 1)

Transcript 2 = $\{E_2, E_3, E_4, \cdots, E_{n-1}\}$, $\hat{t}_2$ = (0, 1, 1, 1, 0, 0, 0, …, 1, 0)

…

Transcript m = $\{E_1, E_3, E_4, \cdots, E_{n-2}, E_n\}$, $\hat{t}_i$ = (1, 0, 1, 1, 0, 0, 0, …, 1, 0, 1)

Then we use A_i to represent abundance of each transcript $\hat{t}_i$.

$\sum_{i=1}^{m} A_i \hat{t}_i$ is the sum of all transcripts in the sample weighted by their abundance.

If we define n column vectors such as: $e_1 = \begin{pmatrix} 1 \\ 0 \\ \dots \\ 0 \end{pmatrix}$, $e_2 = \begin{pmatrix} 0 \\ 1 \\ \dots \\ 0 \end{pmatrix}$, …, $e_n = \begin{pmatrix} 0 \\ 0 \\ \dots \\ 1 \end{pmatrix}$, and a matrix

$$B = \begin{bmatrix} b_{11} & b_{12} & \dots & b_{1n} \\ b_{21} & b_{22} & \dots & b_{2n} \\ \dots & \dots & b_{jk} & \dots \\ b_{n1} & b_{n2} & \dots & b_{nn} \end{bmatrix}$$ to represent the signals from the reactions,

Then we can obtain equations:

$\sum_{i=1}^{m} A_i \hat{t}_i \bullet e_1 = b_{11}$, which means the number of occurrence of exon1 in the sample.

$\sum_{i=1}^{m} A_i \hat{t}_i \bullet e_n = b_{nn}$, and so on.

$\sum_{i=1}^{m} A_i (\hat{t}_i \bullet e_j)(\hat{t}_i \bullet e_k) = b_{jk}$, which is corresponding to the PCR product primed by the forward primer (k) and reverse primer (j). Note when k>j, $b_{jk} = 0$.

Furthermore, if we define another vector $\vec{t}_i = \hat{t}_i / \sqrt{A_i}$, and transform the equation, then

$$\sum_{i=1}^{m} A_i \left(\hat{t}_i \bullet e_j\right)\left(\hat{t}_i \bullet e_k\right) = \sum_{i=1}^{m} \left(\vec{t}_i \bullet e_j\right)\left(\vec{t}_i \bullet e_k\right) = \sum_{i=1}^{m} t_{i,j} t_{i,k} = \sum_{i=1}^{m} \left(t_{j,i}\right)^{transpose} t_{i,k} = b_{j,k},$$

which can be rewritten briefly as $T'T = B$.

Therefore, decoding the mystery of Dscam isoform transcripts is essentially involved with finding a solution to the above equation, where B is a known, n×n, symmetric, and sparse matrix with values corresponding to fluorescent intensities of PCR assays from our chips. T is a non-negative matrix representing alternative splicing vectors. Currently we are working on a Matlab code to factorize the matrix B with an algorithm of nonnegative matrix factorization (NMF). The algorithm starts by randomly initializing matrices T and T transpose, and then iteratively updates them to minimize a divergence functional[100, 101]. The Matlab code has passed our preliminary tests.

Concluding Remarks

We have developed an important approach of applying matrix PCR for gene expression studies. We have obtained quantitative profiles of the lola gene isoforms at different developmental stages of fruit fly. The information can be conveniently extracted to include absolute abundances of expressed genes in individual cells. Quantitative expression profiles of lola isoforms will be very useful in understanding how this transcription factor is involved with regulating downstream neural activities. We have developed a theoretical method to devolve extremely diverse Dscam isoforms by alternative splicing in fruit fly. To our knowledge, this method represents the best tool for decoding the mystery of Dscam

isoforms. We also wish to point out a possible expansion of using matrix PCR in a more general case. Our approach of matrix PCR can be useful to map exons, to profile transcripts, or to explore unknown genes in the future.

Chapter 5

MICROFLUIDIC CHAOTIC MIXING FOR DNA MICROARRAYS

Introduction

Nucleic acid hybridization techniques have been widely used in both fundamental and clinical research to identify genes and mutants, to map their correlations, and analyze their expression. DNA microarrays immobilize thousands of oligonucleotides, cDNA clones or PCR products on the solid substrate, thus providing a powerful tool for large-scale detection of target genes[16, 102]. However, hybridization in conventional microarray experiments is performed in a diffusion-limited manner, which is quite inefficient. The hybridization process may take 8 to 24 hours, during which period the characteristic distance (1 or 3 mm, table 1) that a target DNA molecule can diffuse is still one order of magnitude less than the typical size of most microarrays (>10 mm)[103, 104]. This chapter describes an effective solution to that problem using microfluidic chaotic mixing. Our polydimethylsiloxane (PDMS) devices use integrated peristaltic pumps to circulate the solution between two large chambers, while chaotically mixing the components of the solution in bridge channels at the same time. We have demonstrated that this approach is able to dramatically enhance hybridization signals and improve sensitivity by nearly one order of magnitude, compared with the conventional static hybridization method for the same duration time. Alternatively, for a desired sensitivity, dynamic mixing can be used to accelerate the hybridization process by a factor of 3 or more. This approach offers many

benefits, including high sensitivity, rapid results, better reproducibility, low cost, compatibility with commercial microarray slides, and ease of large-scale integration.

***Table 1*:** Distances of DNA fragments by passive diffusion (estimated with $(2Dt)^{0.5}$)

	Diffusion Coefficient (cm^2/s)	1 hour	12 hours
25-mer	$1.3x10^{-6}$	0.97 mm	3.4 mm
250-mer	$2x10^{-7}$	0.38 mm	1.3 mm
1000-mer	$8x10^{-8}$	0.24 mm	0.83 mm

Challenge

Hybridization of DNA microarray experiments is generally performed with a small volume (< 50 mL) of solution containing target DNA molecules, in an effort to cover a large area of substrate surface immobilized with probes. Therefore, the hybridization chambers are designed to be very thin, typically around dozens of microns. The rationale behind the design is to increase the valid concentration of target DNA molecules by reducing the sample volume, while hybridizing as many printed features as possible. This design also allows target DNA molecules to travel shortened distance from the bulky solution to the substrate surface. However, the Reynolds number in such thin chambers is very low, ranging between 0.0002 and 0.04 in most cases.

$$\mathrm{Re} = \frac{\rho V D}{\mu},$$

where ρ is the density of fluid; V and D are a fluid characteristic velocity and distance; μ is fluid viscosity. Thus laminar flow, which is notorious for its inefficiency in mixing, plays a dominant role if there exists any movement of fluid. Subsequently, once the solution is loaded into the hybridization chambers, it is very difficult to mix individual components of the solution again. On the other hand, local depletion of target DNA molecules occurs after a period of hybridization, compromising the chances of DNA samples to equally react with all the probes of the microarray.

The fundamental challenge faced by DNA microarray practitioners is to continuously mix a sample solution at low Reynolds number and transport the DNA molecules to the proximity of the probes more rapidly than diffusion alone, thereby increasing valid molar hybridization events. There have been many methods of active mixing developed, including surface acoustic wave micro-agitation[105], bubble-induced acoustic microstreaming[103], alternative convection induced through several ports[104], "drain and fill" or air driven bladders[106, 107], magnetic stirring bar[108], and shuttling sample plugs in a serpentine microtrench[109]. Some researchers developed electrokinetic methods to accelerate the transportation of DNA molecules[110-112]. While these methods have all allowed reduced hybridization time and improved signals, they appear to suffer from either one or several shortcomings as follows: inhomogeneous mixing[103-105], small arrays[110-112], relatively lower sensitivity level[103, 104, 106, 108-112], or incompatibility with the widely used Cy dye microarray format[110-112].

On the other hand, chaotic mixing has gained the interests of many researchers as a promising method to mix solutions in microchannels[113-115]. Those designs are featured with a chain of repeating units with customized profile of the microchannel, which can introduce a three-dimensional flow with stretching and folding the streams of individual components of the solution. Therefore chaotic mixing can be realized in a fashion of steady, passive flow in the microchannel without additional actuation of the device.

Chip Design and Fabrication

We have developed a microfluidic device to meet the challenge of DNA microarray experiments, while maintaining compatibility with the widely used microarray format. The silicone rubber device can be conveniently sealed onto a printed microarray slide to perform dynamic hybridization. It is composed of two layers, integrated with valves, pumps, and active mixing elements[116].

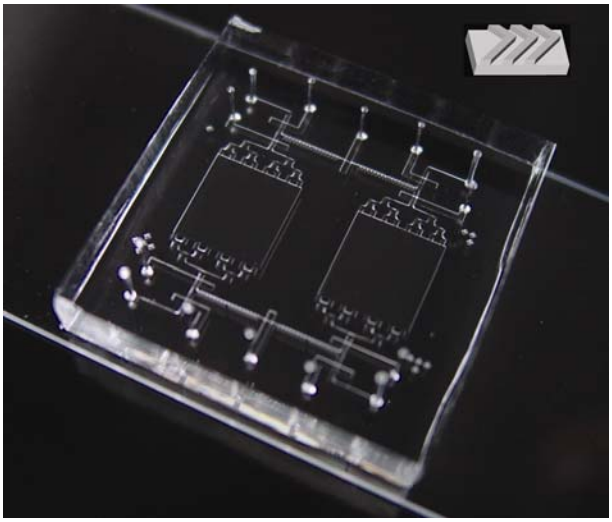

Figure 1: *Optical micrographs of the PDMS device sealed on a glass slide (25mm×7.5mm). The inset on the upper right corner schemes the 3D structure of the bridge channel with herringbone indentations. The size of each chamber is 6 mm×6.5 mm×65 micron.*

As shown in figure 1, the fluidic layer of the device contains two symmetric hybridization chambers (6mm×6.5mm×65 microns, 5㎖). They are connected to each other by bridge channels, whose ceiling incorporates indentations with a herringbone pattern to produce chaotic mixing[114]. The bridge channels (400 microns wide, 40 microns high) are adapted to the chambers with bifurcating channels to equalize the solution distributed into the chambers after mixing. Four input/output through-holes with corresponding micromechanical valves are used for loading samples or disposing waste solutions. These valves are actuated to form closed chambers during hybridization. Additionally, two sets of peristaltic pumps[56] are integrated to circulate the fluid between the hybridization chambers. The design allows different components in the solution to mix in a chaotic manner when they pass through the bridge channels, and then to be delivered through the hybridization chambers. The images (figure 2) show that effective mixing of colors occurred in the bridge channel with the herringbone indentations, producing a mixed color of brown. It is known that the blue and red colors would not mix well in a plain microchannel or microchamber because laminar flow is dominant. The peristaltic pumps create a fluid flux of 5.2 nL/sec. It takes about 16 minutes to complete one round of circulation between the two chambers. The flux can be further raised by increasing the cross-sectional area of the individual pumps.

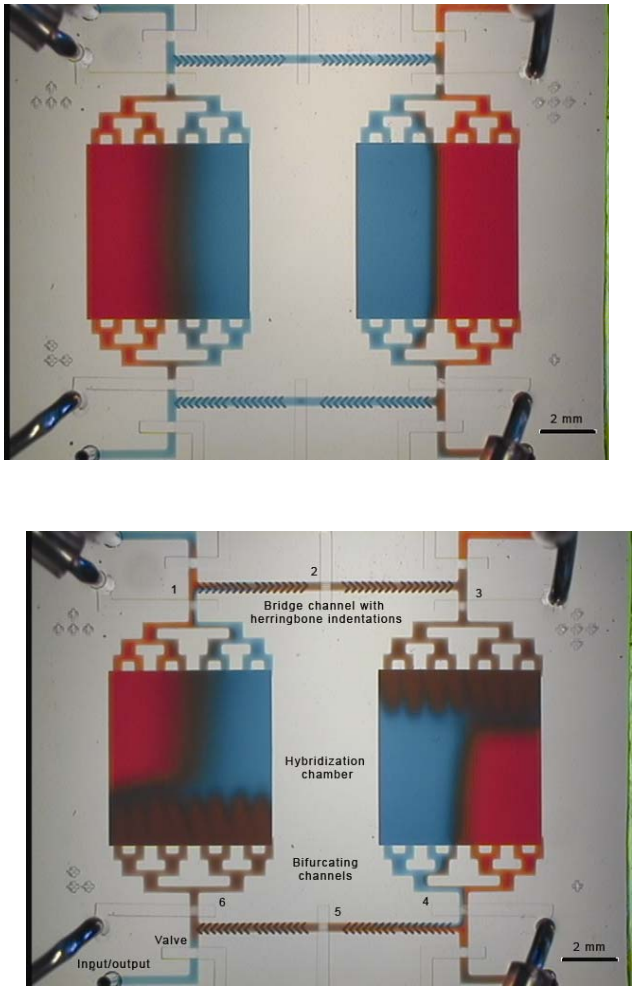

Figure 2: *Chaotic mixing of food colors. The chambers were loaded half with the red and half with the blue color. The peristaltic pumps (123, 456) circulated the solutions clockwise in the device. The herringbone indentations in the bridge channel produced chaotic mixing of the colors.*

The device has some unusual geometrical features, compared with other microfluidic devices that our lab fabricates in a routine procedure. These include thicker and wider channels, and as well as larger chambers. Thicker and wider channels allow more efficient transportation of fluid between the chambers during circulation. Many geometrical

parameters should be taken into account together in designing to make a workable device. The most important ones include the aspect ratio of channels, cross-sectional area of valves and thickness of the thin membrane. If the aspect ratio of the channel falls into the range of 8 (up to12) : 1 (width : height), it is generally safe with the minimum chance of collapse, while maintaining workable valves. Choices of cross-sectional area of valves can be determined by testing combinations of control channels and flow channels of different widths (figure 3).

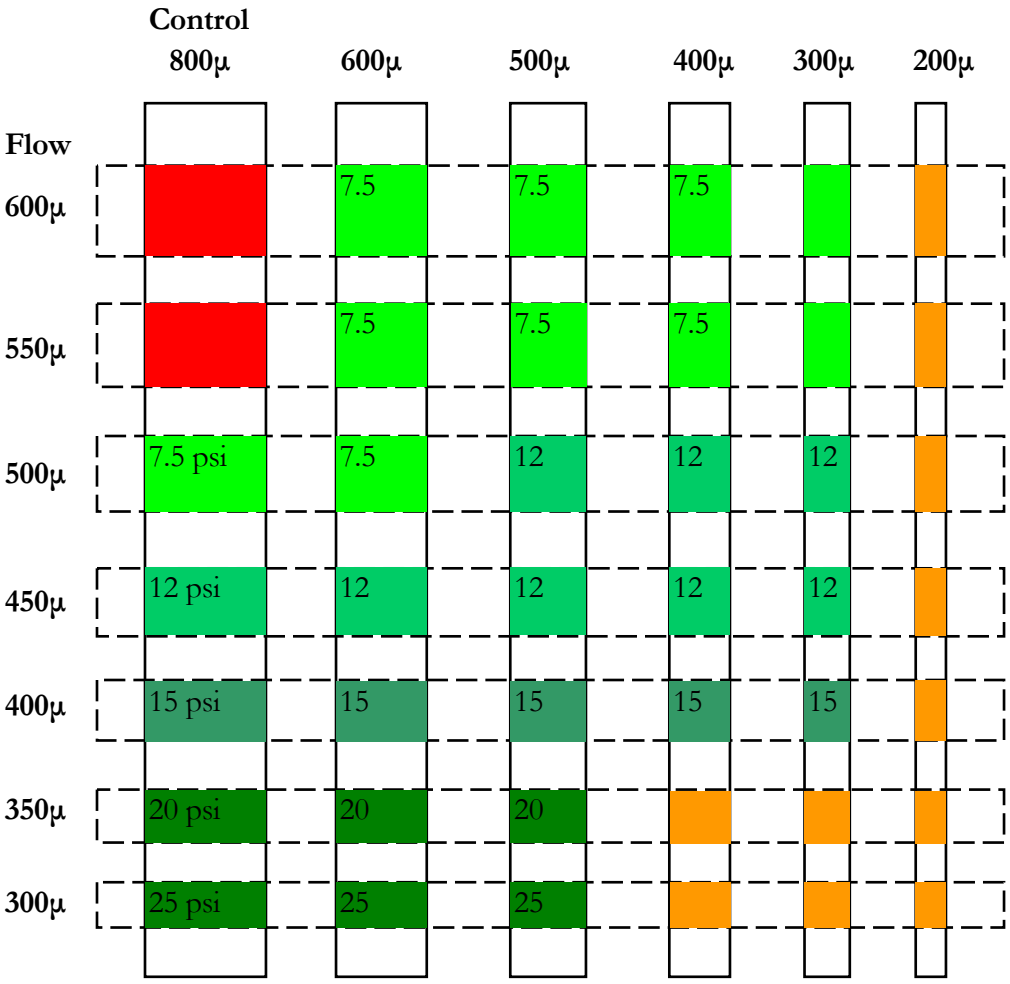

Figure 3: *Valve tests with combinations of flow channels and control channels of different widths. Columns: control channels; rows: flow channels; color rectangles: cross-sectional area of valves. Red: collapsed valves; green: workable valves with different switch-off pressures in the unit of psi; orange: nonworkable valves. The flow channels are approximately 40 microns high. The PDMS flow layer was spun with 1500 RPM for 25 seconds.*

As a brief review, the flow channel is designed to be 400 microns wide, and 40 microns high; the cross-sectional area of valves is 400 microns (flow) by 500 microns (control). The thickness of the thin membrane can be controlled by the speed of spincoating. In this project, it has been demonstrated that a single chamber can cover an area as large as 36mm ×7.5mm without collapse. The shape of the area matters. Given the same area, a rectangular shape has a better chance of reducing collapse than a shape of square.

The mold of control layer (50μm high) can be prepared using photoresist SU-8 with suggested protocol from the manufacturer (Microchem Corp.). The mold of flow layer can be prepared by two steps using photolithography. I developed a protocol using positive photoresist such as SJR 5740 (Shipley Corp.) to prepare thick features (up to 40 microns high) on the silicon wafer. Some features on the flow mold must be prepared with positive photoresist so that they can be rounded by heating to avoid leaky valves. After hard baking photoresist SJR 5740 at 180 ^{o}C for 2 hours, it becomes invulnerable to organic solvents. And then a second procedure of photolithography using Su-8 can be performed to prepare the remaining features, including the chambers on the wafer and the herringbone protrusions on the features of photoresist SJR 5740.

Evaluation of Mixing Efficiency

The efficiency of mixing was evaluated by loading the each chamber half with the blank solution and half with the solution containing fluorescent beads, actuating the pumps, and performing fluorescence measurements. A fluorescent inverted microscope with a CCD camera was set up to take images of the device. Chaotic mixing was confirmed by independent observations of the beads' zigzag motion and crossing one another through the bridge channels (images not shown). Ten windows along the equator of one chamber were specified to monitor the fluorescent intensity in real time. As shown in figure 4a and figure 4b, within minutes chaotic mixing dramatically reduced the fluorescence gradient along the equator. The control experiment followed all the same conditions except for using a device without the herringbone indentations on the bridge channels. In this case (figure 4c and figure 4d), the fluorescence difference along the equator was still substantial after a circulation of the solutions for 2 hours, owing to the absence of effective lateral mixing. Therefore, the chaotic mixing introduced by the herringbone indentations is critical in homogenizing the solutions into the chambers. Ripples in fluorescent intensity were observed (figure 4a and figure 4c) because the extra blank solution initially loaded in the bridge channels took part in the fluid circulation. Interestingly, they became a good index of the periodicity of the circulation (about 8 minutes/ripple). In these experiments, a home-written program in Labview was used to control the movable stage of the microscope. After the PDMS device was mounted on the stage and loaded with the solutions, the coordinates of ten windows were recorded along the equator of one chamber. Other parameters can be specified in the program, such as the periodicity of moving the stage. After each round of

scanning, the device was moved far away from the illumination in order to reduce the effect of bleaching. The images were taken automatically with a periodicity of 95 seconds on average. Each image recorded a window of 340 microns by 260 microns with the format of bmp file. And then the mean values of fluorescent intensity of individual images can be measured and normalized, as shown in the figure 4.

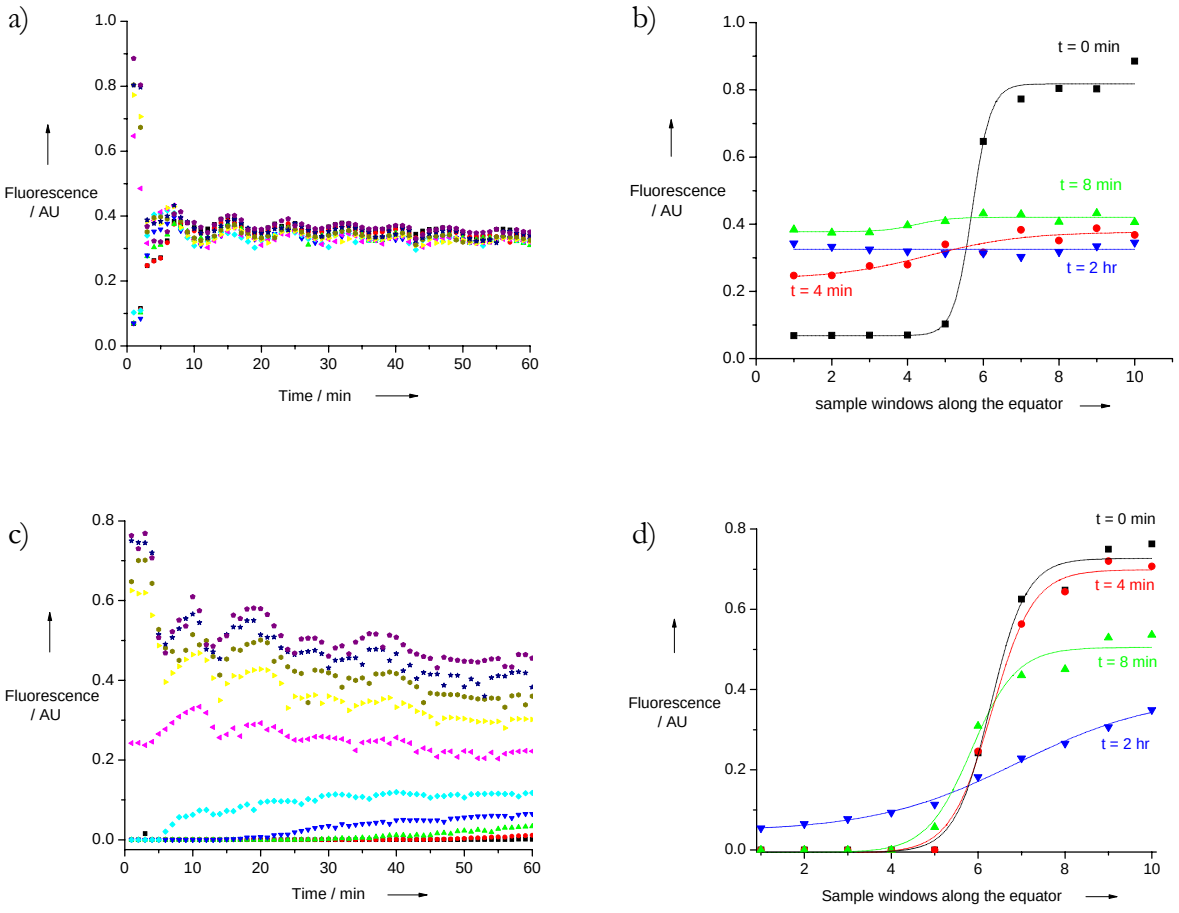

Figure 4: *Evaluation of mixing efficiency of two different devices with (a and b)/ without (c and d) the herringbone indentations in the bridge channels. A solution containing 0.1m fluorescent beads and a blank solution were loaded into the chambers with a pattern*

similar to figure 2a. Ten windows along the equator of one chamber were specified to monitor the fluorescent intensity changes in real time. figure 4a (with chaotic mixing) and figure 4c (without chaotic mixing but with circulation) compare the fluorescent changes of these windows in the time course. figure 4b and figure 4d show different gradient curves at four specified moments (0 min, 4 min, 8 min, 2 hours). Chaotic mixing is much more effective at eliminating heterogeneity in the solution than simple circulation. The Stokes-Einstein diffusion coefficient of 0.1 m beads was estimated to be 4.4x10^{-8} cm^{2}s^{-1}, within the comparable range of DNA molecules (1k bp).

Fluorescent beads with a diameter of 100 nm were taken into use in these experiments. The Stokes-Einstein diffusion coefficient of 100 nm beads was estimated to be 4.4 x 10^{-8} cm^2s^{-1}, within the comparable range of DNA molecules of 1k base pairs (table 1)[117].

$$D = \frac{k_B T}{6\pi\mu\sigma},$$

where μ is the viscosity of suspending fluid; σ is the sphere's radius.

Indeed, the behavior of passive diffusion of these beads was examined in the chambers of our devices. We measured the time for the beads to diffuse cross a certain distance in the chamber. The experimental result (4.7 x 10^{-8} cm^2s^{-1}) matches the calculation using the formula of Stokes-Einstein diffusion coefficient very well.

Preparation of Microarrays and Labeled cDNA Samples

Arrayers (Cartesian Tech microarray workstation and Labnext Xact microarrayer) were used to prepare home-spotted microarrays with Epoxy slides (VEPO-25C, CEL Associates, Inc.). 70-mer DNA oligonucleotides of interested genes were modified with amino-C6 group at 5' ends, which can be ordered from Qiagen or Operon. The sequences of the oligonucleotides are available in the appendix. Typically the solution contains 20 mM oligonucleotides for printing. Some researchers reported that surface probe density higher than 2.0×10^{12} molecule/cm^2 actually reduced the efficiency of target/probe hybridization[118]. Therefore it is advisable to avoid using too concentrated oligonucleotides during spotting. As shown in figure 5, the lone electron pairs of the primary amino group attack the electrophilic carbon on the epoxide group, immobilizing the DNA molecule onto the substrate by a covalent bond. Without additional modification, oligonucleotides, cDNA or RNA molecules contain primary amino group on A, G, and C residues, which are also available to covalently bind to the substrate. However, the modified oligonucleotides produced stronger signals in hybridization, indicating a better controlled surface chemistry in the process of immobilization. As shown in figure 5, the lone electron pairs of the primary amino group attack the electrophilic carbon on the epoxide group, immobilizing the DNA molecule onto the substrate by a covalent bond. Without additional modification, oligonucleotides, cDNA or RNA molecules contain primary amino group on A, G, and C residues, which are also available to covalently bind to the substrate. However, the modified oligonucleotides produced stronger signals in hybridization, indicating a better controlled surface chemistry in the process of immobilization.

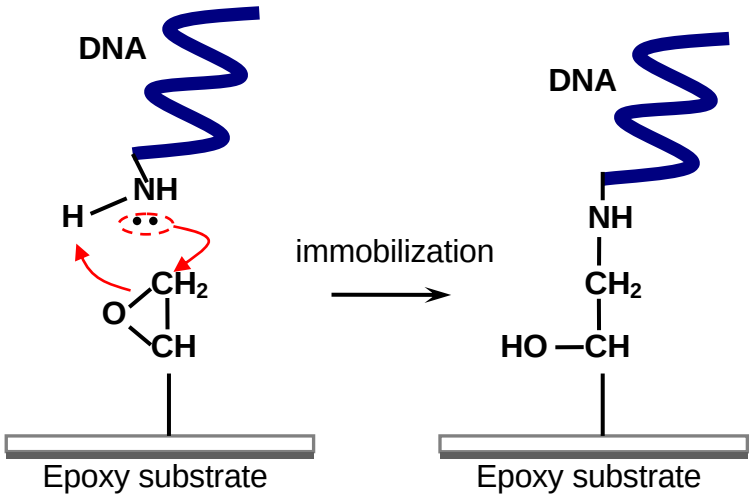

Figure 5: *Schematic of immobilization of a DNA molecule onto the epoxy substrate*

After printing, the slides were kept in a well-sealed plastic box overnight, saturated by water vapor (with salt slurry). Elevated temperature (37 ^{o}C) may facilitate bonding between the printed DNA molecules and the substrate. And then the slides were treated with the following procedures (2 x SSC + 0.1% SDS, 2 minute; 2 x SSC, 2 minute; Boiling DI water, 1 minute; Ice-bathed ethanol, 1 minute). Two PDMS devices were sealed onto a single home-spotted microarray slide, covering areas of identical probe patterns. Each area consisted of four identical blocks. As shown in figure 7a or figure 7b, every block included 18 features (6 spotting solutions repeated 3 times). Six of them were negative control features.

We prepared Cy3-labeled cDNA from the C2C12 mouse skeletal muscle cell line, adding *A. thaliana* CAB spikes (cat # 2552201, Stratagene) as a positive control. Details of total RNA isolation, mRNA extraction, and the reverse transcription protocols have been

described elsewhere[119]. Preparation of samples should be processed in an RNase-free environment to reduce the degradation of RNA samples. A method of indirect labeling was primarily put into use. This method can incorporate aminoallyl labeled nucleotides into cDNA during synthesis, and then couple cyanine fluorescent molecules to the aminoallyl groups in the subsequent step. Another method of direct labeling of cDNA also worked well (see the section of discussion). Nucleotides and cyanine molecules in the labeled cDNA can be analyzed using:

$$nucleotides = \frac{OD_{260} \times volume \times 37 \times 1000}{324.5},$$

$$Cy3 = \frac{OD_{550} \times volume \times 1000{,}000}{150{,}000 \times 1},$$

$$Cy5 = \frac{OD_{650} \times volume \times 1000{,}000}{250{,}000 \times 1},$$

where 324.5 pg/pmol is average molecular weight of a dNTP; 1 OD_{260} = 37 ng/**m**L for cDNA; The extinction coefficients of Cy3/Cy5 are 150,000 $cm^{-1}M^{-1}$ and 250,000 $cm^{-1}M^{-1}$, respectively. The length of the cuvette is 1 cm. The unit of the volume is microliter. The number of one thousand (or one million) is introduced to compensate the difference between picogram and nanogram (or between micromolar and molar).

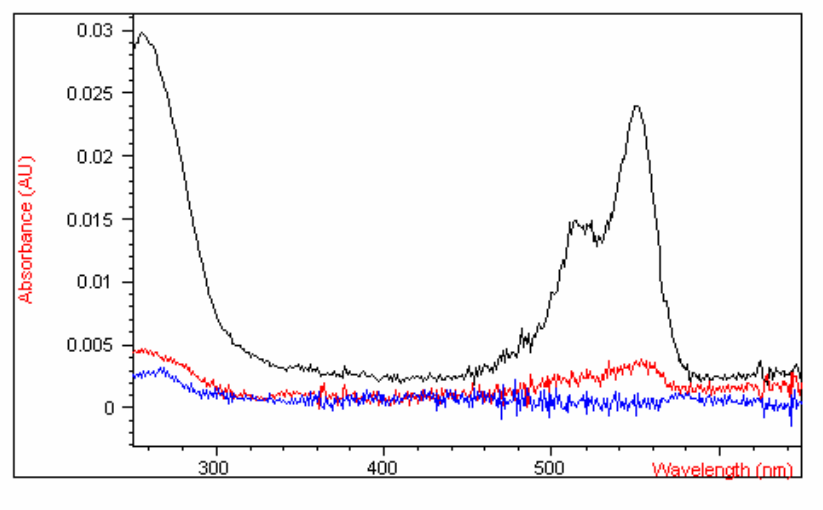

Figure 6: *UV/visible spectra of the Cy3 labeled cDNA. The sample was dried under vacuum spin and then suspended with DI water, making a series of diluted solutions. Black curve: diluted by 100 times; red curve: diluted by 1000 times; blue: diluted by 10000 times. The absorbance values at 260 nm and 550 nm were used to calculate molecules of nucleotides and Cy3 dye in the labeled cDNA sample.*

figure 6 shows the UV/visible spectra of labeled cDNA samples in dilutions. Typically there was a cyanine molecule incorporated in every 20 or 30 nucleotides of the cDNA sample. The cDNA sample was diluted into a series of solutions and then aliquoted. They were spin-dried under vacuum and kept in 4 ^{o}C before use.

Dynamic Hybridization with Homemade Microarrays

A series of dynamic and static (control) hybridizations were performed for the purpose of comparison. Two identical aliquots were used to prepare the hybridization solutions with ArrayHyb buffer (A-7718, Sigma-Aldrich Co). They were loaded into the PDMS devices

sealed on the shared slide, which had been mounted on the flat bed of a thermocycler (PTC-200, MJ Research) and pre-hybridized (5X SSC, 1% BSA, 0.1% mg/mL denatured salmon sperm DNA, 0.1% SDS, at 44 ^{o}C for 1 hour). Dynamic hybridization was performed by actuating the peristaltic pumps in one of the devices; while static hybridization was performed in the other device as a control. After a hybridization at 52 ^{o}C for 2 hours (or other specified duration time), the PDMS devices were peeled away from the slide. The slide was immediately removed into a plastic tube for programmed post-hybridization washing (4X SSC+0.1% SDS at 46 ^{o}C for 20 seconds for twice; 1X SSC+0.1% SDS at 57 ^{o}C for 3 minutes, and then repeat the step with fresh solution; 0.2X SSC at room temperature for 1 minute; 0.1X SSC at room temperature for 1 minute, using AdvaWash 400, Advalytix). The slide was then spin-dried using a centrifuge (5804R, Eppendorf) and scanned (ArrayWorx, Applied Precision LLC) to obtain fluorescent images.

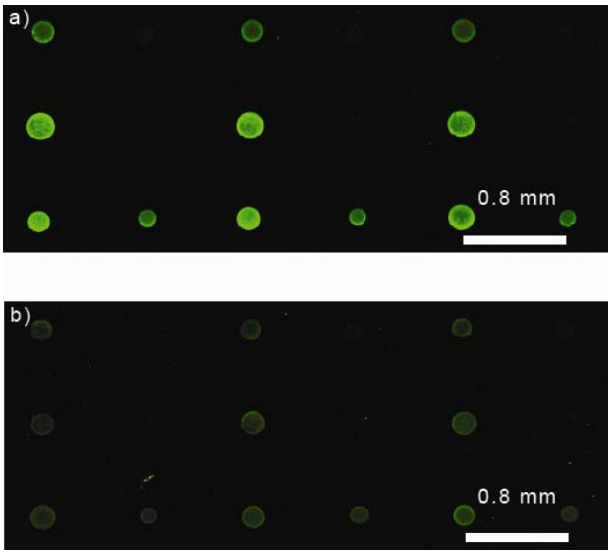

Figure 7: *Signal improvement by microfluidic chaotic mixing. (a) and (b) show one out of four identical blocks of the home-spotted microarray. (a) Dynamic. (b) Static. Typically the diameter of features is around 200 microns.*

As shown in figure 7, hybridization using microfluidic chaotic mixing produced stronger signals, compared with the static control. After we analyzed the data from a series of "side-by-side" experiments, we obtained figure 8, showing that dynamic hybridization also achieved better sensitivity and reduced the required time for hybridization, than the static control.

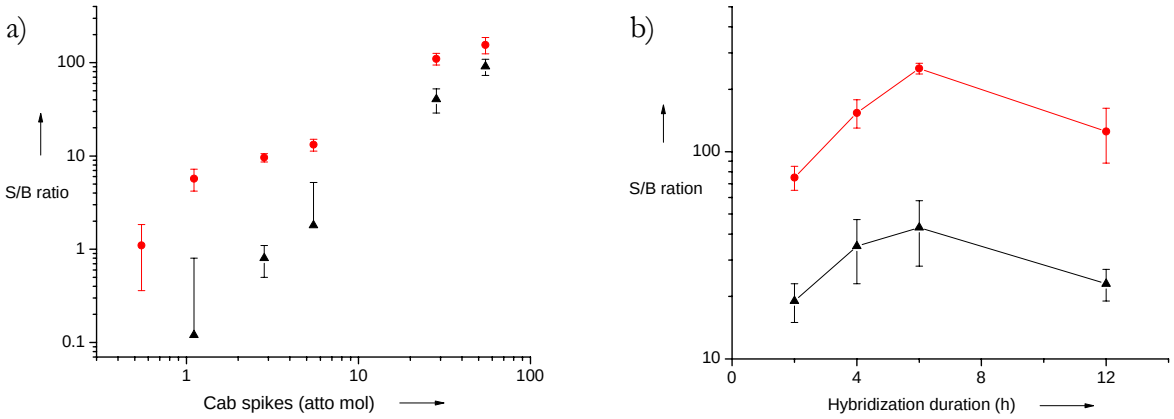

Figure 8: *(a) The titration curves with positive spikes (CAB gene). (b) The hybridization kinetics, data analyzed from the features of myosin light chain sense. In the above figures, red dots represent dynamic hybridization, while black triangles symbol static control. The signal-to-noise ratio or S/N ratio is calculated as the mean of the fluorescent signals subtracted by the mean of the background, then divided by the standard deviation of the background.*

When the input molecules of CAB spikes were reduced to 5.5 attomol, the signal-to-noise ratio of the static method was slightly larger than 1, indicating that the signals were nearly indistinguishable from background at that point. However, the S/N ratio of dynamic hybridization did not collapse to 1 until the input CAB molecules further decreased to 0.55 attomol. There is an enhancement in sensitivity of nearly one order of magnitude by comparing the two titration curves around the S/N ratio of 3. To our knowledge, the sensitivity level using our approach is better than any other reported method designed for active mixing in hybridization. The above enhancement of signals was reproducible, confirmed by independent hybridization experiments. Active mixing also reduced the spot-to-spot fluctuation of signals. The coefficients of variation (CV) of the dynamic hybridization were reduced to nearly half of the values of the conventional static method, as shown by Table 2 and also indicated by figure 8a.

***Table 2*:** The spot-to-spot CVs (n=12) of dynamic vs. static hybridization.

	Dynamic hybridization	Static Hybridization
myogenin sense	0.11	0.18
MCK sense	0.08	0.27
myosin light chain sense	0.12	0.24
CAB (positive control)	0.10	0.23

The features of negative control were spotted using a blank buffer and a solution containing oligonucleotides for the A. thaliana RCA gene (not spiked in the sample). CAB = chlorophyll a/b-binding protein, MCK = muscle creatine kinase.

Hybridization kinetics results (figure 8b) showed that dynamic mixing produced signals with higher S/B ratios than the static method consistently. The signal of dynamic hybridization for 2 hours was nearly twice than its static control hybridized for 6 hours. We noticed that the signals of both methods decreased after a longer hybridization (>6 hours), which might be attributed to partial dehydration of the arrays because the PDMS material is known to be permeable to water vapor.

In order to evaluate the separate contributions of the signal enhancement by circulatory motion of the fluid and by chaotic mixing, we independently performed comparison experiments which included an additional hybridization control with fluid circulation but without chaotic mixing. Identical aliquots of DNA target solutions were hybridized at 52 ^{o}C for 2 hours in three conditions: static (control 1), simple fluid circulation using the devices without the herringbone indentations (control 2), and fluid circulation with chaotic mixing.

***Table 3*:** Fold increases of the background-subtracted fluorescence

	Circulation without chaotic mixing	Circulation With chaotic mixing
myogenin sense	2.1	4.2
MCK sense	1.6	6.9
myosin light chain sense	2.2	3.4
CAB (positive control)	2.3	4.5

Note: The fold increases were referred to the hybridization signals from the static control.

The experimental result (Table 3) clearly showed that chaotic mixing played a significant part in the overall signal enhancement. Compared with the static control, simple circulation of the fluid increased the signal intensity by about 2-fold, while circulation with chaotic mixing improved the signals by 3- or 7-fold. Therefore, microfluidic chaotic mixing has a major effect on the mass transfer of the DNA targets to a solid reactive boundary by effectively homogenizing the solution.

Dynamic Hybridization with High-Density Microarrays

We tested the compatibility of this approach with larger arrays, and demonstrated that microfluidic chaotic mixing can improve hybridization of high-density microarray experiments. A PDMS device was fabricated with similar geometry, but larger hybridization chambers (7.5mm×36mm×65 microns, 35mL). It was sealed onto a commercial microarray (mouse printed oligonucleotides array, 17K, 70-mer, J. David Gladstone Institutes). Approximately 9,500 spots on the slide were accessible within the hybridization chambers. All the experimental procedures followed the previous description except that two identical microarray slides were put into use for comparison. The signals from hybridization using microfluidic chaotic mixing were dramatically enhanced, as shown in figure 9a and c and figure 9b and d (control).

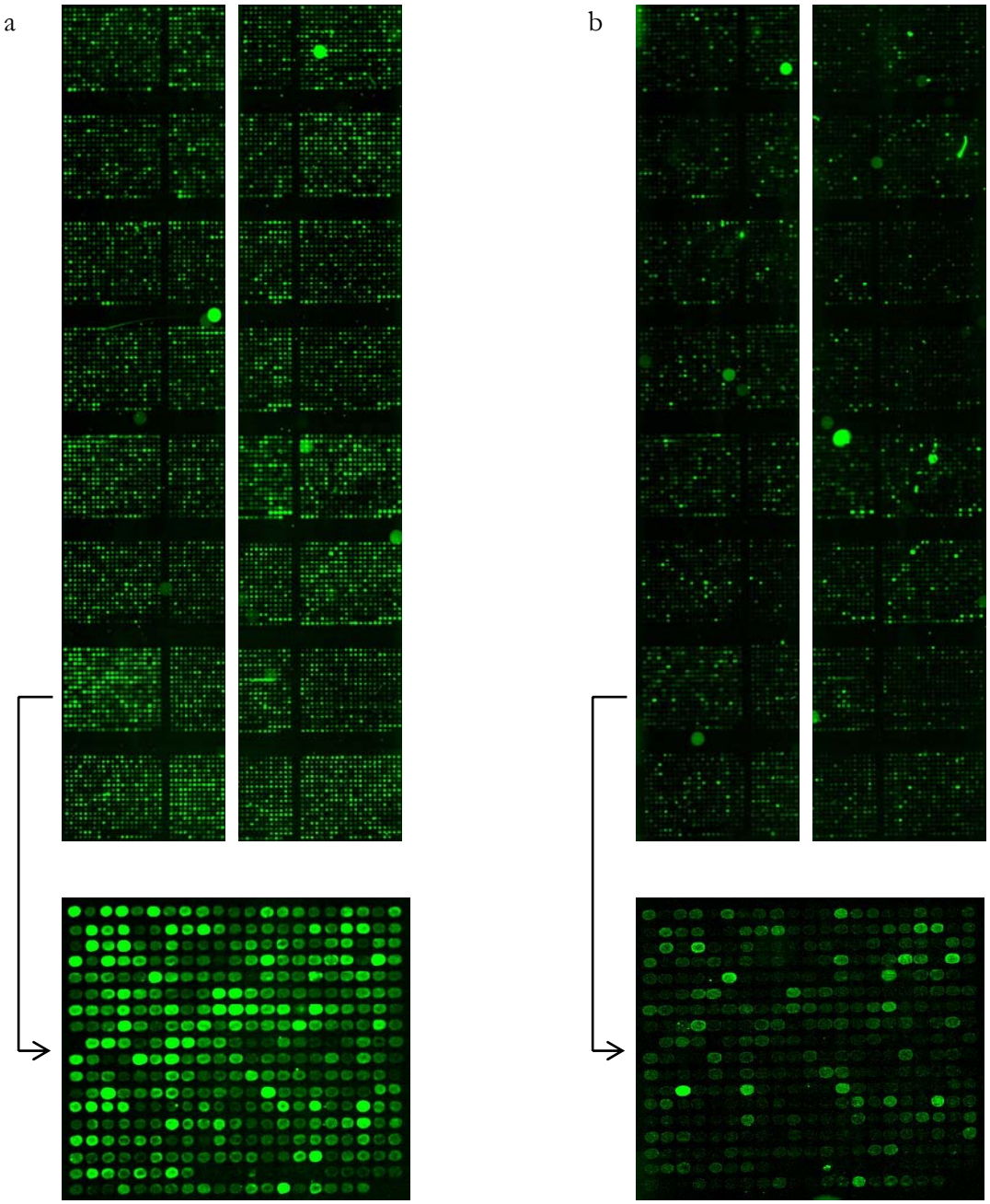

Figure 9: *Fluorescent images of two side-by-side hybridization experiments (17 K microarray). (a) Dynamic; (b) Static. (c) and (d) respectively show a zoom-in view of the block #33 from (a) and (b). A PDMS device with larger chambers (7.5mm×36mm×65m) was used in each experiment. Notice that a gap existed between the two chambers.*

For individual features, we calculated the fold increase in the background-subtracted fluorescence by dynamic mixing over static method, and then made a histogram (figure 10).

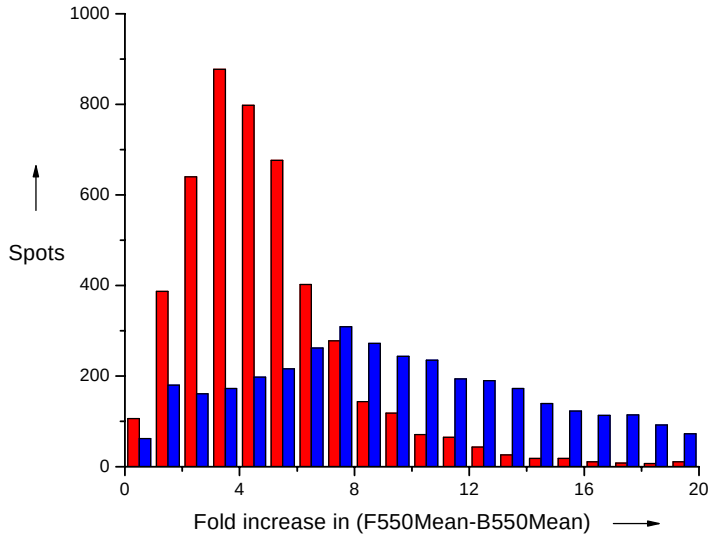

Figure 10: *Histogram of the fold increase in the background-subtracted fluorescence by the dynamic over static hybridization. The red and the blue represent two sets of independent hybridization experiments using different dilutions of the Cy3 labeled cDNA. The red: 1.6 ng/mL; the blue: 0.8 ng/mL. The wider spread in the distribution of the blue columns may result from a greater fluctuation of signal intensities when the static method was used with the more diluted labeled target.*

The peak of the red columns (input sample concentration 1.6 ng/mL) was located between 3- and 4-fold. When the input Cy3 labeled cDNA was diluted to 0.8 ng/mL (the blue

columns), the peak shifted to 7- and 8-fold. That was consistent with our previous observation (figure 8a): the fold increase of signals by dynamic over static hybridization became larger in lower concentration of input samples. Static hybridization may suffer more from local depletion of target DNA molecules around the probes when the concentration of input samples was decreased. But microfluidic chaotic mixing can circumvent this problem effectively. This may explain the above observation. The signal enhancement of our approach was comparable or slightly better than other reported values (mostly ranging from 2- to 5-fold) in literature[103, 104, 106-108].

The specificity of signals of the dynamic vs. static method was further examined (figure 11) using the receiver operating characteristic (ROC) analysis[120]. Dynamic hybridization reduced the overlap between the intensity distributions of the negative control features and the positive probe features. The increase in the area (figure 11b vs. Fig11d) under ROC curves[120] also suggested that the dynamic approach achieved better signal specificity than the static method.

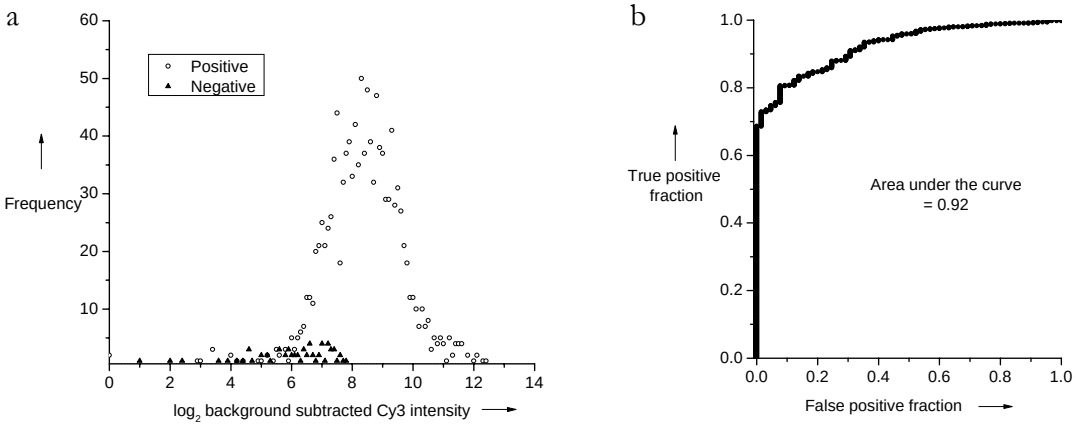

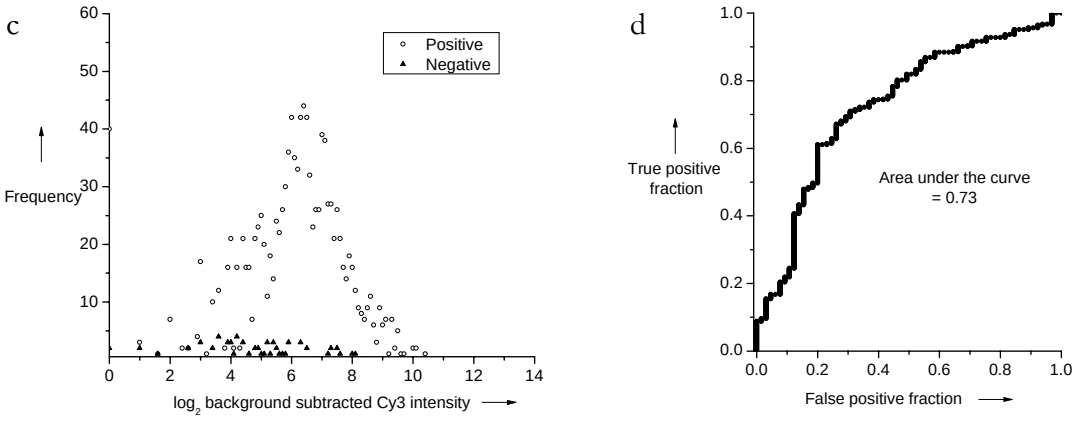

Figure 11: *Distribution of positive/negative signals and ROC curves. a) Distribution of the positive probe signals (open circles) and the negative control signals (black triangles) for the dynamic experiment. b) Receiver operating characteristic (ROC) curve for the dynamic experiment, with an area under the curve of 0.92. c) Distribution of positive/negative signals for the static experiment. d) ROC curve for the static experiment, with an area under the curve of 0.73. Negative control features (Operon) are the sequences that have been determined to be absent from the mouse genome. Positive features were identified from previous independent experiments (data not shown) as having signal intensity greater than 3SD above the median negative control intensity in 72 hour diffusion hybridization experiments using labeled 36 hour C2C12 cDNA. The true positive fraction is defined as the fraction of all positive probe features encountered at any given rank on the intensity scale. The true negative fraction is the fraction of all negative control features encountered at any given rank on the intensity scale.*

Discussions

We attempted to determine how many cDNA molecules were actually hybridized onto the slide from the solution. The nucleotide concentration of the CAB spiked cDNA solution was determined by UV absorption. We manually deposited volume-defined droplets of Cy3 labeled cDNA molecules onto the slide using microcapillary tubes (0.2 mL, Drummond), giving a standard curve of the fluorescence intensity vs. the amount of deposited nucleotides. Using an estimate of the CAB cDNA length, we could calculate the number of hybridized CAB molecules on a given spot. The analysis was based on 2-hour hybridization experiments. The data (table 4) reveal that only a small percentage of target DNA molecules are actually hybridized with the static method, while a large portion of them remain in the solution. Dynamic mixing can increase the percentage of molar hybridization events by 4- to 7-fold. A new challenge may emerge to make better use of the unhybridized target DNA molecules in the solution.

***Table 4*:** Percentages of hybridized CAB molecules out of the total initial spikes.

Input CAB (atto mol)	Dynamic hybridization (%)	Static Hybridization (%)
55	9.4	1.3
28	4.1	0.66
5.5	1.2	0.20
2.8	1.6	0.20
1.1	1.9	0.54

Note: The yield of the labeling reaction was approximately 54% by the measurements of absorption. The full length of the CAB spikes (500 bp) was used in the above estimation. This represents a conservative lower limit as the hexamer priming reaction may yield a distribution of cDNA lengths.

It is particularly attractive to profile the expression levels of multiple genes from a single cell. Current techniques require two rounds of amplification of the mRNA extracted from individual cells so that the sample can be sufficient to perform DNA microarray experiments. It is a labor-intensive procedure, requiring expensive reagents. Moreover, it is debatable whether the bias of measurement is significantly induced by multiple rounds of amplification. We have demonstrated that hybridization with microfluidic chaotic mixing can improve the sensitivity level of DNA microarray experiments by nearly one order of magnitude compared with the static control. Here we discuss a possibility of improving detection limit of DNA microarrays furthermore by decreasing the size of printed features (figure 12). Detection limit represents the minimum amount of sample from which a detection system can produce reliable signals and quantify them accurately. Signal-to-noise (S/N) ratio is a measurement widely used for characterizing detection limit. Some researchers reported that the concentration of Cyanine dye (Cy3 or Cy5) down to 1 molecule/μm^2 can produce signals with an S/N ratio of 10 using a fluorescent scanner of GenePix 4000B [Pickett, 2003]. This critical information allows calculation of the minimum necessary amount of samples within a hybridization chamber (approximately 5 in μL, with an assumption of 100% valid hybridization efficiency from the solution to the solid surface). It is apparent that this putative detection limit is related to the area of

immobilized probes on the substrate surface, or the feature size. Although this relationship is likely to be non-linear beyond certain range of the feature size, decreased feature size would make it possible for smaller number of target DNA molecules to maintain the same density of dye molecules on the surface (1 molecule/μm^2), therefore improving the detection limit of experiments.

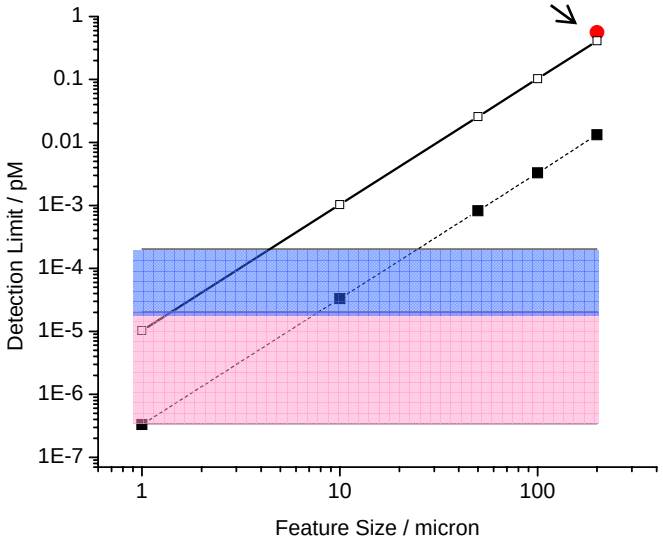

Figure 12: *Putative limits of detection with different sizes of printed features. Red dot indicated by the arrow: detectable concentration of the positive spike (CAB gene) with an S/N ratio of 10 by the actual experiment of dynamic hybridization. Open squares: putative limits of detection (see discussion). Solid squares: putative limits of detection with an additional assumption of efficiency of 100% valid hybridization. Blue region: calculated concentration for genes expressed in medium abundance (60 to 600 copies/cell) from a single cell. Pink region: calculated concentration for genes expressed in low abundance (1*

to 60 copies/cell) from a single cell. A representative volume of 5 microliters was used in the calculation.

As shown in figure 12, the color regions represent expected detection levels for genes in medium (60 to 600 copies/cell, blue) or rare (1 to 60 copies/cell, pink) abundance from a single cell. The red dot symbols the actually detectable concentration of the positive spike (CAB gene) with an S/N ratio of 10 by dynamic hybridization in our experiments. Solid squares represent putative limits of detection with an assumption of 100% valid hybridization efficiency. After the efficiency of valid hybridization is corrected to 1.6% (refer to the experimental data in table 4), the theoretical detection limits (open squares) is reasonably close to the actual detection level by dynamic hybridization in our experiments (the red dot). This also reinforces the conclusion that microfluidic chaotic mixing is an effective approach to enhance hybridization signals, thereby improving the detection limit of experiments. Regarding the issue of feature sizes, a linear extrapolation reveals that microarrays with a feature size of 1 micron may have a chance to directly report detectable signals for genes in rare abundance from a single cell. We anticipate that our approach of dynamic hybridization using microarrays with decreased feature size would dramatically reduce the consumption of samples, potentially profiling gene expression from several hundred cells without any preamplification. However, this extrapolation should be treated with caution because little is known about the nonlinearity of the detection system.

The microfluidic device with smaller chambers was tested for *in situ* cDNA synthesis and labeling, followed by dynamic hybridization. The PDMS device was sealed onto a home-

printed slide. The alignment allowed the printed features accessible only within one chamber for hybridization, leaving the other chamber (blank) for cDNA synthesis and labeling, as schemed in figure 13a and figure 13b.

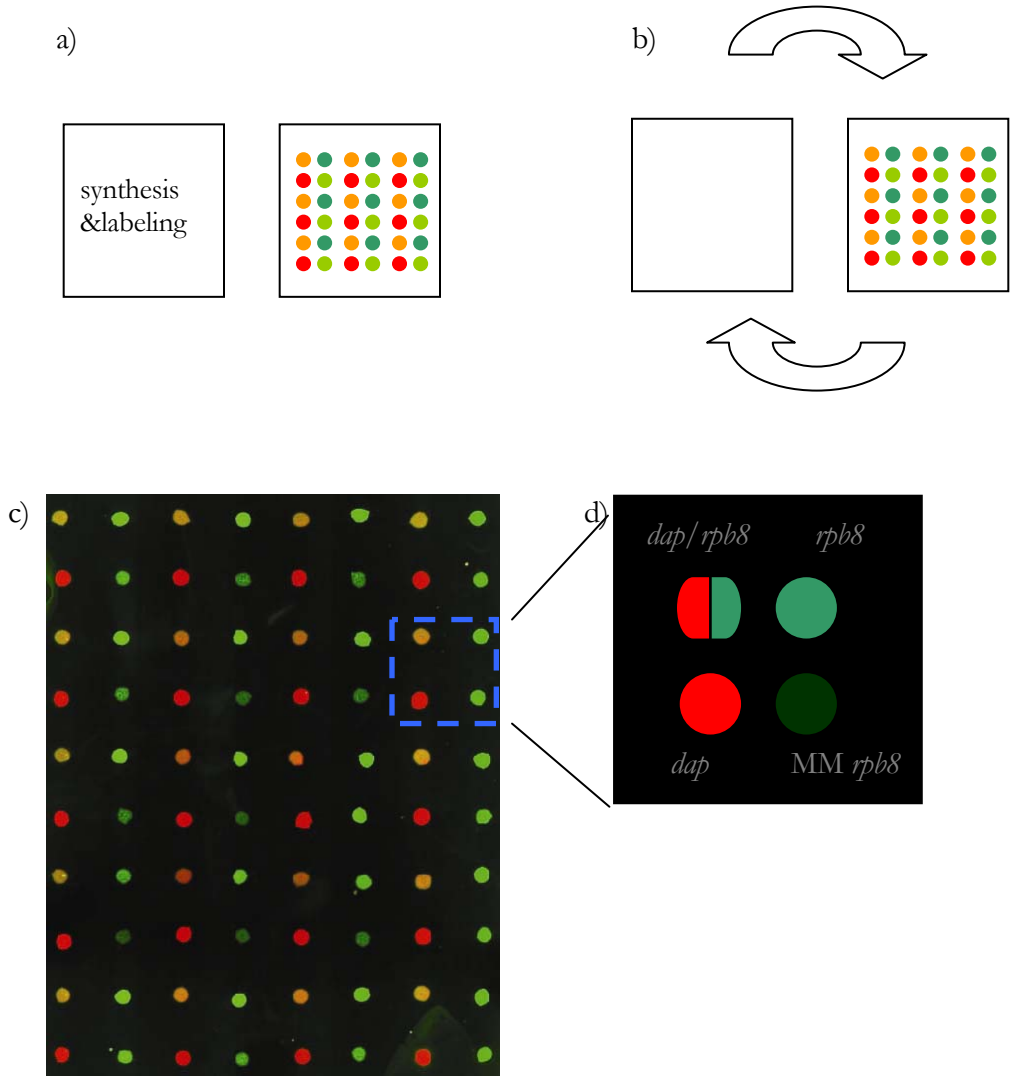

Figure 13: *Dynamic hybridization after cDNA synthesis and cyanine dye labeling using a single chip. The schematic (a) shows that cDNA can be synthesized and labeled in one blank chamber of the device. The schematic (b) shows that dynamic hybridization can be*

performed in the other chamber afterwards. (c) The scanned fluorescent image of dynamic hybridization in the wavelengths of 570nm and 670nm, after cDNA synthesis and labeling. (d) A schematic subunit of the printed pattern of probe sequences.

A reagent kit of LabelStar Array (Qiagen) was used in the experiment for direct incorporation of cyanine 3-dCTP in the synthesis of cDNA. Synthetic RNA with poly(A) tail (37-mer, 2 mM in the final solution) was loaded in the reaction chamber as a mimic of mRNA of the interested Yeast *rpb8* gene. The suggested protocol by the supplier was followed for cDNA labeling with minor changes, including the use a flatbed heating block of the thermocycler (MJ Research). After the reaction of labeling was finished, the hybridization solution was loaded into the other chamber, containing cyanine 5 labeled DNA molecules (control, 2.3 mM) for yeast *dap* gene. Then dynamic hybridization and subsequent washing was performed similar to previous description. As shown in figure 13, the experiment was successful to combine *in situ* cDNA synthesis and labeling and subsequent hybridization in a single chip. All the features produced strong fluorescent signals. The features of hybrid probes (*rpb8/dap*) reported a color of orange, which was a mix of green and red. The signals from mismatch *rpb8* were slightly weak than their counterpart of perfect-match. The data of individual features were displayed in the scatter plot (figure 14), suggesting a detectable difference of a single nucleotide mismatch in the experiment.

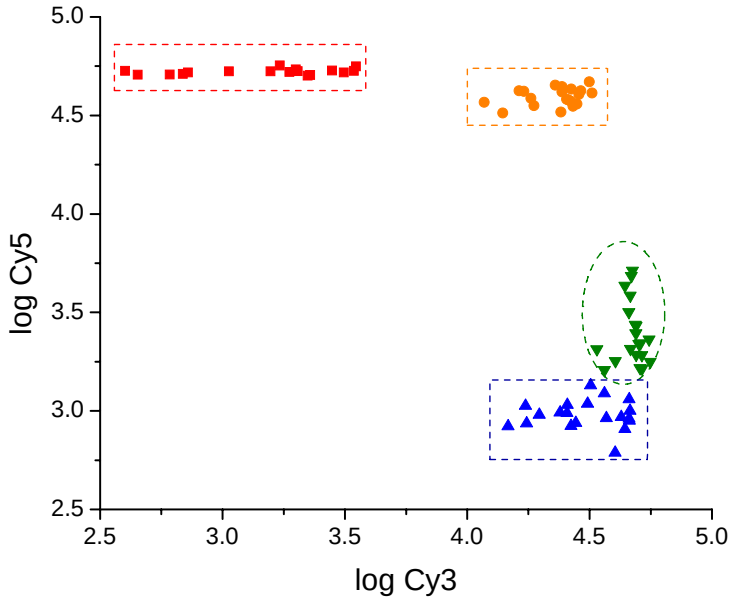

Figure 14: *Scatter plot of the fluorescent intensity of Cy5 vs. Cy3. Data represent the experimental result described in figure 13. Notice that a single nucleotide difference of the probe sequences (rpb8 vs. Mismatch rbp8) reports detectable change of fluorescent intensity. Red: rpb8, orange: rpb8/dap, green: dap, blue: mismatch dap.*

This prototype of integrating *in situ* cDNA synthesis and labeling and dynamic hybridization could facilitate automation of the whole procedure of gene expression studies using DNA microarrays. Interestingly, the design of the experiment gets rid of the step of product cleanup after labeling by a simple method of dilution, which may provide an option to simplify the design of integrated devices with multiple steps of sample preparation.

Concluding Remarks

We have demonstrated that microfluidic chaotic mixing is able to enhance hybridization signals by 3- to 8-fold, through introducing lateral mixing, facilitating the delivery of target DNA molecules, and then increasing the molar hybridization events. Our approach has improved the sensitivity of DNA microarray experiments by nearly one order of magnitude and achieved better signal specificity than the static method. The time-consuming hybridization step of the conventional method has been reduced to 2 hours using this approach. Our PDMS device is disposable, and compatible with high-density microarray slides. The device with larger chambers has a potential ability to hybridize around 135,000 array features in a single experiment, if new generation array printing tips[121] are used to spot ultrahigh-density microarrays (25,000 spots/cm^2).

APPENDIX A: SEQUENCES OF OLIGOS

Chapter 2 and Chapter 3

human beta-actin gene (294 bp)

Forward	5'-TCA CCC ACA CTG TGC CCA TCT ACG A-3'
Reverse	5'-CAG CGG AAC CGC TCA TTG CCA ATG G-3'
Taqman Probe	5'-(FAM)ATG CCC-X(TAMRA)-CCC CCA TGC CA CCT GCG T-3'

λ phage DNA (199 bp)

Forward	5'- GGT TAT CGA AAT CAG CCA CAG CGC C -3'
Reverse	5'- GGA TAC GTC TGA ACT GGT CAC -3'

Chapter 4 (Taqman Probes: 5' end modified with 6-FAM, 3'end modified with 3BHQ_1.)

Lola isoform RA (79 bp)

Forward	5'- GATGAACTCCCGCAGCAT -3'
Reverse	5'- GCAGTTGCTGCCGGTAATAG -3'
Taqman Probe	5'- CAACGGAGGAGTCGACCACCA -3'

Lola isoform RB (73 bp)

Forward	5'- TTACGCGTATAGCGGGACTC -3'
Reverse	5'- TCGCGTAGGGTCACCAGT -3'
Taqman Probe	5'- AATGCCCGCCTGGCCATG -3'

Lola isoform RD (86 bp)

Forward	5'- CCCCAAGACCTGAAGTACGA -3'
Reverse	5'- CAGTGGAAACGCTCCTTGTA -3'
Taqman Probe	5'- TGGCAGCGATGATGCGGA -3'

Lola isoform RF (124 bp)

Forward	5’- CTCGCTGCAACGACATATCA -3’
Reverse	5’- GACACAGACACCGCTCTCAA -3’
Taqman Probe	5’- TGTCTGATGTGCGGCAAAGCA -3’

Lola isoform RG (103 bp)

Forward	5’- GATCCCCAAGATTTGAGCAG -3’
Reverse	5’- GCTGCTTGCCATTGAGAAT -3’
Taqman Probe	5’- ACCGCCGAGATTCAGCGCAG -3’

Lola isoform RH (94 bp)

Forward	5’- AACGAAGGTGGTGAGTCCAG -3’
Reverse	5’- AGACTGAGGGCTCGTCTGAG -3’
Taqman Probe	5’- TCCGTAATTGGCTAATGCTGGCTG -3’

Lola isoform RI (81 bp)

Forward	5’- GATTATACCGGCAACCACAA -3’
Reverse	5’- TGAATGATGTGATGGGGATG -3’
Taqman Probe	5’- TGCCACACATCATCCGCACA -3’

Lola isoform RJ (87 bp)

Forward	5’- ACCATAGGTTTCGGGTCCTT -3’
Reverse	5’- CGCTCTGGACTGGACTGAAC -3’
Taqman Probe	5’- TGCCGGGTTTGCTTCAGTCTG -3’

Lola isoform RK (96 bp)

Forward	5’- CAGCACGACAGATCTCAGGA -3’
Reverse	5’- GGCGTGCTGATACCAGGTTA -3’
Taqman Probe	5’- CACAGCAACGGGATCCCCAA -3’

Lola isoform RL (120 bp)

Forward	5’- CAGCACGACAGATCTCAGGA -3’
Reverse	5’- CGGCATTTCGCTGTCATAG -3’
Taqman Probe	5’- CACAGCAACGGGATCCCCAA -3’

Lola isoform RM (111 bp)

Forward	5’- CAGCACGACAGATCTCAGGA -3’
Reverse	5’- GTTCATAGCTCATATTATCGATTTCA -3’
Taqman Probe	5’- CACAGCAACGGGATCCCCAA -3’

Lola isoform RN (99 bp)

Forward	5’- GAGGAGTGCCAGGATTTCAA -3’
Reverse	5’- GGCATCGTGGAGTTTCTTGT -3’
Taqman Probe	5’- TGGTTCAAGCGACGATCCCA -3’

Lola isoform RO (76 bp)

Forward	5’- CAAGTCCCATCAGAAACTGC -3’
Reverse	5’- GCACGACACGCACTTGTACT -3’
Taqman Probe	5’- TGCGCAAGTACTGCCTCAAGCA -3’

Lola isoform RP (71 bp)

Forward	5’- GACCTGAAGCTGGGCAGTC -3’
Reverse	5’- TCCTCGAACTCCTCATTCTCA -3’
Taqman Probe	5’- TCGTGGACCTACGATGCGGTGA -3’

Lola isoform RQ (79 bp)

Forward	5’- ATGCTCCCTCCACATCCAC -3’
Reverse	5’- GCATCTGACGATTTGCATTT -3’
Taqman Probe	5’- TCATCGGCTACCACCGCATCC -3’

Lola isoform RS (158 bp)

Forward	5’- ATCCCCAAGCGAGGACAC -3’
Reverse	5’- TGGGTTTTTGTCTAAGATTTGC -3’
Taqman Probe	5’- CACACAACACCACCCGCCA -3’

Lola isoform RT (85 bp)

Forward	5’- GGATCCCCAAGAAAACTCCT -3’
Reverse	5’- AATGTGCGAGTTGTTCGATG -3’
Taqman Probe	5’- CGTGAAATCGGTCACCTCGCTG -3’

Lola isoform RV (185 bp)

Forward	5’- GGGATCCCCAAGATGTCTCT -3’
Reverse	5’- TGTTTCTTGCAGATCGTTGC -3’
Taqman Probe	5’- AGCCGACCGAACCGTATCCG -3’

Lola isoform RW (91 bp)

Forward	5’- TGGACTAATGGCACAGGATG -3’
Reverse	5’- AGCACTCGCAATCGAATAGG -3’
Taqman Probe	5’- CAACGGGATCCCCAAGATGGC -3’

Lola isoform RX (103 bp)

Forward	5’- CAGCACGACAGATCTCAGGA -3’
Reverse	5’- GGGTGCGCAGATTGTACTTC -3’
Taqman Probe	5’- CACAGCAACGGGATCCCCAA -3’

Actin 42 (86 bp)

Forward	5’- GCAGACAAAGGATGGGAGTC -3’
Reverse	5’- CTTCTGAAGGAGCGGAAGTG -3’
Taqman Probe	5’- TAATACCGGGAGCAGGCGCA -3’

Lim1 (136 bp)

Forward	5’- GGCATAATAGAAGCGGAGGA -3’
Reverse	5’- TAAAGACTGGGTGGCAAGGT -3’
Taqman Probe	5’- CGCCGGCACACACGTGCTAT -3’

Chapter 5 (These oligos were modified with AminoC6 group at their 5’ ends.)

myogenin sense	5’-TTTGTGTGTTGTTTGTAAAGCTGCCGCCTGACCAAG GTCTCCTGTGCTGATGATACCGGGAACAGGCAGG -3’
MCK sense	5'-AGTCGAACAGGTGCAGCTGGTGGTGGATGGCGTGA AGCTTATGGTGGAGATGGAGAAGAAGCTGGAAAAG-3'
myosin light chain sense	5’-CCTTTGCAGCCATGGGCCGTCTCAATGTGAAGAATG AGGAACTCGACGCTATGATGAAGGAAGCCAGTGG -3’
CAB (positive control)	5'-TGCTCGCTGTTCCTGGGATTTTGGTACCAGAAGCA TTAGGATATGGAAACTGGGTTAAGGCTCAGGAATG-3'
RCA (negative control)	5'-ACGCTGGTGCGGGTCGTATGGGTGGTACTACTCAG TACACTGTCAACAACCAGATGGTTAACGCAACACT-3'
dap	5’- AGGGATCGGAGCCATCATCGCGCCA-3’
Rpb8	5’-CTCATTCGGTGGCCTCTTAATGAGA -3’
Mismatch rpb8	5’-CTCATTCGGTGGACTCTTAATGAGA -3’

APPENDIX B: CORRESPONDING NAMES OF LOLA ISOFORMS*

Names from NCBI (March 9, 2006)	*Names from Goeke's paper (2003)*
RA (NM_170623)	D (AB107275)
RB (NM_170619)	L (AB107283)
RC (identical interesting region with RB)	-
RD (NM_170620)	F (AB107277)
RE (identical interesting region with RD)	-
RF (NM_170621)	I (AB107280)
RG (NM_080027)	T (AB107291)
RH (NM_170617)	M (AB107284)
RI (NM_176133)	K (AB107282)
RJ (NM_176130)	O (AB107286)
RK (NM_176136)	H (AB107279)
RL (NM_176138)	C (AB107274)
RM (NM_176140)	A (AB107272)
RN (NM_176128)	R (AB107289)
RO (NM_176129)	P (AB107287)
RP (NM_176131)	N (AB107285)
RQ (NM_176139)	B (AB107273)
RR (identical interesting region with RG)	-
RS (NM_176137)	E (AB107276)
RT (NM_176134)	J (AB107281)
RU (identical interesting region with RT)	-
RV (NM_206085)	G (AB107278)
RW (NM_206084)	Q (AB107288)
RX (NM_206083)	S (AB107290)
RY (identical interesting region with RN))	-
RZ (identical interesting region with RS))	-

* The right column of this table shows the names of lola mRNA isoforms [Goeke et al., 2003]. They were renamed by NCBI, as shown in the left column. The transcript sequences were blasted against each other to choose the pair with maximum identity, therefore establishing the correspondence between these two naming systems.

In this manuscript, the primers and Taqman probes for individual lola isoforms (listed in Appendix A) were designed on the sequences from NCBI (the new naming system). The figures in Chapter 4 are shown with the names by Goeke et al.

Bibliography

1. Giaever, G., Chu, A. M., Ni, L. & al., e. Functional profiling of the Saccharomyces cerevisiae genome. Nature 418, 387-391 (2002).

2. Mattick, J. S. The functional genomics of noncoding RNA. Science 309, 1527-1528 (2005).

3. Rueter, S. M., Dawson, T. R. & Emeson, R. B. Regulation of alternative splicing by RNA editing. Nature 399, 75-80 (1999).

4. Hannon, G. J. RNA interference. Nature 418, 244-251 (2002).

5. Eisenberg, D., Marcotte, E. M., Xenarios, I. & Yeates, T. O. Protein function in the post-genomic era. Nature 405, 823-826 (2000).

6. Check, E. Proteomics and cancer - Running before we can walk? Nature 429, 496-497 (2004).

7. Zhu, Y. Y. et al. Genetic diversity and disease control in rice. Nature 406, 718-722 (2000).

8. Sander, C. Genomic medicine and the future of health care. Science 287, 1977-1978 (2000).

9. Nevins, J. R. et al. Towards integrated clinico-genomic models for personalized medicine: combining gene expression signatures and clinical factors in breast cancer outcomes prediction. Human Molecular Genetics 12, R153-R157 (2003).

10. Margulies, M., Egholm, M., Altman, W. E. & al., e. Genome sequencing in microfabricated high-density picolitre reactors (vol 437, pg 376, 2005). Nature 439, 502-502 (2006).

11. NIH News Release http://www.genome.gov/12512130 (2004).

12. Yeakley, J. M. et al. Profiling alternative splicing on fiber-optic arrays. Nature Biotechnology 20, 353-358 (2002).

13. Chan, W. C. W. & Nie, S. M. Quantum dot bioconjugates for ultrasensitive nonisotopic detection. Science 281, 2016-2018 (1998).

14. Unger, M. A., Chou, H. P., Thorsen, T., Scherer, A. & Quake, S. R. Monolithic microfabricated valves and pumps by multilayer soft lithography. Science 288, 113-116 (2000).

15. Craighead, H. Future lab-on-a-chip technologies for interrogating individual molecules. Nature 442, 387-393 (2006).

16. Schena, M., Shalon, D., Davis, R. W. & Brown, P. O. Quantitative Monitoring Of Gene-Expression Patterns With A Complementary-Dna Microarray. Science 270, 467-470 (1995).

17. Thorsen, T., Maerkl, S. J. & Quake, S. R. Microfluidic large-scale integration. Science 298, 580-584 (2002).

18. Hansen, C. L., Skordalakes, E., Berger, J. M. & Quake, S. R. A robust and scalable microfluidic metering method that allows protein crystal growth by free interface diffusion. Proceedings Of The National Academy Of Sciences Of The United States Of America 99, 16531-16536 (2002).

19. Takayama, S. et al. Laminar flows - Subcellular positioning of small molecules. Nature 411, 1016-1016 (2001).

20. Beebe, D. J. et al. Functional hydrogel structures for autonomous flow control inside microfluidic channels. Nature 404, 588-+ (2000).

21. Whitesides, G. M. The origins and the future of microfluidics. Nature 442, 368-373 (2006).

22. Duffy, D. C., McDonald, J. C., Schueller, O. J. A. & Whitesides, G. M. Rapid prototyping of microfluidic systems in poly(dimethylsiloxane). Analytical Chemistry 70, 4974-4984 (1998).

23. McDonald, J. C. et al. Fabrication of microfluidic systems in poly(dimethylsiloxane). Electrophoresis 21, 27-40 (2000).

24. Liu, J., Hansen, C. & Quake, S. R. Solving the "world-to-chip" interface problem with a microfluidic matrix. Analytical Chemistry 75, 4718-4723 (2003).

25. Balagadde, F. K., You, L. C., Hansen, C. L., Arnold, F. H. & Quake, S. R. Long-term monitoring of bacteria undergoing programmed population control in a microchemostat. Science 309, 137-140 (2005).

26. Squires, T. M. & Quake, S. R. Microfluidics: Fluid physics at the nanoliter scale. Reviews Of Modern Physics 77, 977-1026 (2005).

27. Lucchetta, E. M., Lee, J. H., Fu, L. A., Patel, N. H. & Ismagilov, R. F. Dynamics of Drosophila embryonic patterning network perturbed in space and time using microfluidics. Nature 434, 1134-1138 (2005).

28. Park, J. U. et al. In situ deposition and patterning of single-walled carbon nanotubes by Laminar flow and controlled flocculation in microfluidic channels. Angewandte Chemie-International Edition 45, 581-585 (2006).

29. Ferrigno, R., Stroock, A. D., Clark, T. D., Mayer, M. & Whitesides, G. M. Membraneless vanadium redox fuel cell using laminar flow. Journal of the American Chemical Society 124, 12930-12931 (2002).

30. Kenis, P. J. A. et al. Fabrication inside microchannels using fluid flow. Accounts of Chemical Research 33, 841-847 (2000).

31. Knight, J. B., Vishwanath, A., Brody, J. P. & Austin, R. H. Hydrodynamic focusing on a silicon chip: Mixing nanoliters in microseconds. Physical Review Letters 80, 3863-3866 (1998).

32. Simonnet, C. & Groisman, A. Two-dimensional hydrodynamic focusing in a simple microfluidic device. Applied Physics Letters 87 (2005).

33. Yantz, G., Gilmanshin, R. & Larson, J. W. Two-dimensional hydrodynamic flow focusing for enhancement of DNA stretching in elongational flow. Biophysical Journal 88, 664A-665A (2005).

34. Jacobson, S. C., McKnight, T. E. & Ramsey, J. M. Microfluidic devices for electrokinetically driven parallel and serial mixing. Analytical Chemistry 71, 4455-4459 (1999).

35. Johnson, T. J., Ross, D. & Locascio, L. E. Rapid microfluidic mixing. Analytical Chemistry 74, 45-51 (2002).

36. Lu, L. H., Ryu, K. S. & Liu, C. A magnetic microstirrer and array for microfluidic mixing. Journal Of Microelectromechanical Systems 11, 462-469 (2002).

37. Tanthapanichakoon, W., Aoki, N., Matsuyama, K. & Mae, K. Design of mixing in microfluidic liquid slugs based on a new dimensionless number for precise reaction and mixing operations. Chemical Engineering Science 61, 4220-4232 (2006).

38. Mullis, K. et al. Specific Enzymatic Amplification Of Dna Invitro - The Polymerase Chain-Reaction. Cold Spring Harbor Symposia On Quantitative Biology 51, 263-273 (1986).

39. Dallapiccola, B., Novelli, G. & Spinella, A. Pcr Dna Typing For Forensics. Nature 354, 179-179 (1991).

40. Wiesner, R. J., Beinbrech, B. & Ruegg, J. C. Quantitative Pcr. Nature 366, 416-416 (1993).

41. Woolley, A. T. et al. Functional integration of PCR amplification and capillary electrophoresis in a microfabricated DNA analysis device. Analytical Chemistry 68, 4081-4086 (1996).

42. Kopp, M. U., de Mello, A. J. & Manz, A. Chemical amplification: Continuous-flow PCR on a chip. Science 280, 1046-1048 (1998).

43. Burns, M. A. et al. An integrated nanoliter DNA analysis device. Science 282, 484-487 (1998).

44. Hong, J. W., Fujii, T., Seki, M., Yamamoto, T. & Endo, I. Integration of gene amplification and capillary gel electrophoresis on a polydimethylsiloxane-glass hybrid microchip. Electrophoresis 22, 328-333 (2001).

45. Lagally, E. T., Emrich, C. A. & Mathies, R. A. Fully integrated PCR-capillary electrophoresis microsystem for DNA analysis. Lab on a Chip 1, 102-107 (2001).

46. Khandurina, J. et al. Integrated system for rapid PCR-based DNA analysis in microfluidic devices. Analytical Chemistry 72, 2995-3000 (2000).

47. Chiou, J., Matsudaira, P., Sonin, A. & Ehrlich, D. A closed cycle capillary polymerase chain reaction machine. Analytical Chemistry 73, 2018-2021 (2001).

48. Belgrader, P. et al. Infectious disease - PCR detection of bacteria in seven minutes. Science 284, 449-450 (1999).

49. Cheng, J., Shoffner, M. A., Hvichia, G. E., Kricka, L. J. & Wilding, P. Chip PCR.2. Investigation of different PCR amplification systems in microfabricated silicon-glass chips. Nucleic Acids Research 24, 380-385 (1996).

50. Wilding, P., Shoffner, M. A. & Kricka, L. J. Pcr in a Silicon Microstructure. Clinical Chemistry 40, 1815-1818 (1994).

51. Liu, J., Enzelberger, M. & Quake, S. A nanoliter rotary device for polymerase chain reaction. Electrophoresis 23, 1531-6 (2002).

52. Yang, J. N. et al. High sensitivity PCR assay in plastic micro reactors. Lab on a Chip 2, 179-187 (2002).

53. Dabiri, D. & Gharib, M. Digital Particle Image Thermometry - The Method And Implementation. Experiments In Fluids 11, 77-86 (1991).

54. Chaudhari, A. M., Woudenberg, T. M., Albin, M. & Goodson, K. E. Transient liquid crystal thermometry of microfabricated PCR vessel arrays. Journal Of Microelectromechanical Systems 7, 345-355 (1998).

55. Fraden, J. A two-point calibration of negative temperature coefficient thermistors. Review Of Scientific Instruments 71, 1901-1905 (2000).

56. Chou, H. P., Unger, M. A., Scherer, A. & Quake, S. R. Biomed. Microdevices 3, 323-330 (2001).

57. Shi, M. M. Enabling large-scale pharmacogenetic studies by high-throughput mutation detection and genotyping technologies. Clinical Chemistry 47, 164-172 (2001).

58. Schweitzer, B. & Kingsmore, S. Combining nucleic acid amplification and detection. Current Opinion In Biotechnology 12, 21-27 (2001).

59. Kwiatkowski, R. W., Lyamichev, V., de Arruda, M. & Neri, B. Clinical, genetic, and pharmacogenetic applications of the invader assay. Molecular Diagnosis 4, 353-364 (1999).

60. Mitchell, P. Microfluidics-downsizing large-scale biology. Nat. Biotechnol. 19, 717-721 (2001).

61. El-Ali, J., Sorger, P. K. & Jensen, K. F. Cells on chips. Nature 442, 403-411 (2006).

62. Psaltis, D., Quake, S. R. & Yang, C. H. Developing optofluidic technology through the fusion of microfluidics and optics. Nature 442, 381-386 (2006).

63. Janasek, D., Franzke, J. & Manz, A. Scaling and the design of miniaturized chemical-analysis systems. Nature 442, 374-380 (2006).

64. Hadd, A. G., Raymond, D. E., Halliwell, J. W., Jacobson, S. C. & Ramsey, J. M. Microchip device for performing enzyme assays. Anal. Chem. 69, 3407-3412 (1997).

65. Fu, A., Chou, H., Spence, C., Arnold, F. H. & Quake, S. R. An integrated microfabricated cell sorter. Anal. Chem. 74, 2451-2457 (2002).

66. Meldrum, D. R. & Holl, M. R. Microscale bioanalytical systems. Science 297, 1197-1198 (2002).

67. Ramsey, J. M. The burgeoning power of the shrinking laboratory. Nat. Biotechnol. 17, 1061-1062 (1999).

68. Ross, D. & Locascio, L. E. Microfluidic temperature gradient focusing. Anal. Chem. 74, 2556-2564 (2002).

69. Farinas, J., Chow, A. W. & Wada, H. G. A microfluidic device for measuring cellular membrane potential. Analytical Biochemistry 295, 138-142 (2001).

70. Bings, N. et al. Microfluidic devises connected to fused-silica capillaries with minimal dead volume. Anal. Chem. 71, 3292-3296 (1999).

71. Macounova, K., Cabrera, C. R. & Yager, P. Concentration and separation of proteins in microfluidic channels on the basis of transverse IEF. Anal. Chem. 73, 1627-1633 (2001).

72. VanDam, R. M., Unger, M. & Quake, S. R. Patent No.:US 6,508,988 B1 (2003).

73. Kikutani, Y. et al. Glass microchip with three-dimensional microchannel network for 2 x 2 parallel synthesis. Lab on a Chip 2, 188-192 (2002).

74. Ismagilov, R. F., Ng, J. M. K., Kenis, P. J. A. & Whitesides, G. M. Microfluidic arrays of fluid-fluid diffusional contacts as detection elements and combinatorial tools. Anal. Chem. 73, 5207-5213 (2001).

75. Liu, J., Hansen, C. & Quake, S. R. Solving the "world-to-chip" interface problem with a microfluidic matrix. Anal Chem 75, 4718-23 (2003).

76. Tettelin, H., Radune, D., Kasif, S., Khouri, H. & Salzberg, S. L. Optimized multiplex PCR: Efficiently closing a whole-genome shotgun sequencing project. Genomics 62, 500-507 (1999).

77. Unger, M. A., Chou, H. P., Thorsen, T., Scherer, A. & Quake, S. R. Monolithic microfabricated valves and pumps by multilayer soft lithography. Science 288, 113-116 (2000).

78. Hansen, C. L., Skordalakes, E., Berger, J. M. & Quake, S. R. A robust and scalable microfluidic metering method that allows protein crystal growth by free interface diffusion. Proc. Natl. Acad. Sci. U.S.A. 99, 16531-16536 (2002).

79. Chou, H. P., Unger, M. A. & Quake, S. R. Biomedical Microdevices 3, 323 (2001).

80. Liu, J., Enzelberger, M. & Quake, S. A nanoliter rotary device for polymerase chain reaction. Electrophoresis 23, 1531-1536 (2002).

81. Berg, J. M. et al. A two-stage discrete peristaltic micropump. Sensors and Actuators A-Physical 104, 6-10 (2003).

82. Belgrader, P. et al. PCR Detection of Bacteria in Seven Minutes. Science 284, 449-450 (1999).

83. Eliopoulos, G. M. & Moellering, R. C. Antibiotic Synergism And Antimicrobial Combinations In Clinical Infections. Reviews Of Infectious Diseases 4, 282-293 (1982).

84. Black, D. L. Mechanisms of alternative pre-messenger RNA splicing. Annual Review Of Biochemistry 72, 291-336 (2003).

85. Graveley, B. R. Alternative splicing: increasing diversity in the proteomic world. Trends In Genetics 17, 100-107 (2001).

86. Smith, C. W. J., Patton, J. G. & Nadalginard, B. Alternative Splicing In The Control Of Gene-Expression. Annual Review Of Genetics 23, 527-577 (1989).

87. Brett, D. et al. EST comparison indicates 38% of human mRNAs contain possible alternative splice forms. Febs Letters 474, 83-86 (2000).

88. http://www.ceolas.org/fly/intro.html.

89. Goeke, S. et al. Alternative splicing of lola generates 19 transcription factors controlling axon guidance in Drosophila. Nature Neuroscience 6, 917-924 (2003).

90. Ohsako, T., Horiuchi, T., Matsuo, T., Komaya, S. & Aigaki, T. Drosophila lola encodes a family of BTB-transcription regulators with highly variable C-terminal domains containing zinc finger motifs. Gene 311, 59-69 (2003).

91. Madden, K., Crowner, D. & Giniger, E. lola has the properties of a master regulator of axon-target interaction for SNb motor axons of Drosophila. Developmental Biology 213, 301-313 (1999).

92. Schmucker, D. et al. Drosophila Dscam is an axon guidance receptor exhibiting extraordinary molecular diversity. Cell 101, 671-684 (2000).

93. Schmucker, D. & Flanagan, J. G. Generation of recognition diversity in the nervous system. Neuron 44, 219-222 (2004).

94. Zhan, X. L. et al. Analysis of Dscam diversity in regulating axon guidance in Drosophila mushroom bodies. Neuron 43, 673-686 (2004).

95. Watson, F. L. et al. Extensive diversity of Ig-superfamily proteins in the immune system of insects. Science 309, 1874-1878 (2005).

96. Lee, T. & Luo, L. Q. Mosaic analysis with a repressible cell marker for studies of gene function in neuronal morphogenesis. Neuron 22, 451-461 (1999).

97. Marin, E. C., Watts, R. J., Tanaka, N. K., Ito, K. & Luo, L. Q. Developmentally programmed remodeling of the Drosophila olfactory circuit. Development 132, 725-737 (2005).

98. Fernandes, J. J. & Keshishian, H. Nerve-muscle interactions during flight muscle development in Drosophila. Development 125, 1769-1779 (1998).

99. Zhu, J., Shendure, J., Mitra, R. D. & Church, G. M. Single molecule profiling of alternative pre-mRNA splicing. Science 301, 836-838 (2003).

100. Lee, D. D. & Seung, H. S. Learning the parts of objects by non-negative matrix factorization. Nature 401, 788-791 (1999).

101. Brunet, J. P., Tamayo, P., Golub, T. R. & Mesirov, J. P. Metagenes and molecular pattern discovery using matrix factorization. Proceedings Of The National Academy Of Sciences Of The United States Of America 101, 4164-4169 (2004).

102. Duggan, D. J., Bittner, M., Chen, Y. D., Meltzer, P. & Trent, J. M. Expression profiling using cDNA microarrays. Nature Genetics 21, 10-14 (1999).

103. Liu, R. H., Lenigk, R., Druyor-Sanchez, R. L., Yang, J. N. & Grodzinski, P. Hybridization enhancement using cavitation microstreaming. Analytical Chemistry 75, 1911-1917 (2003).

104. McQuain, M. K. et al. Chaotic mixer improves microarray hybridization. Analytical Biochemistry 325, 215-226 (2004).

105. Guttenberg, Z. et al. Flow profiling of a surface-acoustic-wave nanopump. Physical Review E 70 (2004).

106. Adey, N. B. et al. Gains in sensitivity with a device that mixes microarray hybridization solution in a 25-mu m-thick chamber. Analytical Chemistry 74, 6413-6417 (2002).

107. Schaupp, C. J., Jiang, G. J., Myers, T. G. & Wilson, M. A. Active mixing during hybridization improves the accuracy and reproducibility of microarray results. Biotechniques 38, 117-119 (2005).

108. Yuen, P. K., Li, G. S., Bao, Y. J. & Muller, U. R. Microfluidic devices for fluidic circulation and mixing improve hybridization signal intensity on DNA arrays. Lab On A Chip 3, 46-50 (2003).

109. Wei, C. W., Cheng, J. Y., Huang, C. T., Yen, M. H. & Young, T. H. Using a microfluidic device for 1 mu l DNA microarray hybridization in 500 s. Nucleic Acids Research 33 (2005).

110. Edman, C. F. et al. Electric field directed nucleic acid hybridization on microchips. Nucleic Acids Research 25, 4907-4914 (1997).

111. Erickson, D., Liu, X., Krull, U. & Li, D. Electrokinetically Controlled DNA Hybridization Microfluidic Chip Enabling Rapid Target Analysis. Analytical Chemistry 76, 7269-7277 (2004).

112. Gurtner, C. et al. Microelectronic array devices and techniques for electric field enhanced DNA hybridization in low-conductance buffers. Electrophoresis 23, 1543-1550 (2002).

113. Liu, R. H. et al. Passive mixing in a three-dimensional serpentine microchannel. Journal Of Microelectromechanical Systems 9, 190-197 (2000).

114. Stroock, A. D. et al. Chaotic mixer for microchannels. Science 295, 647-651 (2002).

115. Simonnet, C. & Groisman, A. Chaotic mixing in a steady flow in a microchannel. Physical Review Letters 94 (2005).

116. Liu, J., Williams, B. A., Gwirtz, R. M., Wold, B. J. & Quake, S. Enhanced signals and fast nucleic acid hybridization by microfluidic chaotic mixing. Angewandte Chemie-International Edition 45, 3618-3623 (2006).

117. Pluen, A., Netti, P. A., Jain, R. K. & Berk, D. A. Diffusion of macromolecules in agarose gels: Comparison of linear and globular configurations. Biophysical Journal 77, 542-552 (1999).

118. Peterson, A. W., Heaton, R. J. & Georgiadis, R. M. The effect of surface probe density on DNA hybridization. Nucleic Acids Research 29, 5163-5168 (2001).

119. Williams, B. A., Gwirtz, R. M. & Wold, B. J. Genomic DNA as a cohybridization standard for mammalian microarray measurements. Nucleic Acids Research 32, e81 (2004).

120. Khodarev, N. N. et al. Receiver operating characteristic analysis: a general tool for DNA array data filtration and performance estimation. Genomics 81, 202-209 (2003).

121. Reese, M. O., van Dam, R. M., Scherer, A. & Quake, S. R. Microfabricated fountain pens for high-density DNA arrays. Genome Research 13, 2348-2352 (2003).